U.PORTO

FACULDADE DE MEDICINA
UNIVERSIDADE DO PORTO

Master in Metabolism – Biopathology and Experimental

Nanomedicines targeting intestinal Fc receptor to enhance the oral delivery of antidiabetic peptides

Student: João David Batista da Costa Almeida

Supervisor: Doctor Professor Bruno Sarmento, Instituto de Investigação e Inovação em Saúde (i3S), Universidade do Porto; Instituto Universitário de Ciências da Saúde (IUCS-CESPU).

Co-supervisor: Doctor Soraia Pinto, Instituto de Investigação e Inovação em Saúde (i3S), Universidade do Porto

FACULDADE DE **MEDICINA**

Acknowledgments

Primeiramente, gostaria de agradecer aos meus orientadores, Professor Doutor Bruno Sarmento e Doutora Soraia Pinto. Ao professor Bruno por me ter, desde o início, aberto as portas e permitido explorar uma área que eu desconhecia quase que por completo, mas pela qual eu já tinha um grande interesse. Pela oportunidade, paciência, apoio, compreensão, por sempre se ter mostrado disponível ao longo do desenvolvimento deste projeto, por me ter ensinado e por se mostrar um exemplo do que significa produzir ciência de qualidade, muito obrigado. Deixe-me também não só agradecer, como parabenizá-lo, por construir e nutrir continuamente um grupo de investigação que me mostrou que a ciência é mais especial e divertida quando partilhada com outras pessoas. O *Nanomedicines and Translational Drug Delivery* (NTDD) é um grupo do qual eu sinto muito orgulho de pertencer. E assim, o meu mais profundo "obrigado" vai para a pessoa que personifica para mim o quão profissional, brilhante, interessante, simpática e alegre a ciência pode ser: "Muito obrigado, Soraia!". Muito obrigado por me teres aceitado e acompanhado sempre de perto desde o primeiro dia, por me teres ensinado todas as técnicas - que se estendem para além das que estão neste trabalho - discussões de resultados e dúvidas, por me permitires não ter medo de errar e nunca hesitares em estender a mão para me orientar na procura da melhor solução. Muito obrigado pela infinita paciência, amizade, preocupação, por seres uma inspiração e modelo do que é ser um investigador profissional deve ser, e por acreditares em mim. Ter-te como orientadora foi crucial e tornou toda esta experiência ainda mais valiosa!

Muito obrigado a todos os membros do NTDD, por me terem acolhido tão bem, e por sempre me apoiarem. Guardo com carinho todos os momentos do último ano, e apesar de todos serem importantes para mim, deixo um obrigado especial à Carolina (por todos os lanches e alegria), à Juliana por me ter ajudado e se mostrar sempre disponível para esclarecer todas e quaisquer dúvidas, à Vânia, ao Paulo, Helena, Margarida, Daniel, Diogo, Sofia(s), Sónia, Bárbara, Adriana, Mariana and to both Valentina(s), Pedro Fuentes and Marina. Thank you so much for making all the days even happier!!

Por fim, agradeço aos meus amigos por todo o apoio, compreensão e muita paciência e à minha família pelo suporte incondicional e por toda a disposição e esforço para que eu pudesse aproveitar esta oportunidade ao máximo.

A gratidão que eu tenho todos por tornarem esta dissertação em algo palpável, mas acima de tudo, prazeroso de construir ultrapassa, em muito, o seu número de caracteres.

Muito obrigado!

Table of Contents

Acknowledgments III

Figure Index VII

Table Index X

List of abbreviations XI

Resumo XV

Abstract XVI

1. Introduction 1

1.1. Diabetes *mellitus* 1

1.1.1. Type 2 diabetes *mellitus* 2

1.1.2. Current type 2 diabetes *mellitus* therapy 3

1.2. Oral drug delivery for diabetes therapy 6

1.2.1. Gastrointestinal barriers 6

1.2.2. Intestinal epithelial transport mechanisms 9

1.3. Neonatal Fc Receptor 10

1.3.1. Neonatal Fc Receptor mechanisms 11

1.3.2. Therapeutical strategies 13

1.4. Nanomedicines for oral drug delivery 15

1.4.1. Nanoparticles as drug delivery systems 17

1.4.2. The biological relevance of nanoparticles properties 18

1.4.3. Nanoparticles for oral drug delivery in diabetic treatment 19

1.4.4. Lipid-based anoparticles for oral drug delivery in diabetic treatment 20

2. Aims 22

3. Materials and Methods 23

3.1. Materials 23

3.2. Production of lipid-based nanoparticles 24

3.2.1. Thin-film hydration followed by extrusion method 24

3.2.2. Microfluidics method 26
3.2.3. Vortex-mixing method 27
3.2.4. Thin-film hydration followed by sonication method 28
3.3. Physicochemical characterization of lipid-based nanoparticles 29
3.3.1. Average particle size, polydispersity index, and zeta potential ... 29
3.3.2. Transmission electron microscope analysis 29
3.3.3. Association efficiency and drug loading 29
3.4. Determination of the Isoelectric Point and solubility of tirzepatide 31
3.4.1. Determination of the isoelectric point of tirzepatide 31
3.4.2. Determination of the solubility of tirzepatide 31
3.5. Functionalization of lipid-based nanoparticles with the affibody 32
3.5.1. Affibody conjugation strategy 32
3.5.2. Conjugation efficiency 32
3.5.2.1. Fluorescamine assay 32
3.5.2.2. Ellman's assay 33
3.6. *In vitro* release study 33
3.7. *In vitro* biological assays 34
3.7.1. Cell culture maintenance 34
3.7.2. Metabolic activity assay 34
3.7.3. *In vitro* interaction studies 35
3.7.4. *In vitro* intestinal permeability assay 36
3.8. Data analysis and statistics 37
4. Results and discussion 38
4.1. Production and physicochemical characterization of lipid-based nanoparticles 38
4.1.1 Thin-film hydration followed by extrusion method 38
4.1.2 Microfluidics method 39
4.1.3 Vortex-mixing method 46

4.1.4 Thin-film hydration followed by sonication method 47

4.2. Functionalization of lipid-based nanoparticles with FcRn-targeting affibody 50

4.3. *In vitro* biological assays 52

4.3.1. Effect of FcRn-targeted lipid-based nanoparticles in the metabolic activity of intestinal cells 52

4.3.2. Interaction studies between the FcRn-targeted lipid-based nanoparticles and intestinal cells 53

4.3.3. *In vitro* permeability profile of FcRn-targeted lipid-based nanoparticles through an intestinal double-culture model 55

5. Conclusion 58

6. Future Perspectives 60

7. References 62

Figure Index

Figure 1. Dysregulation of blood glucose control in T1DM and T2DM. In healthy individuals, food intake stimulates pancreatic insulin secretion, enabling cellular glucose uptake via insulin receptor-mediated transporter activation. In contrast, T1DM results from autoimmune destruction of pancreatic β-cells causing an absolute insulin deficiency, whereas T2DM arises from peripheral insulin resistance and impaired glucose transporter signaling. Both pathologies lead to persistent hyperglycemia. Created in Biorender. 2

Figure 2. Scheme of FcRn-mediated recycling and transcytosis. (A) Vascular endothelial recycling: (1) IgG and albumin are internalized into endothelial cells via pinocytosis. **(2)** Within acidic endosomes (pH ≤ 6.5), ligands bind FcRn, (**3)** and the FcRn-ligand complex is recycled to the cell surface, **(4)** where the ligands are released into circulation at neutral pH (7.4). **(5)** Unbound cargo is degraded in lysosomes. **(B) Intestinal epithelial transcytosis**: **(1)** FcRn-mediated uptake starts at the intestinal lumen. **(2)** Following internalization, ligands bind FcRn in acidic endosomes (pH ≤ 6.5), **(3)** and this complex is transcytosed to the opposite membrane (lamina propria), where the exposure to the physiological pH result in the release of the ligands. Created in BioRender. 13

Figure 3. Representative scheme of the thin-film hydration followed by extrusion method to produce lipid-based nanoparticles (LNPs). Created in BioRender. 25

Figure 4. Representative scheme of the microfluidic production method for lipid-based nanoparticles (LNPs) formulation. Created in BioRender. 27

Figure 5. Representative scheme of the vortex-mixing production method for lipid-based nanoparticles (LNP) formulation. Created in BioRender. 28

Figure 6. Representative scheme of the thin-film hydration followed by extrusion method for lipid nanoparticles (LNPs) production. Created in BioRender. 29

Figure 7. Representative scheme of the Transwell® co-culture setup (Caco-2/HT29-MTX) used for assessing LNP permeability. Created in BioRender. 37

Figure 8. Size, PdI, and surface charge characterization of LNPs prepared by thin-film hydration followed by extrusion. (A) Z-Average (nm), (B) PdI, and (C) ζ-potential (mV). Data corresponds to formulations F0 and FA after 2.5 extrusion cycles through a 200 nm membrane. Full compositions and process parameters are provided in **Table 2** of **section 3.2.1**. Measurements were performed in 10 mM KCl;

Data are shown as mean ± SD and three technical replicates were performed per condition (n = 1)..... 39

Figure 9. Physicochemical characterization of LNPs produced by microfluidics. (A) Z-Average (nm), (B) PdI, (C) ζ-potential (mV), (D) Directly measured AE (%), (E) Directly measured DL (%). Full compositions and process parameters are provided in **Table 3** of **section 3.2.2**). Data is shown as mean ± SD from three independent replicates (n = 3). An ANOVA one-way was applied to compare the samples FMIL – FD, FMIL EtOH, FMIL EtOH:DMSO and FMI DMSO in both panel D and E and did not find any statistical difference between the groups (p-value = 0.3321 in panel D and p-value = 0.3669 in panel E). 40

Figure 10. Transmission electron microscopy (TEM) images of LNPs produced by microfluidic technique. TEM images show LNPs with a spherical shape for empty FMI LNPs and loaded FMI (FMIL) LNPs. Full compositions and process parameters are provided in **Table 3** of **section 3.2.2**. Scale bars represent 100 nm. 42

Figure 11. Tir isoelectric point (pI). The pI was determined by pH titration combined with assessment of peptide charge and solubility across pH 2–12. Tir demonstrated to be cationic at strongly acidic pH, electrically neutral at pH 4.3 (pI), and anionic at physiological pH (~7.4). Error bars denote mean ± SD..... 44

Figure 12. In vitro release profile of Tir from loaded LNPs. Mean percentage of Tir released over 480 min from formulation FMI (**blue squares**), formulation F1 (**red triangles**) and free Tir control (**black circles**). The experiment comprised an initial gastric phase conditions (pH 1.2) from 0 to 120 min followed by transfer into intestinal buffer (pH 6.8) at 120 min, indicated by the dashed vertical line. Full compositions and process parameters are provided in **Table 3** of **section 3.2.2**. Error bars denote mean ± SD. 45

Figure 13. Physicochemical characterization of LNPs produced by vortex-mixing. (A) Z-Average (nm), (B) PdI, (C) ζ-potential (mV), (D) Directly measured AE (%) and (E) Directly measured DL (%) for different LNP microfluidic formulations. Full compositions and process parameters are provided in **Table 4** of **section 3.2.3**. Data is shown as mean ± SD from three independent replicates (n = 3). 47

Figure 14. Physicochemical characterization of LNPs produced by thin-film hydration followed by sonication. (A) Z-average (nm), (B) PdI, (C) ζ-potential (mV, (D) Directly measured AE (%), (E) Directly measured DL (%) and (F) indirect CE (%) detected using both fluorescamine assay (black bars) and Ellman's assay (grey bars). (Data correspond to the formulations indicated on the x-axis (F17, BLNP, Tir-LNP, Affi-BLNP, Affi-Tir-LNP, BLNP-FITC, Affi-BLNP-FITC). Full compositions and process parameters are provided in **Table 4** of **section 3.2.4**. Data is shown as mean ± SD from three independent replicates (n = 3). 49

Figure 15. Transmission electron microscopy (TEM) images of thin-film hydration followed sonication and functionalized LNPs. The images show BLNPs, Tir-LNPs, Affi-BLNPs, and Affi-Tir-LNPs. Spherical morphology of the particles was preserved upon Tir loading, whereas functionalization with FcRn-targeting Affi induced surface roughness, most observed in Affi-Tir-LNPs, suggesting increased structural heterogeneity. Scale bars represent 100 nm. 50

Figure 16. Metabolic activity of Caco-2 and HT29-MTX cells after incubation with LNPs and free Tir. The cellular metabolic activity of both intestinal cells was measured by resazurin, after 4 h and 24 h of exposure to: free tirzepatide (Free Tir), empty LNPs (BLNPs), affibody-functionalized empty LNPs (Affi-BLNPs), tirzepatide-loaded LNPs (Tir-LNPs), affibody-functionalized tirzepatide-loaded LNPs (Affi-Tir-LNPs), and PBS as a control group. LNPs samples were applied at peptide-equivalent concentrations of 0.2, 1.0, 5.04, 25.2 and 126 µg/mL. Fluorescence values were blank-corrected (medium without cells) and normalized to untreated control cells, which are set to 100% viability. Data are shown as mean ± SD and six technical replicates were performed per condition (n = 1). The dotted horizontal line marks 70% metabolic activity, the cytotoxicity threshold. 53

Figure 17. Intestinal cellular interaction of BLNPs and Affi-BLNPs in Caco-2 cells after 4 h incubation. Results are expressed as (A) percentage of FITC-positive cells and (B) mean fluorescence intensity (MFI) at 100–1000 µg/mL. T-test student revealed a statistically significant difference in the percentage of FITC-positive cells between BLNPs and Affi-BLNPs at 100 µg/mL ($p = 0.000038$) and 500 µg/mL ($p = 0.006720$). Data represent the mean ± SD of three technical replicates measurements (n = 1). Significance is denoted as *$p < 0.05$, **$p < 0.01$, ***$p < 0.001$ and ****$p < 0.0001$. 54

Figure 18. Transepithelial electrical resistance (TEER) of Caco-2:HT29-MTX (90:10) co-culture during 21 days. TEER values increased from 330 $\Omega \cdot cm^2$ at day 7 to 630 Ω/cm^2 at day 21. The TEER values are represented as mean ± SD. Twelve technical replicates were performed per condition (n = 1). Values represent the mean ± SD. 56

Figure 19. TEER values and permeability profile (% of the initial amount) of free Tir, Tir-LNPs, and Affi-Tir-LNPs through the Caco-2/HT29-MTX co- culture in vitro model. All results are represented as mean ± SD (n = 3) 57

Table Index

Table 1. FDA-approved GLP-1 and dual GIP/GLP-1 receptor agonists, their routes and dosing, approximate human half-lives, and principal molecular/formulation modifications relative to endogenous incretins[57]. 5

Table 2. Lipid-based nanoparticles (LNPs) formulations tested in thin-film hydration followed by extrusion method. 25

Table 3. Formulations tested in microfluidics method. 26

Table 4. Formulations tested in vortex-mixing method. 27

Table 5. Formulations tested in thin-film hydration followed by extrusion method...... 28

Table 6. Solubility assessment of Tir in EtOH, DMSO, ultrapure water, PBS (pH 7.4) and citrate buffer (pH 4.3). 43

List of abbreviations

ADA: American Diabetes Association

AE: Association Efficiency

Affi-BLNPs: Affibody-functionalized empty lipid-based nanoparticles

Affi-Tir-LNPs: Affibody-functionalized Tir-loaded lipid-based nanoparticles

APC: Allophycocyanin

ATP: Adenosine triphosphate

ATCC: American Type Culture Collection

BBB: Blood brain barrier

BLNPs: Empty lipid-based nanoparticles

CE: Conjugation efficiency

Cys: Cysteine

CVD: Cardiovascular diseases

DLS: Dynamic Light Scattering

DL: Drug Loading

DM: Diabetes *mellitus*

DMEM: Dulbecco's Modified Eagle Medium

DMSO: Dimethyl sulfoxide

DOTAP: 1,2-dioleoyl-3-trimethylammonium-propane

DOTMA: 1,2-dioleoyl-3-trimethylammonium methane

DSPE: 1,2-distearoyl-sn-glycero-3-phosphoethanolamine

DSPE-PEG2k: DSPE functionalized with methoxy-polyethylene glycol (2 kDa)

DSPE-PEG10k: DSPE functionalized with methoxy-polyethylene glycol (10 kDa)

DSPE-PEG2k-Mal: DSPE-PEG2k conjugated with maleimide (maleimide-functionalized DSPE-PEG2k)

DSPE-PEG2k-FITC: DSPE-PEG2k conjugated with fluorescein isothiocyanate

DTNB: 5,5'-dithiobis-(2-nitrobenzoic acid) (Ellman's reagent)

DPP-4: Dipeptidyl peptidase-4

ELS: Electrophoretic light scattering

EtOH: pure ethanol

FBS: Fetal bovine serum

FcRn: Neonatal Fc receptor

FD: Freeze dry

FDA: Food and Drug Administration

FITC: Fluorescein isothiocyanate

FRR: Flow rate ratio

FSC: Forward Scatter

GIP: Glucose-dependent insulinotropic polypeptide

GLP-1: Glucagon-like peptide-1

GLP-1RA: Glucagon-like peptide-1 receptor agonist

GIT: Gastrointestinal tract

HBSS: Hank's Balanced Salt Solution

HPLC: High-Performance Liquid Chromatography

HSA: Human serum albumin

IESCs: Intestinal epithelial stem cells

IgG: Immunoglobulin G

iDPP-4: Dipeptidyl peptidase-4 inhibitors

KCl: Potassium chloride

LNP: Lipid-based nanoparticle

MASLD: Metabolic dysfunction-associated steatotic liver disease

MFI: Median Fluorescence Intensity

MODY: Maturity-Onset Diabetes of the Young

MPT: Mucus penetration testing

NEAA: Non-Essential Amino Acids

NP: Nanoparticle

PBS: Phosphate-Buffered Saline

Papp: Apparent Permeability Coefficient

PdI: Polydispersity Index

PEG: Poly(ethylene glycol)

Phe: Phenylalanine

pI: Isoelectric point

PLGA-PEG: poly(lactic-co-glycolic acid) conjugated with poly(ethylene glycol)

RF: Raw Fluorescence

RP-HPLC: Reversed-Phase High-Performance Liquid Chromatography

Rpm: rotations per minute

RT: Room temperature

SD: Standard deviation

SGLT-2i: Sodium-glucose cotransporter-2 inhibitors

SNAC: Salcaprozate sodium

SSC: Side Scatter

T1DM: Type 1 diabetes *mellitus*

T2DM: Type 2 diabetes *mellitus*

TCEP: Tris(2-carboxyethyl)phosphine

TEER: Transepithelial Electrical Resistance

TEM: Transmission Electron Microscopy

TFA: Trifluoroacetic acid

Tir: Tirzepatide

Trp: Tryptophan

Tyr: Tyrosine

Z-Average: hydrodynamic diameter

λem: Emission wavelength

λex: Excitation wavelength

ζ-potential: Zeta potential

Resumo

A diabetes *mellitus* é uma doença metabólica caracterizada pela hiperglicemia crónica, sendo que a diabetes *mellitus* tipo 2 (DMT2) constitui aproximadamente 90% de todos os casos diagnosticados da doença. O tirzepatide (Tir), um péptido agonista duplo dos recetores do polipéptido insulinotrópico dependente da glucose (GIP) e do péptido-1 semelhante ao glucagon (GLP-1), com eficácia clínica demonstrada no tratamento da DMT2, está atualmente disponível apenas em formulações injetáveis devido às barreiras gastrointestinais físicas e químicas que impedem a absorção oral. Este trabalho teve como objetivo desenvolver nanopartículas lipídicas (LNPs) para a administração oral de Tir, procurando ultrapassar essas barreiras e explorar a via de transcitose intestinal mediada pelo recetor Fc neonatal (FcRn) através da funcionalização com um *affibody* específico (Z_{FcRn_16}).

Foram avaliadas diferentes estratégias de produção, incluindo hidratação de filme fino, microfluídica e mistura por vortex. A hidratação de filme fino seguida de sonicação revelou-se a mais promissora, originando LNPs com diâmetro hidrodinâmico de 133 nm, índice de polidispersão de 0,35, potencial zeta de −7 mV, eficiência de associação (AE) de 70% e quantidade de fármaco incorporado em LNPs (DL) de 2,4%. A funcionalização com o *affibody* Z_{FcRn_16}, recorrendo a química maleimida–tiol, atingiu elevada eficiência de conjugação (>85%), mas levou ao aumento do tamanho e da heterogeneidade das partículas, além de reduzir a quantidade de Tir associada à partícula (AE = 35% e DL = 0,7%). *In vitro*, as formulações apresentaram boa biocompatibilidade, e as LNPs funcionalizadas demonstraram maior internalização celular relativamente às não funcionalizadas em linha celular Caco-2 que mimetiza os enterócitos e expressa endogenamente o recetor FcRn. No entanto, os ensaios de permeabilidade em co-cultura intestinal revelaram que nem o Tir livre, nem as Tir-LNPs não funcionalizadas, nem as LNPs direcionadas ao FcRn conseguiram atingir transporte transepitelial detetável através da barreira intestinal.

Em conclusão, a hidratação de filme fino com sonicação produziu partículas capazes de se associar eficiente com o Tir e de interagir com as células, mas que não conseguem permear o epitélio intestinal. Os esforços futuros deverão focar-se em assegurar um encapsulamento eficaz do fármaco no núcleo da nanopartícula (para excluir a mera adsorção superficial), minimizar a perda de fármaco durante a funcionalização, e demonstrar transcitose efetiva através do epitélio intestinal.

Palavras-chave: Diabetes *mellitus* tipo 2; Nanopartículas direcionadas ao recetor Fc neonatal; Affibody; Administração oral; Tirzepatide.

Abstract

Diabetes *mellitus* is a metabolic disease characterized by chronic hyperglycemia, with type 2 diabetes *mellitus* (T2DM) constituting approximately 90% of all diagnosed cases. Tirzepatide (Tir), a dual agonist peptide of the glucose-dependent insulinotropic polypeptide (GIP) and glucagon-like peptide 1 (GLP-1) receptors with demonstrated clinical efficacy in the treatment of T2DM, is currently only available in injectable formulations due to the physical and chemical gastrointestinal barriers that prevent oral absorption. This work aimed to develop lipid nanoparticles (LNPs) for the oral administration of Tir, seeking to overcome these barriers and explore the pathway of intestinal transcytosis mediated by the neonatal Fc receptor (FcRn) through functionalization with a specific affibody (Z_{FcRn_16}).

Different production strategies were evaluated, including thin-film hydration, microfluidics, and vortex mixing. Thin-film hydration followed by sonication proved to be the most promising, yielding LNPs with a hydrodynamic diameter of 133 nm, a polydispersity index of 0.31, a zeta potential of −7 mV, an association efficiency (AE) of 70%, and a drug loading (DL) of 2.4%. Functionalization with the ZFcRn_16 affibody, using maleimide-thiol chemistry, achieved high conjugation efficiency (>85%) but led to an increase in particle size and heterogeneity, in addition to reducing the amount of Tir associated with the particle (AE = 35% and DL = 0.7%). In vitro, the formulations showed good biocompatibility, and the functionalized LNPs demonstrated greater cellular internalization compared to the non-functionalized ones in a Caco-2 cell line that mimics enterocytes and endogenously expresses the FcRn receptor. However, permeability assays using an intestinal co-culture model revealed that neither free Tir, non-functionalized Tir-LNPs, nor FcRn-targeted LNPs achieved detectable transepithelial transport across the intestinal barrier.

In conclusion, thin-film hydration with sonication produced particles capable of efficiently associating with Tir and interacting with cells, but which were unable to permeate the intestinal epithelium. Future efforts should focus on ensuring effective drug encapsulation in the nanoparticle core (to exclude mere surface adsorption), minimizing drug loss during functionalization, and demonstrating effective transcytosis across the intestinal epithelium.

Keywords: Type 2 diabetes *mellitus*; Neonatal Fc receptor-targeted nanoparticles; Affibody; Oral delivery; Tirzepatide.

1. Introduction

1.1. Diabetes *mellitus*

Diabetes *mellitus* (DM) is characterized by a state of chronic hyperglycemia, marked by persistently elevated blood glucose levels[1,2]. This condition, however, is not a single disorder but a spectrum of diseases with distinct etiologies. The classification of DM is based on its underlying cause: autoimmune destruction of pancreatic β-cells defines type 1 diabetes (T1DM), while insulin resistance coupled with a progressive secretory deficiency characterizes type 2 diabetes (T2DM). Other forms include gestational diabetes, which emerges during pregnancy, and monogenic varieties such as MODY (Maturity-Onset Diabetes of the Young), caused by specific genetic mutations[1,3].

A central feature of diabetic pathophysiology is the impairment of pancreatic β-cell function, which is responsible for the production and release of insulin[4] (**Figure 1**). These critical cells can be compromised by genetic defects, targeted for autoimmune pancreatic β-cells destruction (*e.g.* T1DM), or damaged by chemical toxins, drugs, or infections[4,5]. Beyond the pancreas, the clinical manifestation of DM is further driven by peripheral insulin resistance. The action of insulin on metabolic tissues, easily seen on the liver, muscle, and adipose tissue, can be hindered by inherent defects in the insulin molecule or, more frequently, by a loss of tissue sensitivity to its signal (*e.g.* T2DM). This resistance manifests as a failure of insulin-responsive pathways and glucose transporters, rendering the body unable to respond effectively to circulating insulin[6,7] (**Figure 1**).

One of the mains role of insulin, is to be responsible for promoting glucose uptake by peripheral tissues, which will be then metabolized by them to be able to execute their functions, being their energy source[8]. Thus, a deficiency in insulin production, secretion or action will be translated in the absence of recognition of glucose by the cells, accumulating in the bloodstream, leading to hyperglycemia[9]. Although various of the reasons explain why this hormone malfunction exactly initiates and is perpetuated, the gathering evidence clearly attributes its development due to genetic, environmental, and lifestyle factors[9,10]. A major factor associated with the development of T2DM is a sedentary lifestyle compounded by malnutrition; the disease is therefore frequently comorbid with other metabolic disorders, including obesity, metabolic dysfunction-associated steatotic liver disease (MASLD), and hypertriglyceridemia[9,11].

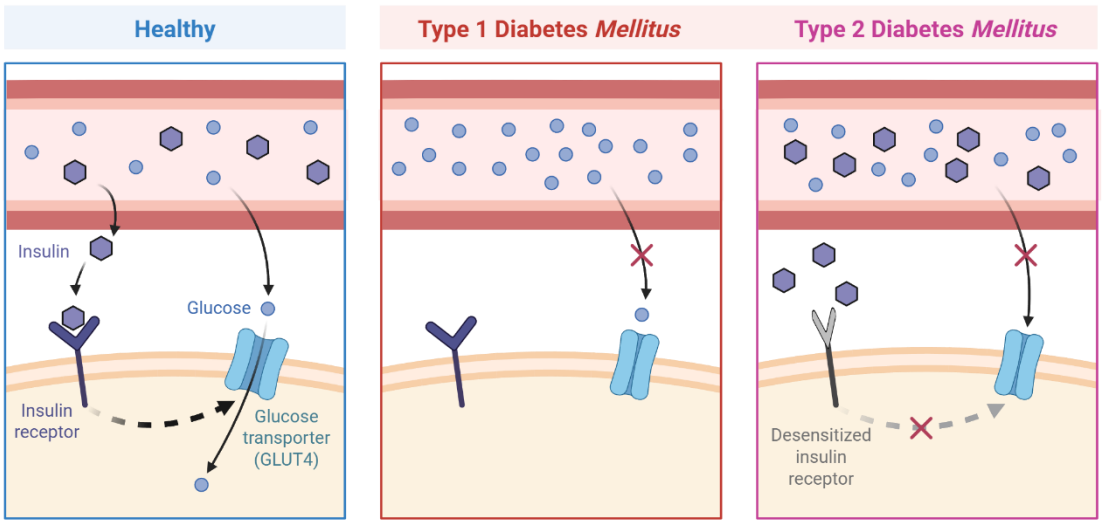


Figure 1. Dysregulation of blood glucose control in T1DM and T2DM. In healthy individuals, food intake stimulates pancreatic insulin secretion, enabling cellular glucose uptake via insulin receptor-mediated transporter activation. In contrast, T1DM results from autoimmune destruction of pancreatic β-cells causing an absolute insulin deficiency, whereas T2DM arises from peripheral insulin resistance and impaired glucose transporter signaling. Both pathologies lead to persistent hyperglycemia. Created in Biorender.

In untreated patients, chronic hyperglycemia leads to a spectrum of severe acute and long-term complications. Acute manifestations include stupor, seizures, and diabetic ketoacidosis, while long-term sequelae encompass cardiovascular disease, kidney failure, hypertension, and neurovascular damage. The latter manifests as extremities necrosis, lower limb amputation (e.g., diabetic foot syndrome), blindness from diabetic retinopathy, and peripheral neuropathy[12-14]. This spectrum of comorbidities contributes to diabetes being one of the most significant causes of mortality worldwide, responsible for approximately 9.3% of all global deaths[2]. The gravity of this situation is amplified by the fact that DM is considered a 21st-century pandemic, as of 2024, it afflicted 11.1% of the global adult population (aged 20-79 years), and its prevalence is projected to rise, potentially affecting one in eight adults by 2050[2,15]. Beyond its profound social impact, the disease imposes a substantial economic burden on national health systems, with costs exceeding 1 trillion USD annually and no foreseeable decrease in expenditures[2,15]. Among the different forms of DM, T2DM is the most prevalent, accounting for approximately 90% of all cases worldwide[2,16].

1.1.1. Type 2 diabetes *mellitus*

In healthy individuals, after a meal, the increase in blood glucose triggers the pancreas to produce and release insulin onto the blood, which will bind to its specific receptors on the cell's surfaces and induce them to activate their glucose

transporters to start uptake the glucose. However, this process is severely disturbed in DM patients[17,18].

Specifically, in the case of T2DM, the patients are not primarily insulin-dependent, as they are able to produce and secrete insulin, however, their peripheral tissues seem to be poorly responsive to insulin, presenting the characteristic of "insulin resistance"[19,20]. This resistance prevents the cells from efficiently uptake glucose from the circulatory system, not reducing hyperglycemia and, in a cyclical response, induces the pancreas to produce and secrete even more insulin. This excessive insulin production eventually results in β-cells damage, affecting their capacity to produce insulin, then adding the insulin secretion deficiency to the disease pathophysiology[19,21]. Although its presence is commonly noticed in adults, it is increasingly starting to be more frequently diagnosed on younger ages[22,23]. T2DM is highly affected by lifestyle habits, being heavily associated with sedentarism, excessive body weight and eating habits[24,25]. Conversely, physical exercise, management of body weight and a healthy diet are seen as crucial in the management of T2DM[25-27]. Nonetheless, T2DM patients may need medication to manage their blood glycemia in the long-term[28].

1.1.2. Current type 2 diabetes *mellitus* therapy

As a chronic metabolic disorder, diabetes *mellitus* currently has no universal cure and necessitates lifelong management to control blood glucose levels and prevent complications. While some cases of Type 2 Diabetes Mellitus (T2DM) remission have been reported with intensive treatment models, disease management for the vast majority of patients demands constant vigilance, including regular blood glucose monitoring, adherence to dietary and lifestyle modifications, and strict timing of medication to effectively respond to glycemic fluctuations[29-32].

The pharmacological arsenal for diabetes includes 10 principal classes of anti-diabetic drugs that target distinct pathophysiological defects[33]. These include agents to address insulin absence (insulin and insulin analogs), stimulate insulin secretion (sulfonylureas and GLP-1 receptor agonists [GLP-1RAs]), inhibit the dipeptidyl peptidase 4 enzyme (iDPP-4), improve insulin sensitivity (GLP-1RAs and thiazolidinediones), suppress exacerbated hepatic gluconeogenesis (biguanides), and delay carbohydrate absorption (α-glucosidase inhibitors and sodium-glucose cotransporter 2 inhibitors [SGLT-2i])[28,34]. Notably, GLP-1RAs have emerged as a particularly impactful class, not only for their glucose-lowering efficacy but also for their association with disease remission in some T2DM patients and their demonstrated cardioprotective and other organ-specific benefits[29,35-38].

Despite this progress in therapeutic options over recent decades, modern treatment strategies still present significant room for improvement. The observable

trend towards the development of peptide-based therapeutics, including dual and triple agonists—for T2DM underscores the urgent need for administration formulations to accompany this innovation[39-41]. A primary reliance on injectable delivery is often distressing and inconvenient for patients, contributing to poor adherence to therapy. The associated high consumption of needles and other invasive medical devices, coupled with the high-cost production of sterile, single-use injectables, presents a substantial barrier to treatment and places a strain on healthcare systems[42,43].

Thus, the path to an ideal diabetes treatment paradigm involves several key milestones. A concerted effort from both industry and academia is required to surpass these challenges, which range from identifying more suitable, patient-centric drug delivery routes to developing enhanced therapies that move beyond management toward the ultimate goal of a cure[44].

1.1.2.1. The pharmacological incretin hormones

The incretin hormones is a family of hormones released in the body in response to oral glucose intake, helping to regulate the blood glucose levels. In healthy individuals, incretin hormones are responsible for triggering the insulin release after food intake[45]. The two most recognized members of this group are the glucagon-like peptide-1 (GLP-1) and the glucose-dependent insulinotropic polypeptide (GIP), that thus produce a glucose-dependent response that stimulates the pancreatic insulin secretion and help maintain healthy glycemia levels[46,47]. Their powerful action rendered them as very interesting molecules in the therapy of T2DM, and that made molecules like GLP-1 rise in the pharmacological field, being the most commonly used for this disease[46,47].

GLP-1 is a 37 amino acid peptide secreted by intestinal L cells in its inactive form. It only activates after intracellular post-translational cleavage of the first six amino acids from its N-terminal[45]. GLP-1 has several glycemic features, namely: (1) increase insulin sensitivity in peripheral tissues (muscle and adipose tissue) (2) increase insulin secretion in a glucose-dependent way; (3) decrease glucagon secretion and (4) inhibit gastric emptying[48-50]. The incretin effects are compromised in T2DM patients, as some of the incretin hormones, are found to be less secreted in this disease, and so, the administration of GLP-1 may compensate for that reduction[46,48].

The physiological GLP-1 has a very short half-life of 1 to 2 min in plasma, with its active peptide being promptly metabolized by the DPP-4 protease, which is found all over plasma and in the endothelial cells of blood vessels[51]. This protease cleaves the peptide bond between the 8th alanine and 9th glutamine from the peptidyl N-terminal, disabling the GLP-1 efficient binding to its receptor, thus making it lose its biological activity[52]. Hence, to solve this limitation, GLP-1 analogs, such as

liraglutide, exenatide and semaglutide, have been developed, with changes in their peptide sequence that retracted the modified GLP-1 clearance, extending the analogs half-life to a week, in cases like exenatide and semaglutide[51]. Additionally, more advanced molecules started to appear, like the hybrid peptide "twincretin" Tir that is capable to bind to the GLP-1 and to the GIP receptors, potentializing the insulin sensitivity effect, besides the insulinotropic effect. SURPASS/SURMOUNT trial showed that Tir is, for now, the most effective Food and Dug Administration (FDA)-approved GLP-1RA for T2DM treatment, outperforming the GLP-1 analogs in glycemic control (HbA1c reduction)[48,51]. Nonetheless, as easily degradable peptides, all the GLP-1RA are administered as subcutaneous injectable formulation. Being usually in the format of injectable pens, this antidiabetic class also need specific conditions of storage, adding some more inconvenience to their usage, besides their embarrassing public application[48,53-55]. In 2019, it was approved by FDA for T2DM treatment, the first oral GLP-1RA formulation Rybelsus® (oral semaglutide form). This oral semaglutide was developed to tackle the patients concerns and inconveniences of invasive and painful injections, but their modest oral bioavailability (< 1%) is still a limitation[56]. To provide a clearer overview of current therapeutic options, Table 1 summarizes all FDA-approved GLP-1 and dual GIP/GLP-1 receptor agonists, listing administration routes, approximate human half-lives, and the key molecular or formulation modifications that enhance their pharmacological activity relative to endogenous incretins[57] — note that all listed drugs target GLP-1 except tirzepatide, which is a dual GLP-1/GIP agonist.

Table 1. FDA-approved GLP-1 and dual GIP/GLP-1 receptor agonists, their routes and dosing, approximate human half-lives, and principal molecular/formulation modifications relative to endogenous incretins[57].

Agent (Trade name(s))	Route of administration	Half-life	Main modifications vs endogenous GLP-1
Exenatide (Byetta®)	Subcutaneous (twice daily)	2–3 h	Exendin-4 backbone (exogenous peptide, DPP-4 resistant), C-terminal amidation.
Exenatide (Bydureon®)	Subcutaneous (once weekly) (PLGA depot)	≈2 weeks (depot release)	Encapsulated in PLGA microspheres for sustained release (formulation, not peptide modification).
Lixisenatide (Adlyxin® / Lyxumia®)	Subcutaneous (once daily)	2–4 h	Exendin-4 derivative with C-terminal substitutions; C-terminal amidation; DPP-4 resistance.
Albiglutide (Tanzeum®)	Subcutaneous (once weekly)	6–7 days	Tandem GLP-1 repeats genetically fused to human albumin

			(albumin fusion extends half-life); Ala8→Gly for DPP-4 resistance.
Dulaglutide (Trulicity®)	Subcutaneous (once weekly)	≈5 days	Two GLP-1 analogue chains fused to an IgG4 Fc (Fc-fusion) to increase size/half-life; Ala8→Gly substitution.
Liraglutide (Victoza® / Saxenda®)	Subcutaneous (once daily)	11–15 h	C16 fatty-acid acylation at Lys (via spacer) promoting albumin binding; C-terminal amide.
Semaglutide (Ozempic®)	Subcutaneous (once weekly)	≈160 h (≈1 week)	Ala8→Aib (DPP-4 resistance); Lys26 acylation with C18 diacid via spacer → strong albumin binding;
Semaglutide (Rybelsus®)	Oral (once daily)	≈160 h (≈1 week)	Ala8→Aib (DPP-4 resistance); Lys26 acylation with C18 diacid via spacer → strong albumin binding; absorption/ formulation tech (SNAC).
Tirzepatide (Mounjaro® / Zepbound®)	Subcutaneous (once weekly)	≈120 h (≈5 days)	Unimolecular dual **GIP/GLP-1** backbone; Lys20 acylation with C20 diacid for albumin binding; Aib substitutions; engineered biased agonism.

1.2. Oral drug delivery for diabetes therapy

The oral route always had the tendence to be preferred as the most convenient for drug delivery, as its the most simple and least invasive, being specially highlighted in case of treatment for chronic diseases[58-60]. Moreover, oral medications are made to be more chemically stable, supporting higher temperature fluctuations, nor needing to be sterile neither storage at strict conditions[59]. For these reasons, the treatment options of T2DM would greatly benefit from oral formulations. However, up to nowadays, there is no oral formulation that enables the effective delivery of medical peptides or proteins, but there is a notable effort to shift this paradigm, specifically for anti-diabetic drugs, as may be seen with the increasing clinical trials to develop a such technology[61]. One of the main challenges that hinders the effective peptide oral drug delivery are the gastrointestinal barriers, both chemical and physical, that those molecules need to overcome until they can successfully reach their target[62,63].

1.2.1. Gastrointestinal barriers

The GIT main function is to digest the nutrients that come from meals, from carbohydrates, proteins and lipids, fragmenting each of these macromolecules into simpler and smaller molecules that can be easily absorbed at the intestine level.

This digestive process is carried out by a myriad of enzymes and other physiological mechanisms, including pH variations and gut peristaltic motility, which break molecular bonds, denature proteins, and alter their ionic states[64]. Moreover, being open to the exterior environment, GIT is equipped with epithelial and mucus barriers that act against external pathogens and xenobiotics, constituting the first line of defense[65]. Thus, this harsh environment also avoids the absorption of oral medical proteins and peptides, like GLP-1RA, in its effective format, which results in very low oral bioavailability of less than 1%, as the case of Rybelsus®[59,61]. Hence, the success of the oral formulation relies on its capacity to avoid the enzymatic action and pH-fluctuations of GIT, but also on a way to permeate the mucus and epithelial barriers.

1.2.1.1 The biochemical barrier

The main agents of the biochemical barrier are enzymes and pH variation. Starting at the mouth, any oral intake faces a pH 6.5 that lowers to pH 1.0-2.0 at the stomach and starts again to increase in the duodenum (pH 4.0-5.5), jejunum (pH 5.5 – 7.0) and stabilizes at pH 7.0-7.5 on the ileum, colon and rectum. These fluctuation are harsh to the peptides and proteins, that can be oxidated, deaminated or hydrolyzed, inactivating them and affecting their pharmacokinetics[62]. Parallelly, the enzymes like proteases also cleave the proteins and peptides, causing their deactivation. Those enzymes are ubiquitous on the GIT, being not only encountered on its luminal space and epithelial surfaces, but also inside the cells, on the cytosol and inside the lysosomes. Examples include the mouth lysozymes and saliva amylase – which does not have a greatly impact considering the minimal time of orally administered drugs in this space – acidic pepsin on the stomach, and trypsin on the intestine[60]. It is notable that the pH variations and enzymatic activity should be considered in the design of the peptides and proteins of oral delivery technologies.

1.2.1.2. The intestinal mucus barrier

The mucus can be found covering the GIT, with a variable thickness along the entire tract, dependent on the digestive activity. The stomach and colon present thicker layers, while the small intestine display a thinner layer, enabling a more absorptive characteristic[66,67]. Mucus is mainly composed of water, mucins, lipids, and proteins that are randomly organized in a viscid matrix. Most of the unique features of the mucus are attributed to the mucins, highly glycosylated glycoproteins, negatively charged, that are continuously secreted by the GIT goblet cells. The mucin fibers are negatively charged due to their sialic acid and sulfate groups[66]. The mucus matrix exhibits a heterogeneous porosity, with pore sizes ranging from 20 to 1,800 nm and a reported mean pore size of approximately 200 nm[68], but this structure is varies depending on the GIT organ and individual health[69].

The GIT mucus layer is organized in an inner layer, closer to the epithelial cells, and an looser outer layer that is constantly replaced[66]. Varying in composition, the pH of these layers is different. In the stomach, the inner layer is more neutral to protect the cells from chloride acid, while the outer layer is much more acidic. Therefore, the mucus acts as an innate first line of defense, preventing xenobiotics and pathogens to directly reach or harm the GIT epithelia, orally administered drugs included[70]. Studies on this mucus layer permeability showed that small molecules easily diffuse through it, contrary to the macromolecules. However, the mucus barrier filtration goes beyond the size, with their negative and hydrophobic nature also keeping strange substances from crossing[70,71]. Thus, to trespass the mucus and reach the epithelial lining, the drug delivery systems need to be able to fit the heterogenous, negatively charged, and hydrophobic mucus net[72].

1.2.1.3 The intestinal epithelial barrier

Even though the GIT is all delineated by an epithelial layer, the grand majority of the absorption occurs in the small intestinal epithelium, since the stomach epithelium has a degradative acidic environment and enzymatic activity and the colon mainly functioning to maintain the electrolyte and fluid homeostasis[73]. Thus, the intestinal epithelial barrier, specifically the small intestinal epithelium, constitutes the last line that needs to be crossed by the oral delivery system to reach the circulatory system[74].

The epithelial cells are tightly bound through the junctional complexes formed by the tight junction, adherent junctions and desmosomes (90). Although these intercellular proteins seal the intercellular space of linked cells, it is a dynamic network that adapts the pore size and charge. This process regulates the selective passage of molecules like nutrients, water, and electrolytes, while being a solid barrier to external and strange substances[75]. The intestinal epithelium has a brush appearance due to the villi, protuberances that arise into the intestinal lumen, maximizing the intestine absorptive area[76]. To add to this absorptive capacity, the monolayer of polarized intestinal epithelial cells, also named enterocytes, present microvilli at their apical side[76,77]. This absorptive efficacy is attested right at the start of the small intestine (duodenum, jejunum and ileum), precisely where the majority of nutrients and substances are effectively absorbed[77].

Besides the enterocytes, the intestinal epithelial layer also possesses other type of cells, namely the mucus-producing goblet cells mentioned above, the pluripotent intestinal epithelial stem cells (IESCs) that regenerate the epithelium, enteroendocrine cells (that include L-cells and K-cells that secrete hormones like the GLP-1 and GIP, respectively), among others[78].

However, it is noteworthy that while intercellular adhesive limit paracellular permeation between epithelial cells, the cell membranes regulate transcellular

transport of molecules. Enterocytes possess dynamic intracellular pathways (e.g., endocytosis, transcytosis, carrier-mediated transport) that facilitate the movement of molecules from the apical intestinal lumen to the basolateral lamina propria, where they subsequently enter the circulatory system via capillaries[79].

Overall, the therapeutical peptide and protein oral delivery technologies should encounter molecular opportunities that help them successfully trespass the absorptive intestinal epithelium before they can finally reach the bloodstream and efficiently get to their target.

1.2.2. Intestinal epithelial transport mechanisms

Large or poorly absorbed molecules depend heavily on cellular transport mechanisms to cross the intestinal epithelium and enter the circulatory system. These substances are transported via two primary mechanisms: (1) passive transport, where the substance transport occurs along the concentration gradient (from high to low concentration) without energy expenditure; and (2) active transport, when the substance transport occurs against the concentration gradient, requiring energy in the form of adenosine triphosphate (ATP)[80,81]. These transport mechanisms operate through two distinct pathways: (1) the transcellular route, where molecules cross both apical and basolateral membranes by moving through the cell itself, and (2) the paracellular route, where substances pass between cells through tight junction-regulated spaces. The paracellular pathway is inherently passive because tight junctions form selective pores that lack energy-dependent transporters[82]. Passive transport, including both transcellular diffusion of small lipids and paracellular movement of ions, occurs along concentration gradients, while active transport is exclusively transcellular. This energy-dependent process requires either specialized membrane transporters - like SGLT1, which couples' glucose uptake to sodium electrochemical gradient - or vesicular mechanisms - such as FcRn-mediated transcytosis[83].

The challenge of overcoming the intestinal epithelial barrier has driven decades of research into various enhancement mechanisms. One primary strategy involves the chemical modification of the therapeutic peptide itself[84]. Key approaches include (i) site-specific mutagenesis to alter amino acid sequences for improved stability or binding affinity; (ii) protein fusion, wherein a secondary protein is fused to the parent peptide to enhance solubility or prolong circulation half-life; (iii) glycosylation, the attachment of carbohydrate groups to shield the molecule from enzymatic degradation; (iv) PEGylation, the covalent conjugation of poly(ethylene glycol) (PEG) chains to reduce immunogenicity and extend plasma half-life; and (v) prodrug approaches, involving chemical or biochemical derivatization to create inactive precursors that convert to active drugs after absorption[84,85]. Other methods that can be used to improve the crossing of the intestinal barrier are formulation-

based strategies, that often provide more immediate translational potential. This latter approach leverages pharmaceutical excipients (e.g., permeation enhancers[86] or enzyme inhibitors) or advanced delivery systems such as NPs, microparticles, emulsions, or microneedles[87-89].

The formulation-based strategies try to take advantage from the natural intestinal epithelium transport mechanisms, adjusting to their barriers depending on their goal. Examples include mucoadhesive formulations that, as their name suggests, are able to interact with the intestinal mucus, increasing their retention time in that layer so their cargo can be released at that target site, or, to trespass this barrier, mucus-penetrating surface moieties that can permeate through the mucus layers to reach the cellular epithelium[90-92]. Other techniques included inhibitors to prevent, for example, the degradation of therapeutical peptides by proteolytic enzyme[93]. One of the most explored strategies is the use of permeation enhancers that modulate the junctional complexes of the epithelium to enable the passage of drugs[59,86,94]. Another highly investigated strategy is the usage of decorating carrying systems with surface modifications, such as targeting ligands that promote cellular uptake and consequent transcellular transport[83,95]. However, despite the intensive research efforts and progress made in non-invasive drug delivery, there is not yet a well-stablished and efficient strategy to promote drugs uptake and transport across cellular barriers, specially of therapeutic peptides, strongly compromising their intestinal absorption and oral bioavailability[62,96].

One of the strategies to trespass the intestinal epithelium barrier is exploit natural transcytosis mechanisms that mediate the transport of molecules from the apical side of the barrier to the basolateral side, while preserving its structure[97]. Transcytosis is an metabolic pathway that enables the shuttle of large molecules across a cell in a receptor-mediated dependent process. This process usually starts with endocytosis of the receptor-binding molecule into an specific endosome that transports their core content from one end of the cell to another without fusing, for example, with lysosomes that would degrade the endocytic content. An example of this transcytosis natural mechanism that occurs in the intestine epithelium is the neonatal Fc receptor-mediated pathway[98,99].

1.3. Neonatal Fc Receptor

Beyond the intestinal epithelium, the neonatal Fc receptor (FcRn) is widely expressed almost ubiquitously throughout the entire body, including in enterocytes, vascular and blood brain barrier (BBB) endothelial cells, hepatocytes, among other cell types[100,101]. It was first identified in the jejunum of neonatal rats, where its role was shown to be the uptake of maternal immunoglobulin G (IgG) from milk, thereby contributing to the establishment of early-life immunity[100]. Focusing specifically on the FcRn relevance on the intestine, this receptor can be found in enterocytes,

goblet cells, and enteroendocrine cells, localized both on the apical membrane facing the lumen and within intracellular endosomes[101]. Its expression is seen over the lifespan, persisting in the adulthood where it continues to mediate immune and absorptive functions of both of its natural ligands: IgG and albumin[100]. This interaction is pivotal for the biological action of IgG and albumin as, by engaging FcRn, both ligands are protected from lysosomal degradation, prolonging their half-lives through the recycling pathway (**Figure 2A**), and they can be transcytosed across epithelial barriers to reach the systemic circulation in the transcytosis pathway (**Figure 2B**)[100,102].

The Fc region of IgG binds selectively to FcRn through an interaction mediated by histidine (His) residues in their protonated state[102]. His, with a side chain pKa of around 6.0, becomes protonated at acidic pH, typically between 5.5 and 6.5. As the pH rises above 6.0, His residues progressively lose their protons, weakening their interaction with FcRn. This confers FcRn with one of its most distinctive features: a pH-dependent binding mechanism, whereby ligands are bound tightly at mildly acidic pH (<6.5) and released as the environment approaches physiological pH (7.4)[100,102]. Because of this property, FcRn can capture its ligands in the acidic environment of the proximal small intestine with nanomolar affinity, transport them across the epithelium, and release them into the systemic circulation at neutral pH, avoiding the lysosomal catabolism route[100]. In addition to IgG, FcRn also binds to albumin at a distinct, non-overlapping site, through an equally pH-dependent mechanism[103]. In this case, protonated His residues in albumin form hydrogen bonds with tryptophan (Trp) residues of FcRn, which are disrupted as the pH increases and His loses its protonation state, thereby releasing the ligand[103].

The functional features of FcRn have gained recognition over the decades, with reports of its involvement in various biological processes. These include mediating passive immunity in offspring during fetal and neonatal stages, transporting IgG and albumin across epithelial barriers, and recycling both molecules to prevent their premature degradation[101,104]. These functions are crucial for sustaining IgG-mediated immune surveillance and for supporting the multiple roles of albumin, including plasma buffering, maintenance of osmotic pressure, and transport of diverse endogenous and exogenous molecules[101,104].

1.3.1. Neonatal Fc Receptor mechanisms

1.3.1.1. Recycling

As previously noted, the FcRn-mediated recycling process occurs predominantly in endothelial cells[102,104]. While the well-characterized recycling pathway focuses on IgG, the analogous mechanism for albumin is not yet fully understood. Since the external environment of these cells is the blood at pH 7.4, FcRn expression on the cell surface would be ineffective for ligand binding due to its pH-dependent affinity,

which requires a mildly acidic environment, explaining its low surface expression[102]. Instead, FcRn is located intracellularly within early endosomes, where the internal pH of approximately 6.0 enables binding to its ligands[101].

Thus, following non-specific uptake of IgG or albumin into endothelial cells (*e.g.*, via pinocytosis), these molecules are incorporated into endosomes that subsequently fuse with FcRn-containing early endosomes[103]. FcRn then binds the internalized ligands, and the resulting FcRn–ligand complexes are sorted into recycling pathways[105]. In contrast, molecules that do not bind FcRn are trafficked to lysosomes for degradation. The recycling process culminates in exocytosis, during which exposure to the physiological pH of the extracellular environment dissociates the FcRn–ligand complex, thereby releasing IgG or albumin back into circulation and significantly extending their plasma half-lives[105] (**Figure 2A**).

1.3.1.2. Transcytosis

Despite sharing mechanistic similarities with the recycling pathway, FcRn-mediated transcytosis is defined by key regulatory specificities that alter the intracellular route[102]. This bidirectional process can be initiated through either FcRn directly bind to its ligands at the cell surface, leading to the receptor-mediated endocytosis of the coupled complex, or the ligands may be internalized non-specifically via fluid-phase pinocytosis into early endosomes, where they subsequently bind to FcRn present in the acidic lumen, similar to what happens in the recycling pathway[102]. Following either uptake mechanism, the FcRn-ligand complex within the mildly acidic endosome is specifically sorted into the transcytosis pathway, which directs the transcytosis from one end of the cell to the other in polarized cells. Upon exocytosis at the opposite membrane, exposure to the physiological pH of the extracellular environment (lamina propria) causes the complex to dissociate, thereby releasing the ligand[99,104] (**Figure 2B**). Any unbound ligands that do not complex with FcRn are routed to lysosomal degradation. Furthermore, it is important to note that both the rate of this transport process and the ligand affinity of FcRn are reported to vary significantly depending on anatomical site and species[104]. This anatomical variability is attributed to multiple factors, namely the proportion of cells expressing FcRn, expression levels within individual cells, the rate of non-specific ligand internalization and the concentration of ligands in the extracellular compartment[104].

Given its ability to translocate ligands across polarized epithelial barriers while avoiding degradation, FcRn has emerged as a promising target for therapeutic delivery strategies[97,98,106].

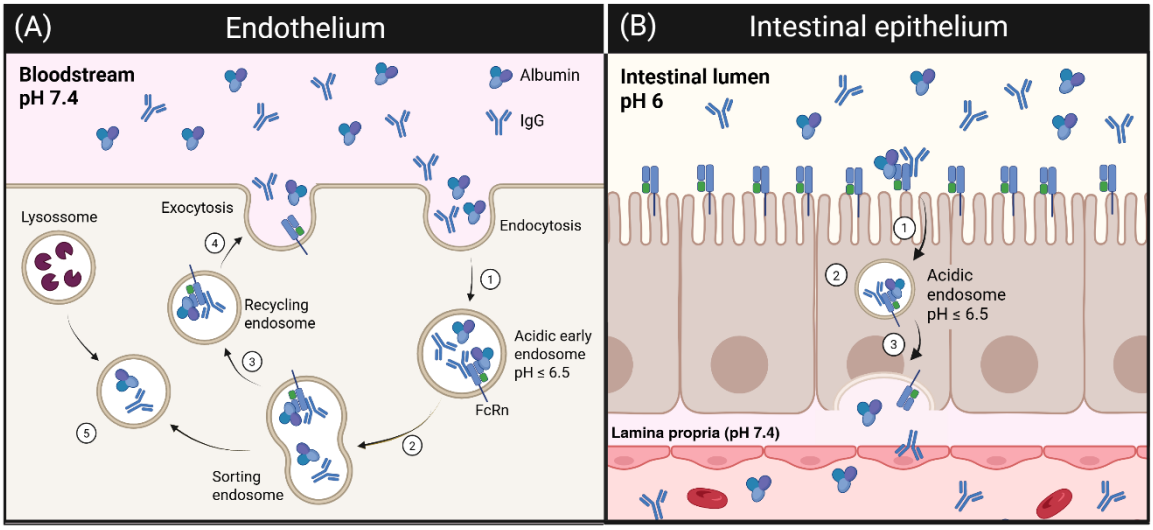


Figure 2. Scheme of FcRn-mediated recycling and transcytosis. (A) Vascular endothelial recycling: (1) IgG and albumin are internalized into endothelial cells via pinocytosis. **(2)** Within acidic endosomes (pH ≤ 6.5), ligands bind FcRn, (**3)** and the FcRn-ligand complex is recycled to the cell surface, **(4)** where the ligands are released into circulation at neutral pH (7.4). **(5)** Unbound cargo is degraded in lysosomes. **(B) Intestinal epithelial transcytosis**: **(1)** FcRn-mediated uptake starts at the intestinal lumen. **(2)** Following internalization, ligands bind FcRn in acidic endosomes (pH ≤ 6.5), **(3)** and this complex is transcytosed to the opposite membrane (lamina propria), where the exposure to the physiological pH result in the release of the ligands. Created in BioRender.

1.3.2. Therapeutical strategies

The non-invasive delivery of labile peptide and protein therapeutics, such as via the conventional oral route, remains a major challenge in drug delivery research[84,88]. A central strategy is enabling the safe passage of these molecules across biological barriers without disruptive penetration. This often involves exploring absorptive mucosal surfaces, such as intestine and lungs, and engineering drug cargoes to exploit natural transport systems present at these interfaces[84]. One such transporter that can be leveraged for this purpose is the FcRn receptor[101].

FcRn-based strategies use two key physiological functions: transcytosis across epithelial layers and recycling to extend the half-life of therapeutic molecules[101]. A common approach involves engineering the therapeutics themselves to incorporate FcRn-binding domains from IgG or albumin. This creates fused molecules that can bind FcRn, facilitating transport across mucosal barriers[107,108]. Once in circulation, these same fused constructs can take advantage of the FcRn recycling mechanism, which reduces degradation rate and significantly enhances their systemic residence time[107,108].

Besides direct fusion to therapeutics, FcRn targeting can also be integrated into nanocarrier systems. Advances in nanotechnology enable the precise functionalization of biomaterials with FcRn-binding motifs such as IgG Fc fragments, albumin derivatives, or even high-affinity synthetic binders designed to outperform natural ligands, like affibodies. These functionalized carriers improve cellular uptake and transport compared to non-functionalized systems[97-99].

Proof-of-concept studies demonstrate that FcRn-engaging formulations can effectively cross biological barriers[109]. This offers a promising platform for the non-invasive delivery of drugs for a wide range of conditions, including cancer chemotherapy[107] and metabolic disorders such as diabetes *mellitus*[98].

However, several limitations must be addressed. A primary limitation is that the FcRn pathway may not transport enough therapeutic molecules to achieve the effective systemic concentration required for a therapeutic effect[99]. Furthermore, IgG Fc-fused constructs risk being phagocytosed by antigen-presenting cells (APC), which could trigger an immune response or lead to unintended degradation[110,111]. The ubiquitous expression of FcRn also raises the possibility of non-specific, off-target uptake in various tissues. However, this broad expression can also be seen as an advantage for treating other conditions[101,104].

Despite these limitations, the growing understanding of FcRn biology, combined with the rapid progress in nanotechnology, is paving the way for more sophisticated solutions[97]. The nanocarrier tailored design allows for more precision in creating targeted delivery systems[97]. As research continues to understand how these nanocarriers interact with the FcRn pathway, the full potential of this transporter can be unlocked[104]. The advancement of these technologies and strategies promises to nurture the development of transformative non-invasive treatments, ultimately shifting the paradigm for how drugs are administered across a wide spectrum of diseases[97].

1.3.2.1. Affibodies

Affibodies represent a class of engineered protein ligands that have emerged as powerful alternatives to conventional antibodies in biomedical applications. These small proteins (~6.5–7 kDa) are based on a three-helix bundle scaffold derived from the Z-domain of staphylococcal protein A. Their minimalist α-helical structure lacks disulfide bonds, which confers exceptional thermal stability and an ability to refold completely after denaturation[112,113]. They are selected by phage-display or synthetic libraries and can be produced efficiently in E. coli or by peptide synthesis, yielding high-affinity, antibody-like specificity often in the nanomolar range[112,114,115]. The absence of native cysteines permits the deliberate introduction of a single cysteine for site-specific conjugation (for example, via maleimide–thiol chemistry) without disrupting structure or binding activity[116].

These properties—small size, robustness, and customizable binding interfaces—make affibodies well suited for both diagnostic imaging and therapeutic targeting. Their compactness favors rapid extravasation, deep tissue penetration and fast clearance from non-target tissues, which is advantageous for molecular imaging[117]. Affibodies are also effective nanoparticle targeting ligands, since its stable conjugation to nanoparticle surfaces enhances specific accumulation, cellular uptake and retention, thereby improving payload delivery and reducing off-target exposure[114,117-120].

A notable translational example is the use of an FcRn-binding affibody (Z_{FcRn}) on poly(lactic-co-glycolic acid) conjugated with PEG (PLGA-PEG) nanoparticles carrying semaglutide. This delivery system showed superior uptake in Caco-2 cells and intestinal organoids and improved glycemic control in diabetic mice versus non-targeted formulations, demonstrating the potential of affibody-mediated receptor-targeting to enable oral delivery of peptide therapeutics[98,106].

Looking forward, the affibodies modularity enables integration into multifunctional constructs (targeting, payload release and imaging) and smart prodrug systems activated by tumor-associated proteases, further enhancing selectivity and safety[118,121-124]. Overall, affibodies combine manufacturability, stability and precise targeting, making them valuable tools for decorating LNPs and other nanocarriers to improve targeted transport and therapeutic efficacy.

1.4. Nanomedicines for oral drug delivery

The medical application of nanotechnology, termed nanomedicine, represents the convergence of nanoscale engineering with biomedical science to develop advanced diagnostic and therapeutic strategies, and it has become the focus of intensive academic and industrial development[122].

Nanomedicine manipulates materials at the nanoscale to build nano-sized biomedical devices, ranging from advanced prostheses and implants to sophisticated drug delivery systems[123]. Drug nanocarriers have revolutionized the formulation of poorly water-soluble compounds and enabled the development and administration of therapeutics that previously had suboptimal pharmaceutical properties[124]. These nanosystems enable targeted drug delivery with improved bioavailability and specificity while minimizing off-target effects[124].

The impact of nanotechnology in therapeutics is evidenced by the substantial growth in publications, patents, and startup companies dedicated to translating nanomedicines into clinical products. The current clinical market includes over 50 approved nanomedicines used worldwide, such as Onivyde® (liposomal irinotecan), Ambisome® (liposomal amphotericin B) and Onpattro® (siRNA in

LNPs)[123,125]. The recent success of nanoparticle-based COVID-19 vaccines, which used LNPs to protect and deliver mRNA intracellularly, demonstrates the remarkable potential of nanoscale delivery systems, as these vaccines were developed, tested and authorized in record time, resulting from years of prior research into lipid nanoparticle platforms[126,127].

Beyond approved therapies, there are several other nanomedicine-based products currently in clinical trials, reflecting sustained investment and continued confidence in the ability of nanoscale engineering to address unmet medical needs[128]. These developments include nanomedicines for therapeutic delivery of both biologics and small molecules, whose efficacy derives directly from their nanoscale architecture[128].

Although intravenous administration remains the dominant route in preclinical and clinical settings[123], as expected since it provides straightforward systemic access, it is an invasive approach, usually requiring strict sterility during manufacturing and storage, has associated high costs[42,43], and ultimately reduces patient compliance, particularly for regimens requiring frequent injections[41].

Consequently, considerable effort is now directed toward alternative administration routes (oral, inhaled, transdermal), formulation strategies that simplify handling and reduce the need for frequent injections[123].

As the understanding of disease complexity deepens, nanotechnology in the direction of a more personalized medicine[129]. Nanoscale platforms are intrinsically modular and tunable, with particle size, surface chemistry, ligand decoration and material composition are possible to being adjusted to match patient phenotypes, payloads and routes of administration, allowing biomarker-guided, stratified therapies (for example, carriers targeted to receptors overexpressed in a patient subgroup), theragnostic that combine imaging and treatment for real-time monitoring, and stimuli-responsive systems that release drug only under specific physiological cues (pH, enzymes, redox state)[129,130]. Collectively, these design flexibilities promise safer, more effective and patient-centric interventions, and researchers are increasingly applying rational, mechanism-driven design principles to translate those promises into clinically meaningful outcomes[129,130]. Realizing this potential will, however, require parallel progress in companion diagnostics, scalable and reproducible manufacturing, adaptive regulatory pathways, and careful attention to ethical and access issues. In short, the field may be entering an era in which nanomedicine, expanding beyond intravenous delivery toward oral, inhaled and other non-invasive routes, can be tailored to individual needs and thereby transform disease treatment[129].

1.4.1. Nanoparticles as drug delivery systems

The search for a "magic bullet", a therapeutic shuttle that selectively targets the desired cells, has driven the development of NPs as advanced drug delivery systems. Engineered to overcome persistent pharmacological challenges, NPs enhance the stability and solubility of encapsulated cargo, promote transport across biological membranes, and prolong systemic circulation to improve therapeutic efficacy and safety[124,131].

Therapeutic molecules can be integrated into nanosystems via encapsulation, embedding, adsorption, or chemical conjugation[132]. This versatility allows for further modification with adjuvants or targeting moieties to achieve optimized release profiles and pharmacological actions[132]. Concurrently, advancements in nanomaterial science have created a library of biocompatible, non-toxic materials for fabricating a wide array of NP platforms. These are broadly classified into two categories based on their core physicochemical properties: organic[133] and inorganic[134]. Each category has multiple subclasses with distinct advantages and limitations depending on cargo type, stabilization, and delivery efficiency. Furthermore, combining organic-organic or organic-inorganic materials can produce hybrid NPs, engineered to synergize the benefits of both components and outperform single-platform systems.

The most commonly investigated nanosystems are polymeric, inorganic and lipid-based NPs. Polymeric NPs are colloidal particles synthesized from natural or synthetic polymers, offering a wide variety of tunable structures for delivering drugs (usually hydrophobic), biomolecules, and nucleic acids[135]. Despite being characterized by a highly flexible and easily modified chemical structure, some of these polymeric materials are associated with moderate toxicity. Advances in production techniques and the development of increasingly biocompatible and innovative polymers have enabled some polymeric NPs to transition into clinical use[125]. Inorganic NPs, fabricated from materials like gold, iron oxide, or silica, are distinguished by their unique physical, electrical, magnetic, and optical properties. Their finely tuned characteristics, high stability, and variety of shapes—from nanospheres and nanorods to nanoshells—make them highly useful for diagnostics, imaging, and photothermal therapy, and they can serve as excellent drug-delivery nanocarriers. However, concerns regarding low solubility and potential long-term toxicity[136], such as metallic accumulation in the organism, prevent their widespread clinical application. Lipid-based NPs, typically comprising vesicular structures formed by phospholipids surrounding one or more aqueous cores, are generally characterized by high biocompatibility, biodegradability, favorable bioavailability, relatively straightforward production and scalability, and an exceptional capacity to carry diverse payloads ranging from hydrophilic to hydrophobic molecules[125,132]. The most common subsets include liposomes, solid-

lipid NPs, and micelles. These favorable properties collectively make lipid-based NPs the most prevalent class of FDA-approved nanomedicines[125].

1.4.2. The biological relevance of nanoparticles properties

The performance of any nanoparticle (NP) platform is dictated by a collection of tunable characteristics, including size, morphology, core material, surface properties, responsiveness to stimuli, and targeting capability[137,138]. Particle size is perhaps the most critical feature, as it directly correlates with loading capacity, release kinetics, stability, biodistribution, and cellular uptake efficiency[139-141]. All parameters must be tuned according to the specific application objective, as the cellular and physiological context of a disease imposes unique constraints.

For example, to trespass the mucus barrier and effectively engage with FcRn to be endocytosed and follow the transcytosis pathway, NPs should be less than 200 nm (see Sections **1.2.1.2** and **1.3.1.2**). This size target is also supported by the dimensions of endosomes (40–200 nm)[142-144] and empirical evidence from various oral delivery nanosystems[98,145-147]. Although the optimal size for efficient transcytosis varies with surface properties and cell type, it must not exceed the size of the endosome that facilitates internalization[140]. A general trend is that smaller NPs are more readily internalized[141,148,149]; however, this comes with a trade-off, as a smaller size reduces the drug encapsulation capacity per particle[148].

The shape of an NP also affects its diffusivity and adhesion to cells and the extracellular matrix[150]. Spherical NPs are typically internalized more efficiently due to their symmetry and constant contact angle with the cell surface, while asymmetric shapes often require a specific orientation for uptake[150,151]. Furthermore, evidence suggests that a rough surface minimizes repulsive forces, thereby promoting cellular adhesion and endocytosis[151,152].

Beyond absolute size, the homogeneity of the NP population, quantified by the polydispersity index (PdI), is a vital indicator of formulation quality and batch-to-batch reproducibility. A narrow size distribution (PdI ≤ 0.3 for lipid-based systems, with PdI ≤ 0.2 considered optimal) ensures consistent performance and predictable *in vivo* behavior[153,154].

Surface chemical properties are equally critical, influencing biodistribution, colloidal stability, and interfacial interactions with biological systems[137]. A strong surface charge is often essential to prevent aggregation. Positively charged NPs typically show more efficient cellular internalization by interacting strongly with negatively charged phospholipids on the cell membrane[137,155,156].

The strategic decoration of LNP surfaces with PEG, that will be explored in detail in the following **section 1.4.4**, is a key design feature to improve mucus permeability and reduce early NP clearance. The incorporation of stimuli-responsive materials is

another advanced strategy, leveraging endogenous (*e.g.*, pH, enzymes, hypoxia) or exogenous triggers (*e.g.*, light, ultrasound) to achieve controlled, on-demand drug release at a specific anatomical site[157]. Finally, functionalizing the NP surface with specific receptor ligands—such as antibodies, peptides, or vitamins—enables selective recognition by target cells or tissues[158,159]. This strategy not only increases the local drug concentration at the intended site but also minimizes off-target effects on healthy tissues, a primary advantage of nanocarriers over free drug administration[160]. The versatility of nanoparticles allows for functionalization with multiple targeting ligands, enabling the development of sophisticated nanosystems designed to simultaneously overcome biological barriers and deliver their cargo to specific targets[158].

1.4.3. Nanoparticles for oral drug delivery in diabetic treatment

Diabetes *mellitus* is a global health challenge that demands innovative therapeutic strategies, particularly for medications that require recurrent injections[161]. An oral formulation represents a popular alternative that could improve the treatment regime for chronic diseases like diabetes[161]. However, the numerous physiological barriers of the GIT, such as wide pH variations, a tight epithelial barrier, dynamic mucus layers, and a myriad of catabolic enzymes that coat the intestinal lining, prevent these oral formulations from effectively reaching the circulatory system[162,163]. In response to these biological challenges, researchers have studied the composition and mechanisms underlying these barriers, leveraging these insights to guide the rational design of NPs capable of overcoming such obstacles. Successfully applying these strategies has led to advanced nanocarriers that improve the oral bioavailability of drugs, with the potential to shift treatment paradigms for chronic diseases, such as diabetes *mellitus*[164,165].

These rationally engineered NPs are designed to: (i) protect drugs from harsh GIT conditions; (ii) target specific regions or cell types within the stomach or intestine; (iii) enhance mucoadhesion and transmucosal penetration; (iv) increase drug solubility and bioavailability; and (v) facilitate spatially and temporally controlled drug release[166].

Several formulations of NPs have been extensively explored as carriers for anti-diabetic drugs, with a primary focus on insulin and GLP-1RA[162]. These NP-based delivery platforms are constructed from a wide range of materials and can be categorized into five main classes: (i) natural polymeric NPs; (ii) synthetic polymeric NPs; (iii) lipid-based NPs; (iv) inorganic NPs; and (v) nanosuspensions[162].

Each category of nanocarrier encompasses distinct material systems with specific relevance to anti-diabetic drug delivery. Natural polymeric NPs commonly employ biocompatible materials, such as chitosan[167], alginate, and dextran[168]. Synthetic polymeric variants include well-established systems like PLGA,

polyallylamine, poly(lactic acid) (PLA), niosomes[169], poly(amidoamine) (PAMAM) dendrimers[170,171], polymeric micelles, and Eudragit®-based formulations[172]. Lipid-based systems represent a particularly significant category, comprising solid lipid nanoparticles (SLNs), liposomes, nanostructured lipid carriers (NLCs), and nanoemulsions[173]. Inorganic nanomaterials explored for diabetes applications include gold[174], zirconium phosphate (ZrP), silica, and porous silicon NPs[175,176]. Finally, drug nanosuspensions, consisting of sub-micron drug crystals stabilized by surfactants, offer particular utility for enhancing the solubility and bioavailability of poorly soluble anti-diabetic compounds, such as glibenclamide and glimepiride[177].

These diverse nanocarrier systems have demonstrated promising glucoregulatory outcomes in multiple preclinical studies, exhibiting sustained blood glucose reduction and prolonged hypoglycemic effects[164,178,179]. While numerous nanocarrier platforms show considerable potential for diabetes treatment, the following section will focus specifically on LNPs and their application in oral anti-diabetic therapy, which will be explored in greater detail in subsequent work.

1.4.4. Lipid-based anoparticles for oral drug delivery in diabetic treatment

LNPs is a vast term that includes classic liposomes, SLNs, NLCs, and related vesicular systems, represent one of the most pragmatic and clinically translatable platforms for drug delivery[180,181]. Composed of physiological or modified lipids (such as phospholipids, triglycerides, and fatty acids) stabilized with surfactants or PEGylated lipids, LNPs offer a unique combination of biocompatibility, biodegradability, and versatile design[181]. Their properties can be finely tuned by adjusting lipid composition, surfactant type, and surface modifications, enabling efficient encapsulation of both hydrophilic peptides and hydrophobic small molecules. This flexibility of characteristics allows LNPs to protect sensitive therapeutics from gastric degradation, control release kinetics, and improve tissue-specific delivery[182], attributes that make them especially attractive for oral anti-diabetic therapies.

Typically engineered in the 50–300 nm size range using methods like high-pressure homogenization or microfluidics[183,184], LNPs exhibit a uniform spherical morphology that promotes consistent biodistribution and cellular uptake. Smaller particles (<200 nm) show improved mucus penetration, while surface modifications, such as cationic coatings (*e.g.,* chitosan) or PEGylation, enhance mucosal adhesion, transiently open tight junctions, and prolong circulation[185-187]. Further functionalization with targeting ligands (*e.g.,* vitamins[188], lectins[189], or affibodies[98]) can facilitate receptor-mediated transcytosis, enhancing oral absorption.

LNPs have demonstrated considerable potential in enhancing the oral delivery of anti-diabetic peptides. For instance, insulin-loaded SLNs and NLCs have achieved 5-fold improvements in relative oral bioavailability in preclinical models[190]. Incorporating mucoadhesive polymers (*e.g.,* chitosan) or enteric coatings further prolongs hypoglycemic effects and increases systemic exposure[185,191,192]. Similarly, GLP-1Ras, such as exenatide and liraglutide, have been successfully encapsulated in NLCs, which not only protect the peptides but also stimulate endogenous GLP-1 secretion and enhance permeability across intestinal epithelia[193]. Another example was the usage of an oral nanomicelle liraglutide formulation that showed 4.6-fold increase in oral exposure and produced significant long-term glycemic control and lipid metabolism benefits in T2DM animal models[194].

Beyond peptides, LNPs significantly improve the oral performance of small-molecule drugs, such as pioglitazone and glibenclamide[195]. By enhancing dissolution and sustaining release, LNPs increase bioavailability and prolong therapeutic action, enabling better glycemic control with reduced dosing frequency[196].

Despite these technological advancements, oral delivery of anti-diabetic peptides remains a challenge, mainly due to the gastrointestinal environment, with its enzymatic activity, pH variability, and mucosal barriers. Additionally, issues related to stability, scalability, and batch-to-batch reproducibility of LNPs must be addressed alongside regulatory and safety considerations, especially when using novel excipients[180]. Nevertheless, LNPs remain one of the most compelling platforms due to their biocompatibility, established manufacturing methods, and multifunctional design capabilities. Coupled with emerging targeting strategies and smart release technologies, LNPs hold strong potential to enable effective oral therapies for diabetes, including complex peptides like Tir, ultimately improving patient adherence and treatment outcomes.

2. Aims

The treatment of T2DM with peptide- and protein-based drugs, such as insulin and GLP-1 receptor agonists (GLP-1RAs), continues to rely heavily on injectable formulations. While effective, these injections remain inconvenient and burdensome for patients. Oral administration offers a more patient-friendly alternative, with the potential to improve treatment adherence, reduce healthcare burdens, and take advantage of physiological delivery routes, making it particularly desirable for chronic therapies requiring frequent dosing. However, the GIT poses multiple barriers, including enzymatic and acidic environments, poor intestinal permeability of peptides, and rapid clearance.

LNPs represent a versatile platform for oral delivery, due to their ability to encapsulate peptides, shield them from enzymatic degradation and acidic pH, and be engineered to enhance residence at and interaction with the intestinal mucosa and epithelium. These features make LNPs an attractive carrier for Tir, a dual GLP-1/GIP receptor agonist with proven clinical benefit but currently limited to subcutaneous administration. In this context, in order to overcome the GIT barriers, the functionalization of the LNPs with a FcRn-specific ligand, may enable the nanosystem to hijack the receptor-mediated transcytosis pathway, thereby opening a new route for enhancing the oral bioavailability of Tir.

Thus, the main objective of this dissertation is to develop and characterize an FcRn-functionalized LNP nanosystem that protects Tir from gastrointestinal degradation and promotes its intestinal absorption via FcRn-mediated transcytosis.

To accomplish this, the following specific objectives were set:

1. To develop Tir-loaded LNPs using different production methods, including microfluidics, nanoprecipitation, and thin-film hydration;
2. To functionalize LNPs with a FcRn-targeting affibody via Mal–thiol chemistry;
3. To explore the impact of the functionalized Tir-loaded LNPs in the metabolic activity of intestinal cell lines, mimicking the enterocytes (Caco-2 cells), and mucus-producing goblet cells (HT29-MTX cells);
4. To evaluate the intestinal interaction of the LNPs with Caco-2 cells via FcRn-mediated endocytosis;
5. To evaluate the ability of FcRn-targeted LNPs to improve the intestinal transport and delivery of Tir.

3. Materials and Methods

3.1. Materials

Drug: For experimental work, Tir was purchased from Pepmic Co., Ltd (Suzhou, China). **Phospholipids and excipients** included soy lecithin (L-α-phosphatidylcholine, from soy), 1,2-dioleoyl-3-trimethylammonium-propane (DOTAP) and 1,2-dioleoyl-3-trimethylammonium-methane (DOTMA) (Lipoid®, Ludwigshafen, Germany), and cholesterol (Sigma-Aldrich, Missouri, USA). Polyethylene-glycolated lipids were 1,2-distearoyl-sn-glycero-3-phosphoethanolamine-N-[methoxy(polyethylene glycol)-10k] (DSPE-PEG_{10k}), 1,2-distearoyl-sn-glycero-3-phosphoethanolamine-N-[methoxy(polyethylene glycol)-2k] (DSPE-PEG_{2k}), 1,2-distearoyl-sn-glycero-3-phosphoethanolamine-N-[maleimide(polyethylene glycol)-2k] (DSPE-PEG_{2k}-Maleimide, DSPE-PEG_{2k}-Mal) and DSPE-PEG_{2k}-FITC (fluorescein-conjugated DSPE-PEG_{2k}) were obtained from Ruixibiotech (Xi'an, China). The **FcRn-targeting affibody** ZFcRn_16 (sequence: VDAKYAKEWMRAAHEIRWLPNLTFDQRVAFIHKLEDDPSQSSELLSEAKKLNSQAPKC), engineered with an N-terminal hexa-histidine tag and a C-terminal cysteine and purified by immobilized metal-ion affinity chromatography under native conditions, was kindly supplied by the Department of Protein Science, School of Engineering Sciences in Chemistry, Biotechnology and Health, KTH Royal Institute of Technology (Stockholm, Sweden). **Solvents**: ethanol (EtOH, HPLC grade), chloroform, methanol and acetonitrile (HPLC grade) were purchased from Sigma-Aldrich (Missouri, USA), as was dimethyl sulfoxide (DMSO). **Buffers** were prepared in-house, like citrate buffer (50 mM, pH 4.3), acetate buffer (1 mM, pH 4), phosphate buffers (pH 7.0) and phosphate-buffered saline (PBS, 1×, pH 7.4). Milli-Q ultrapure water was produced in-house using a MilliQ station (Millipore Corporation, Massachusetts, USA) with conductivity ≈0.055 µS/cm and resistivity ≈18.2 MΩ·cm, and Hank's Balanced Salt Solution (HBSS) was prepared in-house. **Cell lines** and cell culture reagents comprised the Caco-2 clone (C2BBe1) and HT29-MTX cell lines (American Type Culture Collection, ATCC, Virginia, USA), Dulbecco's Modified Eagle Medium (DMEM) High Glucose and trypsin-EDTA (Gibco / Thermo Fisher Scientific, Massachusetts, USA), non-essential amino acids (NEAA) and other supplements (Thermo Fisher Scientific, Massachusetts, USA), fetal bovine serum (FBS) (Biochrom GmbH, Berlin, Germany), penicillin/streptomycin (Invitrogen, Massachusetts, USA) and human serum albumin (HSA) (Sigma-Aldrich, Massachusetts, USA). Analytical reagents and kits included fluorescamine reagent and Ellman's reagent (5,5'-dithiobis-(2-nitrobenzoic acid), DTNB) (Sigma-Aldrich, Missouri, USA), tris(2-carboxyethyl)phosphine (TCEP) (Thermo Fisher Scientific, Massachusetts, USA), L-cysteine and trifluoroacetic acid (TFA) (Sigma-Aldrich, Missouri, USA), and uranyl acetate (Sigma-Aldrich, Missouri, USA). Consumables

and specialized materials included 200 nm extrusion polycarbonate membranes, micro extruder set and 1,000 µL gas-tight syringes (Avanti Polar Lipids, Alabaster, AL, USA), Amicon® Ultra filters (100 kDa MWCO; Ultracel membrane) (Millipore Corporation, Bedford, MA, USA), carbon-coated copper grids (Electron Microscopy Sciences, Hatfield, PA, USA) and Transwell® inserts (12-well format; membrane surface area 1.1 cm^2; pore size 1 µm) (Corning Inc., Corning, NY, USA). Instrumentation comprised a probe sonicator (Vibracell, Sonics & Materials / Bioblock, Connecticut, USA), a Dolomite quartz X-junction microfluidic chip (190 µm etch depth) together with H-interface holder, PTFE tubing and Luer fittings (Dolomite Microfluidics, Royston, UK), syringe pumps (Braintree Scientific, Inc., Braintree, MA, USA), an inverted microscope with digital camera (Leica ICC50 HD; Leica, Zurich, Switzerland), a magnetic stirrer (IKA-Werke, Staufen, Germany), a Malvern Zetasizer Nano ZS for size and ζ-potential analysis (Malvern Panalytical, Malvern, UK), and a Thermo Vanquish HPLC system (Thermo Fisher Scientific, Waltham, MA, USA) equipped with Chromeleon chromatography data system software (v. 7.3.2; Thermo Fisher Scientific) and a Synergi C12 column (Synergi 4 µm MAX-RP 80 Å, 250 × 4.6 mm; Phenomenex, Torrance, CA, USA). Fluorescence and cell-based assays were read on a BioTek Synergy Mx microplate reader (BioTek Instruments Inc., Vermont, USA) using black 96-well plates (black bottom; Greiner Bio-One, Kremsmünster, Austria), and flow cytometry experiments were performed on a BD Accuri™ C6 Plus flow cytometer (BD Biosciences, New Jersey, USA) with data analysis in FlowJo v.10 (BD Biosciences, New Jersey, USA). Data analysis and statistical tests were performed using GraphPad Prism 9 (GraphPad Software Inc., San Diego, CA, USA).

3.2. Production of lipid-based nanoparticles

3.2.1. Thin-film hydration followed by extrusion method

The initial approach to produce LNPs was the thin-film hydration followed by membrane extrusion to obtain unilamellar vesicles (**Figure 3**) with narrow size distribution. The formulations comprised phosphatidylcholine (soy lecithin) and cholesterol at a 9:1 (*w/w*) ratio, representing 70% of the total lipid mass, with the remaining 30% substituted by DSPE-PEG_{10k} (**Table 2**). Batches were first prepared with a total lipid mass of 10 mg and later scaled up to 25 mg to improve Tir loading capacity. All components were weighed directly into a glass scintillation vial, dissolved in chloroform (1 mL per lipid component) and combined in a single glass tube. Further, the solvent was evaporated under a gentle stream of compressed nitrogen while rotating the tube to form a thin, uniform lipid film. The dry film was hydrated with 2 mL of pre-warmed PBS (1×, pH 7.4) at a temperature above the lipid transition (~55 °C) and equilibrated for 30 min with intermittent vortexing to produce a multilamellar dispersion. The dispersion was transferred to a smaller glass tube

and subjected to probe sonication on a Bioblock Vibracell sonicator (Sonics & Materials, Connecticut, USA) for 3 min at 70% amplitude, followed by equilibration at 55 °C.

Table 2. Lipid-based nanoparticles (LNPs) formulations tested in thin-film hydration followed by extrusion method.

Formulation	Lecithin (w/w %)	Cholesterol (w/w %)	DSPE-PEG$_{10k}$ (w/w %)	Extrusion cycles
F0	72%	8%	20%	2.5
FA	63%	7%	30%	2.5

DSPE-PEG: 1,2-distearoyl-sn-glycero-3-phosphoethanolamine-N-[methoxy(polyethylene glycol)]

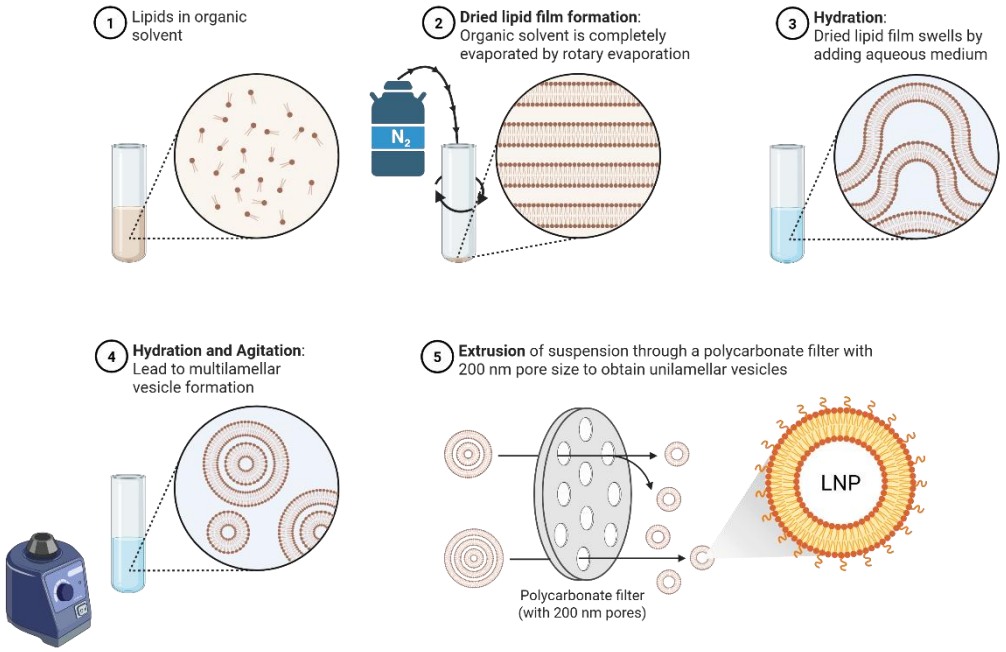


Figure 3. Representative scheme of the thin-film hydration followed by extrusion method to produce lipid-based nanoparticles (LNPs). Created in BioRender.

Size reduction and homogenization were then achieved by extrusion through 200 nm polycarbonate membranes (Avanti Polar Lipids, Alabaster, AL, USA) using a Micro Extruder set (Avanti Polar Lipids, Alabaster, AL, USA) maintained at 55 °C. The lipid suspension was loaded into a 1000 µL gas-tight syringe (Avanti Polar Lipids, Alabaster, AL, USA) and extruded back-and-forth through the membrane into a second empty syringe. This process was repeated until the alternate syringe filled and the suspension appeared homogeneous and slightly opalescent, consistent with light scattering by a uniform vesicle population.

3.2.2. Microfluidics method

Another approach used to produce the LNPs consisted in using a microfluidic X-junction chip, that enables a rapid and controlled mixing of the organic and aqueous phases (**Figure 4**). Formulations were prepared on a 25 mg total mass basis, with various compositions of lecithin, cholesterol, DSPE-PEG_{10K} or DSPE-PEG_{2K}, DOTMA, DOTAP, and Tir tested (**Table 3**). All the components were weighed directly into glass scintillation vials. Lipids and Tir were dissolved in absolute EtOH (organic phase; final organic volume of 4 mL) and the aqueous phase composed of ultrapure water, PBS (1×, pH 7.4) or 50 mM citrate buffer (pH 4.3) depending on the formulation.

The microfluidic setup consisted of a Dolomite quartz X-junction chip (190 µm etch depth) (Dolomite Microfluidics, Royston, UK) mounted on an H-interface holder, connected to syringe pumps (Braintree Scientific, Inc., Braintree, MA, USA) via PTFE tubing and Luer fittings (Dolomite Microfluidics, Royston, UK), and positioned on an inverted microscope equipped with a digital camera (Leica ICC50 HD, Zurich, Switzerland) for visual monitoring.

Table 3. Formulations tested in microfluidics method.

Formulation Code	Lecithin (w/w %)	Cholesterol (w/w %)	DSPE-PEG_{10k} (w/w %)	DSPE-PEG_{2k} (w/w %)	Tir (w/w %)	DOTAP (w/w %)	DOTMA (w/w %)	FRR (O:A) (µL/min)
FMB	63%	7%	30%	-	-	-	-	700:1400
FMC	63%	7%	30%	-	-	-	-	500:1400
FMF	63%	7%	30%	-	-	-	-	500:1600
FMG	68%	7%	25%	-	-	-	-	500:2000
FMH	68%	7%	25%	-	-	-	-	250:1400
FMI	59.5%	7%	30%	-	3.5%	-	-	350:1400
F1	54.5%	7%	30%	-	3.5%	5%	-	350:1400
F2	48.5%	13%	30%	-	3.5%	5%	-	350:1400
F3	74.5%	7%	10%	-	3.5%	5%	-	350:1400
F4	54.5%	7%	-	30%	3.5%	5%	-	350:1400
F5	74.5%	7%	-	10%	3.5%	5%	-	350:1400
F6	54.5%	7%	30%	-	3.5%	5%	-	350:350
F7	65.1%	16.4%	-	10%	3.5%	5%	-	350:1400
F8	62.5%	13%	-	10%	3.5%	11%	-	350:1400
F10	54.5%	7%	30%	-	3.5%	-	5%	350:1400

DSPE-PEG: 1,2-distearoyl-sn-glycero-3-phosphoethanolamine-N-[methoxy(polyethylene glycol)]; **Tir**: Tirzepatide; **DOTAP**: 1,2-dioleoyl-3-trimethylammonium-propane; **DOTMA:** 1,2-dioleoyl-3-trimethylammonium methane; **FRR**: Flow Rate Ratio

Flow-rate ratios (aqueous:organic) and total flow rates were optimized empirically to promote rapid solvent exchange while minimizing chip fouling and clogging. Freshly formed LNP dispersions were collected into a beaker under magnetic stirring (300 rpm) (IKA-Werke magnetic stirrer, Staufen, Germany) at room temperature (RT) to permit EtOH evaporation.

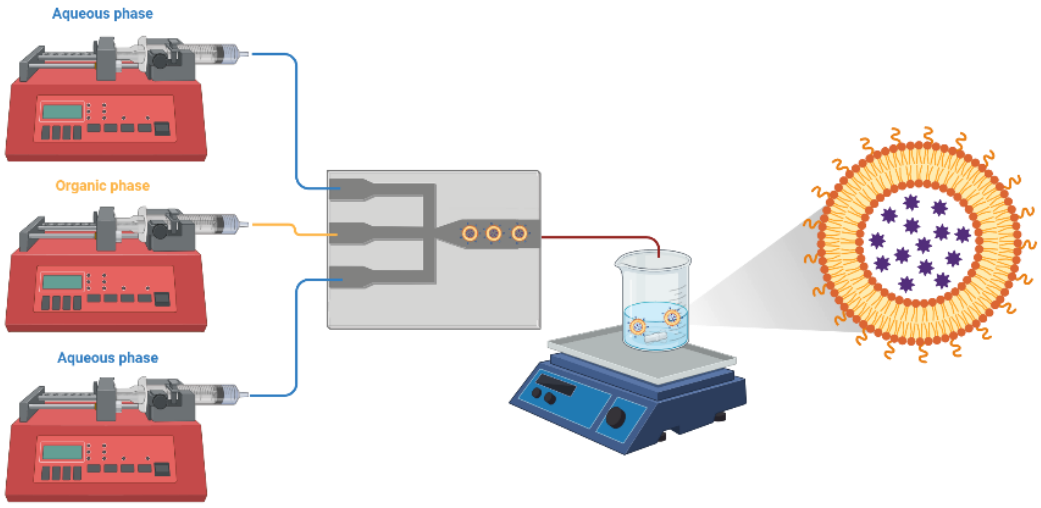


Figure 4. Representative scheme of the microfluidic production method for lipid-based nanoparticles (LNPs) formulation. Created in BioRender.

3.2.3. Vortex-mixing method

In the vortex-mixing method (**Figure 5**), for each batch, 13 mL of 1× PBS (aqueous phase, pH 7.4) was stirred at 300 rpm using a magnetic stirrer in a glass beaker. Formulations were prepared on a 30 mg total mass basis, with the same composition of lecithin, cholesterol, DSPE-PEG_{10K} and Tir, but varied DOTMA, DOTAP tested (**Table 4**). The organic phase (lipids and Tir dissolved in EtOH) was added dropwise at the aqueous surface using a 1 mL pipette to promote controlled solvent mixing and to favor spontaneous lipid self-assembly. After complete addition, the resulting dispersion was left to evaporate at RT for 3 h under continuous stirring to remove the organic solvent and to stabilize the suspension. Afterwards, the crude dispersion was concentrated as described previously in **section 3.2.2**.

Table 4. Formulations tested in vortex-mixing method.

Formulation Code	Lecithin (w/w %)	Cholesterol (w/w %)	DSPE-PEG_{10k} (w/w %)	Tir (w/w %)	DOTAP (w/w %)	DOTMA (w/w %)
F9	54.5%	7%	30%	3.5%	5%	-
F11	54.5%	7%	30%	3.5%	-	5%
F12	54.5%	7%	30%	3.5%	9%	-

DSPE-PEG: 1,2-distearoyl-sn-glycero-3-phosphoethanolamine-N-[methoxy(polyethylene glycol)]; **Tir**: Tirzepatide; **DOTAP**: 1,2-dioleoyl-3-trimethylammonium-propane; **DOTMA:** 1,2-dioleoyl-3-trimethylammonium methane

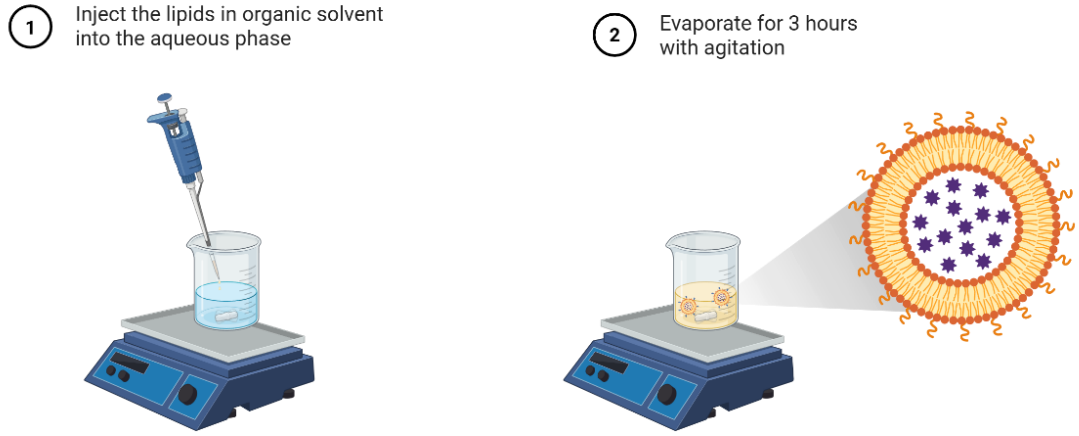


Figure 5. Representative scheme of the vortex-mixing production method for lipid-based nanoparticles (LNP) formulation. Created in BioRender.

3.2.4. Thin-film hydration followed by sonication method

This thin-film hydration alternative replaces extrusion with probe sonication (**Figure 6**), as extrusion proved to be very time-consuming and inefficient. In this method, each lipid was dissolved in 1 mL chloroform. Formulations were prepared on a 30 mg total mass basis, with the same compositions of lecithin, cholesterol, DSPE-PEG_{2K}, but varied DOTMA and DOTAP, and Tir tested (**Table 5**). Lipids were combined, solvent removed as above (**section 3.2.1**), and the dry film hydrated with 2 mL PBS containing Tir. The dispersion was sonicated in an ultrasonic water bath (30 min) and then probe-sonicated (70% amplitude, 3 min continuous) with the vial immersed in an ice bath to control temperature. The resulting suspension was concentrated by Amicon® centrifugal filtration to 1 mL, as described above in **section 3.2.2**.

Table 5. Formulations tested in thin-film hydration followed by extrusion method.

Formulation Code	Lecithin (w/w %)	Cholesterol (w/w %)	DSPE-PEG_{2k} (w/w %)	Tir (w/w %)	DOTAP (w/w %)	DOTMA (w/w %)
BLNP	65.1%	16.4%	10%	-	5%	-
Affi-BLNPs	65.1%	16.4%	10%	3.5%	5%	-
F17	65.1%	16.4%	10%	3.5%	-	5%

DSPE-PEG: 1,2-distearoyl-sn-glycero-3-phosphoethanolamine-N-[methoxy(polyethylene glycol)]; **Tir**: Tirzepatide; **DOTAP**: 1,2-dioleoyl-3-trimethylammonium-propane; **DOTMA:** 1,2-dioleoyl-3-trimethylammonium methane

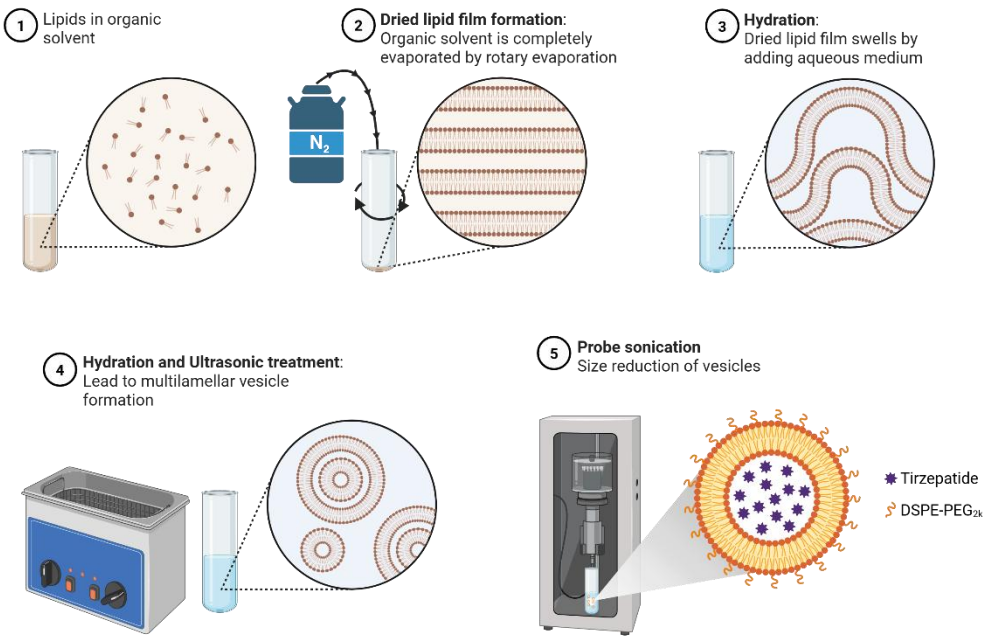


Figure 6. Representative scheme of the thin-film hydration followed by extrusion method for lipid nanoparticles (LNPs) production. Created in BioRender.

3.3. Physicochemical characterization of lipid-based nanoparticles

3.3.1. Average particle size, polydispersity index, and zeta potential

The LNPs hydrodynamic diameter (*Z*-average), polydispersity index (PdI) and zeta-potential (ζ-potential) were measured using a Malvern Zetasizer Nano ZS (Mal-Panalytical, Malvern, UK). Prior to analysis, each sample was diluted 1:50 in 10 mM KCl and measured in triplicate, with the sole exception of microfluidic formulations FMB, FMC, FMF, FMG, and FMH, which were diluted 1:50 in ultrapure water before measurement.

3.3.2. Transmission electron microscope analysis

The morphology of LNPs was assessed by transmission electron microscopy (TEM) analysis. Samples were diluted 1:50 in 1 mM acetate buffer and deposited on carbon-coated copper grids. After a short adsorption period, excess liquid was removed with filter paper, and the grids were negatively stained with uranyl acetate. The samples were imaged at appropriate magnifications to confirm the shape of LNPs.

3.3.3. Association efficiency and drug loading

The amount of Tir incorporated into LNPs was quantified by (a) reversed-phase high-performance liquid chromatography (RP-HPLC) or (b) fluorescence method,

taking advantage from peptide intrinsic fluorescence conferred by the presence of aromatic amino acid residues in its framework, including tyrosine (Tyr), phenylalanine (Phe) and tryptophan (Trp) residues[197-199].

Prior to quantification, several strategies for complete disruption and extraction of Tir from lipid matrices were evaluated. Methods tested included: (1) solubilization in dimethyl sulfoxide (DMSO), (2) solubilization in absolute EtOH, (3) mixed solvent extraction (DMSO:EtOH), and (4) lyophilization of the NPs suspension with subsequent reconstitution of the freeze-dried in either EtOH or DMSO. For lyophilization, samples were frozen at −80 °C for 24 h and subsequently subjected to vacuum freeze-drying. Each extraction procedure was followed by centrifugation (20,000 *g*, 10 min, RT) to remove insoluble lipid debris and the supernatant analyzed by RP-HPLC or sample fluorescence.

Regarding the quantification of Tir by RP-HPLC, it was achieved using an HPLC Thermo Vanquish system (ThermoFisher, Waltham, MA, USA). Control of the equipment, as well as data acquisition and processing were carried out with the Chromeleon chromatography data system software (v. 7.3.2.). A reversed phase Synergi C12 column (Synergi 4 µm MAX-RP 80 Å, 250 × 4.6 mm) was used as the stationary phase, while the mobile phase consisted of (A) 0.1% (*v/v*) trifluoroacetic acid (TFA) in water and (B) pure acetonitrile, run in the following gradient: 0 min, 60% A / 40%; 0-13 min, 40% A / 60% B; 13–14 min, 20% A / 80% B; 14–15, 60% A / 40% B; 15–25, 60% A / 40% B. Chromatographic separation was performed at a flow rate of 1 mL/min**.** Detection of Tir was performed by ultraviolet absorbance at 280 nm and the injection volume was 20 µL. Under these chromatographic conditions the retention time of Tir was around 8 min. Standard curves were prepared by serial dilution of Tir standards ranging from 2.5 to 100 µg/mL, and included in each run. All samples were analyzed in triplicate, and a procedural blank (mobile phase or the solvent used for the solubilization of the NPs) were run alongside unknowns to ensure chromatographic stability and method reproducibility.

Another method of quantification of Tir relied on intrinsic peptide fluorescence because of its aromatic residues (Tyr, Phe and Trp residues)[197-199]. Measurements were performed on a BioTek Synergy Mx microplate reader (BioTek Instruments Inc., Vermont, USA) using black 96-well plates with black bottoms. Aliquots were read at an excitation wavelength (λex) of 295 nm and an emission wavelength (λem) of 350 nm. A calibration curve of Tir in DMSO was prepared in the range 2.5–100 µg/mL. All samples and standards were assayed in triplicate and blank-corrected prior to calculation.

Association efficiency (AE) and drug loading (DL) were determined by both direct and indirect methods. Direct method of AE was calculated as the ratio between the amount of peptide loaded into the NPs and the total amount of

peptide used to produce the formulations (Eq. 1), while direct DL was calculated as the ratio between the amount of peptide loaded into the NPs and the total mass of NPs (lipids and encapsulated peptide) used to produce the formulation (Eq. 2). Indirect method of AE and DL were determined from the amount of free (unencapsulated) Tir recovered in the supernatant after LNPs concentration in Amicon® tubes and calculated as shown in Eq. 3 and Eq. 4, respectively:

(1) $$Direct\ AE(\%) = \frac{\text{Amount of Tir loaded to LNPs}}{\text{Total amount of Tir used}} \times 100$$

(2) $$Direct\ DL(\%) = \frac{\text{Amount of Tir loaded to LNPs}}{\text{Total mass of LNPs + Tir}} \times 100$$

(3) $$Indirect\ AE(\%) = \frac{\text{Total amount of Tir loaded to LNPs} - \text{Free Tir in supernatant}}{\text{Total amount of Tir used}} \times 100$$

(4) $$Indirect\ DL(\%) = \frac{\text{Total amount of Tir loaded to LNPs} - \text{Free Tir in supernatant}}{\text{Total mass of LNPs + Tir}} \times 100$$

3.4. Determination of the Isoelectric Point and solubility of tirzepatide

3.4.1. Determination of the isoelectric point of tirzepatide

To determine the pH at which Tir carries no net surface charge (isoelectric point, pI), a pH-titration experiment was performed through ζ-potential measurements using the Malvern Zetasizer Nano ZS (Malvern Panalytical, Malvern, UK). A 0.2 mg/mL Tir solution in ultrapure water was acidified to pH 2 with 1.0 M HCl and titrated in 0.5 pH-unit steps up to pH 11 using 0.2 M NaOH. At each pH point the solution was equilibrated and the ζ-potential was measured. The pI was taken as the pH at which the ζ-potential crossed zero (interpolated from the ζ-potential versus pH curve).

3.4.2. Determination of the solubility of tirzepatide

To evaluate the solubility profile of Tir in different solvents, 2 mg of the drug was weighed in triplicate for each solvent condition and dissolved in 0.5 mL of solvent. The solvents tested were EtOH, DMSO, ultrapure water, PBS pH 7.4, and citrate buffer (pH 4.3). Samples were incubated at 37 °C under orbital agitation at 120 rpm for 15 minutes to promote dissolution. Following incubation, the suspensions were centrifuged to remove undissolved material, and the supernatants were collected, diluted as necessary, and analyzed by RP-HPLC to quantify Tir concentration, as previously described in **section** 3.3.3.

3.5. Functionalization of lipid-based nanoparticles with the affibody

3.5.1. Affibody conjugation strategy

Surface functionalization of LNPs with the Z_{FcRn_16} affibody was performed using Mal–thiol chemistry to promote directional, covalent attachment to the NPs surface. The protocol below was adapted from Azevedo *et al.*[200] with modifications to the reagent ratios and purification steps to fit the LNPs.

Briefly, LNPs containing DSPE-PEG_{2K}-Mal in their formulation were resuspended in PBS 1× pH 7.0 at a reaction volume of 1 mL. The thiolated affibody (Z_{FcRn_16}, C-terminal Cys) was reduced prior to conjugation using TCEP at a molar ratio TCEP:affibody of 2:1, followed by incubation for 1 h at RT and 400 rpm to expose the C-terminal thiol. The reduced affibody solution was added to LNPs suspension in a DSPE-PEG_{2K}-Mal:affibody molar ratio of 1:0.25. The mixture was incubated overnight at 4 °C under 400 rpm agitation to favor the covalent linkage of the thiol group from the free Cys of the affibody with the Mal ring displayed at the particle surface to further form a thioether bond. The functionalized particles were washed with the purpose of removing unreacted affibody and reducing agent by centrifugal ultrafiltration using Amicon® 100 kDa cut-off filters (centrifugation at 3,000 *g*, 60 min, 20 °C). The LNPs retained in the filter were resuspended in 1 mL of fresh PBS 1× (pH 7.0) and further physicochemical characterized as described in **section 3.3**. The washing solution was used to determine the conjugation efficiency (CE) of the affibody to the LNPs as described in **section 3.5.2**.

3.5.2. Conjugation efficiency

CE of the Z_{FcRn_16} affibody to LNPs was determined by an indirect approach (eq. 5), through the quantification of the unreacted affibody recovered in the combined filtrates and washes, and considering the total amount of the affibody used for the conjugation to the LNPs. The concentration of free, unreacted affibody was quantified using the fluorescamine assay, while the number of unconjugated Cys groups was confirmed with Ellman's assay.

(5) $$Indirect\ CE(\%) = \frac{\text{Total amount } Z_{FcRn_16} - \text{Amount free } Z_{FcRn_16}}{\text{Total amount } Z_{FcRn_16}} \times 100$$

Buffer and non-functionalized LNPs were included in every batch to validate the assays.

3.5.2.1. Fluorescamine assay

Fluorescamine is a non-fluorescent compound that reacts selectively with primary amines to form a highly fluorescent pyrrolone-type product, enabling the quantification of free primary amines and, by extension, the concentration of the

affibody in solution[201]. For this assay, a fresh fluorescamine solution (0.3 mg/mL in DMSO) was prepared. Then, 100 µL of each standard or sample (in triplicate) was added to a black 96-well plate, followed by 50 µL of the fluorescamine solution. The plate was incubated for 15 min at RT in the dark. Fluorescence was measured using a BioTek Synergy Mx plate reader BioTek Instruments Inc., Vermont, USA) with λex at 400 nm and λem at 460 nm, consistent with the spectral characteristics of the fluorescamine-amine adduct[201]. The calibration curve (2.5–100 µg/mL) was prepared using affibody standards dissolved in PBS (pH 7.0).

3.5.2.2. Ellman's assay

Ellman's assay is based on the stoichiometric reaction of DTNB with free thiol groups to form 2-nitro-5-thiobenzoic acid (TNB), a yellow-colored compound that directly correlates with the quantity of free thiol groups in solution after the functionalization of LNPs with the affibody[202]. This assay was performed in phosphate reaction buffer (0.1 M, pH 8.0) containing 1 mM EDTA. A DTNB stock solution was prepared by dissolving 4 mg in 1 mL of reaction buffer. For the assay, 50 µL of DTNB solution was added to 2.5 mL of reaction buffer, and then mixed with 250 µL of sample. The mixture was incubated for 15 min at RT, and its absorbance was read at 412 nm on a BioTek Synergy Mx BioTek Instruments Inc., Vermont, USA). A calibration curve was prepared with L-cysteine (2.5–100 µg/mL), and the affibody quantification was made based on a stoichiometry reaction of 1:1.

3.6. *In vitro* release study

The release of Tir from FMI and F1 (see **Table 3**) was assessed over 8 h to mimic gastric and early intestinal transit. Briefly, LNPs (1 mL, equivalent to an initial Tir mass of 664 µg for FMI and 158 µg for F1) were dispersed in 3 mL of acidic buffer (pH 1.2, gastric conditions) and incubated at 37 °C with orbital stirring (100 rpm) for 2 h. Subsequently, the LNPs were recovered from the gastric medium by high-speed centrifugation (20,000 *g*, 15 min, RT), and the pellet was resuspended in 4 mL of pre-warmed intestinal buffer (pH 6.8, duodenal conditions) to continue the release study for the remaining 6 h.

At predetermined time points (15, 30, 60, 120, 180, 240, 360, and 480 min), aliquots (200 µL) were withdrawn. The withdrawn volume was replaced with an equal volume of pre-warmed respective buffer to maintain a constant volume throughout the experiment. Each aliquot was processed to separate particulate material by centrifugation (21,000 *g*, 15 min, 20 °C), and the supernatant was collected and analyzed by RP-HPLC (as described in **section 3.3.3**) to quantify the amount of Tir released from the LNPs.

3.7. *In vitro* biological assays

3.7.1. Cell culture maintenance

Caco-2 (human colorectal adenocarcinoma cell line) and HT29-MTX (human colorectal adenocarcinoma cell line) cells were cultured separately in 75 cm^2 T-flasks in DMEM High Glucose supplemented with FBS (10% (*v/v*)), NEAA (1% (*v/v*)) and penicillin/streptomycin (1% (*v/v*)) - penicillin (100 U/mL) and streptomycin (100 µg/mL) - inside an incubator with a humidified atmosphere at 37 °C and 5% CO_2. The medium was changed 2-3 times per week. When confluence reached about 70% to 80%, cells were detached by treating with trypsin-EDTA at 37 °C and seeded in other 75 cm^2 T-flasks. HT29-MTX cells were utilized between passages 29 and 48, and Caco-2 cells between passages 78 and 93.

3.7.2. Metabolic activity assay

The metabolic activity of cells mimicking the enterocytes (Caco-2 cells) and mucus-producing goblet cells (HT29-MTX cells)[203-205] was assessed by resazurin assay, a fluorometric method that measures the metabolic capacity of viable cells through the mitochondrial reduction of non-fluorescent resazurin to fluorescent resorufin[206]. For the assay, cells were seeded in 96-well plates at 2.0×10^4 cells/well (Caco-2) or 1.0×10^4 cells/well (HT29-MTX) and allowed to adhere for 24 h. Afterwards, each well was washed once with PBS 1× at pH 7.4, followed by treatment with free Tir, empty non-functionalized LNPs (BLNPs), Tir-loaded LNPs (Tir-LNPs), affibody-functionalized empty LNPs (Aff-BLNPs), and affibody-functionalized Tir-LNPs (Aff-Tir-LNPs).All the samples were diluted into complete medium and applied at the concentrations of 0.2, 1, 5.04, 25.2 and 126 µg/mL, which corresponds to Tir concentration. Cells were incubated with the samples for 4 h and 24 h. Controls included untreated cells (positive control), cells treated with 1% (*v/v*) Triton X-100 (negative control), medium alone (background), and medium containing PBS 1× at a concentration equivalent to that carried over by the highest LNP formulation tested (126 µg/mL), to exclude PBS-related effects.

At each time-point, wells were washed once with 1× PBS (pH 7.4) and resazurin working solution (20% (*v/v*) resazurin diluted in DMEM complete medium) was added. Plates were incubated for 2 h at 37 °C in the dark, followed by transferring the samples to a black, transparent flat-bottom 96-well plate. Fluorescence was measured using a BioTek Synergy Mx microplate reader (BioTek Instruments Inc., Vermont, USA) with λex and λem of 530 nm and 590 nm, respectively. Each condition was assayed in 6 replicas.

The metabolic activity of each cell line was determined according to equation 6:

(6) $$\text{Metabolic Activity (\%)} = \frac{\text{Fluorescence Signal Sample} - \text{Fluorescence Signal Blank}}{\text{Fluorescence Signal Positive Control} - \text{Fluorescence Signal Blank}} \times 100$$

3.7.3. *In vitro* interaction studies

Interaction studies between intestinal cells and fluorescently FITC-labelled LNPs was quantified by flow cytometry in Caco-2 cells, a well-established *in vitro* model for studying nanoparticle cell interaction mechanisms in the intestinal epithelium[207]. Caco-2 cells was selected for this assay due to its closer resemblance with enterocytes and high expression of key transporters and receptors, including FcRn, which is critically involved in transcytosis mechanisms relevant to nanoparticle delivery systems (see **section 1.3.1.2**)[208,209].

Briefly, Caco-2 cells were seeded in 6-well plates at 5.0 × 10^5 cells/well and incubated for 24 h at 5% CO_2 and humidified atmosphere to reach the desired confluence prior to the assay. NPs were fluorescently labelled by substituting 1 mg of lecithin in the formulation for DSPE-PEG_{2K}-FITC. BLNPs and Aff-BLNPs were tested using three NPs concentrations: 100, 500, and 1000 µg/mL. Each condition was tested in triplicates. An untreated cell control was included to remove cellular autofluorescence. Samples were incubated with cells for 4 h at 37 °C in a humidified 5% CO_2 atmosphere. The 4 h exposure was selected to mimic the upper-intestinal residence time relevant to nanoparticle–epithelium interactions[210-212]. At the end of the incubation period, samples were discarded, and each well was washed twice with PBS 1× to remove loosely bound particles and debris. Cells were then detached using trypsin-EDTA, collected, and centrifuged at 1,200 rpm for 5–10 min at 4 °C. The pellet was resuspended in PBS 1×, filtered through a 100 µm nylon mesh to remove aggregates and clumps, and transferred to FACS tubes for acquisition. Flow cytometry analysis was performed on a BD Accuri™ C6 Plus (BD Biosciences, New Jersey, USA). Data acquisition collected a minimum of 20,000 events per sample. A sequential gating strategy was applied: (i) exclusion of debris and non-cellular events on SSC-A vs FSC-A (debris occupies the low FSC/low SSC region), (ii) singlet discrimination using FSC-H vs FSC-A to remove doublets and aggregates, and (iii) identification of the fluorescent-positive population, which translated to FITC-labelled LNPs detection in FL1 channel (λex: 488 nm, λem: 530 nm). The interaction of each sample with Caco-2 cells was expressed as the percentage of positive cells and the median fluorescence intensity (MFI) of the positive population. Raw flow-cytometry data were processed and analysed using the software FlowJo v10 (BD Biosciences, New Jersey, USA).

3.7.4. *In vitro* intestinal permeability assay

Permeability of free Tir, Tir-LNPs, and Aff-Tir-LNPs was evaluated using a 2D Transwell® co-culture model composed of Caco-2 and HT29-MTX cells (**Figure 7**). Co-cultures were prepared on Transwell® inserts (12-well plate, membrane surface area of 1.1 cm^2, and pore size of 1 µm) by seeding Caco-2 and HT29-MTX at a 9:1 ratio (9.9×10^4 Caco-2 cells and 1.1×10^4 HT29-MTX cells per insert), with the apical and basolateral compartments supplemented with 0.5 mL and 1.5 mL of medium, respectively. The model was cultivated for 21 days under standard culture conditions (37 °C, 5% CO_2, and humidified atmosphere), with DMEM medium renewal every 2–3 days.

Transepithelial electrical resistance (TEER) was monitored from day 7 onward (every 2–3 days) using the EVOM2 epithelial volt ohmmeter equipped with an STX2 electrode (World Precision Instruments, Inc., Sarasota, FL, USA) to track barrier formation and integrity. Measurements were initiated at day 7 as the initial culture week is dedicated to cell attachment and proliferation, with the functional barrier, characterized by mature tight junctions, only becoming established after approximately 7-10 days of culture, as it was validated previously[203,204,208].

On day 21, the medium was removed from the apical and basolateral compartments of the inserts, followed by washing twice both apical and basolateral sides with 1× PBS (pH 7.4). Then, the model was equilibrated with 0.5 mL and 1.5 mL of pre-warmed Hank's Balanced Salt Solution (HBSS) on the apical and basolateral compartments, respectively, for 30 min at 37 °C. Afterwards, HBSS was discarded from the apical side and replaced by 0.5 mL of free Tir, Tir-LNPs or Affi-Tir-LNPs at the peptide-equivalent concentration of 126 µg/mL in HBSS, while the 1.5 mL of HBSS from the basolateral side was not replaced. All plates were maintained at 37 °C with gentle orbital agitation (100 rpm). 200 µL aliquots from the basolateral side were collected at different time points: 15, 30, 60, 90, 120, 150, 180 and 240 min. At each time-point, the removed volume was replaced with an equal volume of pre-warmed HBSS. TEER was recorded immediately before sample addition and immediately prior to every sampling time-point. Collected basolateral aliquots were centrifuged at 20,000 *g* for 10 min to remove particulate material, and processed for Tir quantification by RP-HPLC, as described in **section 3.3.3**. At the end of the experiment, samples from the apical compartment were recovered and the Transwell® membranes were carefully excised, submerged in DMSO to solubilize any peptide associated with the filter, incubated for 2 h and centrifuged (14,000 rpm, 10 min). The resulting extracts were also analysed by RP-HPLC to account for peptide retained in the membrane.

Apparent permeability coefficients (P_{app}) would be calculated from the measured mass of Tir (m_{Tir}) that was detected in the basolateral side, the initial

total Tir concentration (Ci_{Tir}), the insert surface area (A_{insert}) and time of the experiment (t) (eq. 7):

(7) $$P_{app} = \frac{m_{Tir}}{Ci_{Tir} \times A_{insert} \times t} \times 100$$

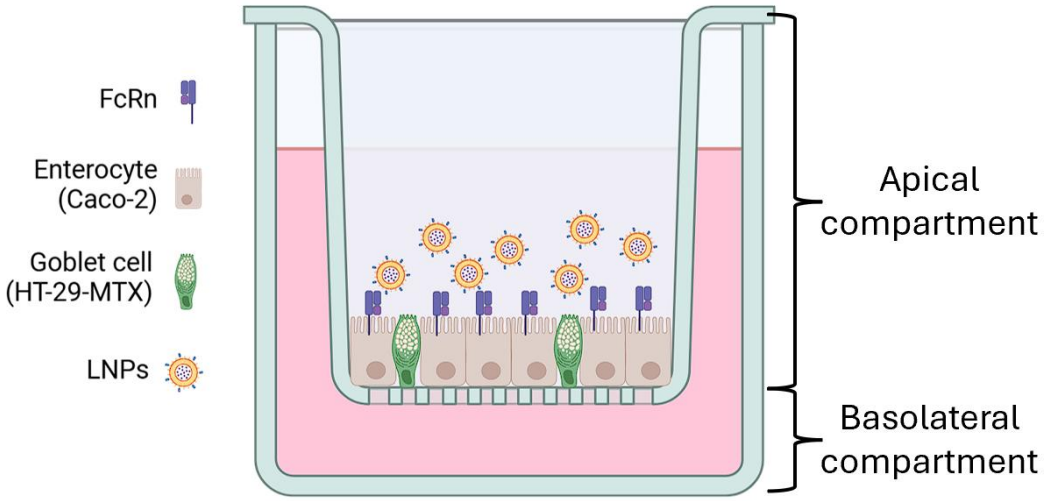


Figure 7. Representative scheme of the Transwell® co-culture setup (Caco-2/HT29-MTX) used for assessing LNP permeability. Created in BioRender.

3.8. Data analysis and statistics

Quantitative values are presented as mean ± standard deviation (SD) from at least three independent experiments (n ≥ 3) unless otherwise stated. Pairwise comparisons employed unpaired two-tailed Student's t-tests, while multi-group comparisons used one-way ANOVA. The levels of significance were considered for *p < 0.05, **p < 0.01, ***p < 0.001 and ****p < 0.0001. Data processing and graphs were produced with GraphPad Prism 9 Software (GraphPad Software Inc., San Diego, California). Exact *n*, tests and *p*-values are reported in **section 4** and in the legends of the figures.

4. Results and discussion

4.1. Production and physicochemical characterization of lipid-based nanoparticles

4.1.1 Thin-film hydration followed by extrusion method

Two LNP formulations (Table 2) were produced by thin-film hydration prior to size reduction by membrane extrusion as described in **section 3.2.1.** with a total lipid content of 10 mg.

The higher DSPE-PEG_{10k} content in the FA formulation, compared to F0, was intended to generate a denser PEG corona. This strategy aimed primarily to reduce opsonization and macrophage uptake[213,214], while simultaneously enhancing transport through the intestinal mucus[213,215] (see **section 1.4.4**).

FA formulations were subjected to repeated passages through a 200 nm polycarbonate membrane until reached 2.5 cycles (**Figure 8**). The production of LNPs by thin-film hydration followed by extrusion produced particles in the target size range for intestinal delivery, which should be below 200 nm to effectively navigate the mucus mesh (see **section 1.4.2**).

As shown in **Figure 8**, after five passes through a 200-nm membrane, F0 showed a Z-average of 117 nm with a PdI of 0.18 ± 0.02, while FA had a Z-average of 152 ± 1 nm and a PdI of 0.23 ± 0.00, indicating that both formulation had a homogeneous size distribution. PdI values ≤ 0.3 fall within commonly used acceptance thresholds for LNPs. However, PdI values ≤ 0.2 are more ideal for drug delivery applications (see **section 1.4.2**). Furthermore, the observation that most of the size reduction and homogenization occurred during the early extrusion cycles is consistent with previous studies on liposomal extrusion[216].

Although the LNPs produced by thin layer followed by extrusion method demonstrated a uniform size distribution, with an overall hydrodynamic diameter compatible for intestinal delivery, in practice, the extrusion workflow showed to be time-consuming and poorly scalable. This was proved when the total lipid content of the formulations increased to 25 mg. In this case, the process could take days to complete. According to these operational limitations and taking into consideration that comparable or suitable *Z*-average values were further achieved by microfluidic method with greater throughput and reproducibility[217,218], which was also reported in previous studies[219], thin-film hydration followed by extrusion was discontinued as a LNPs producing method.

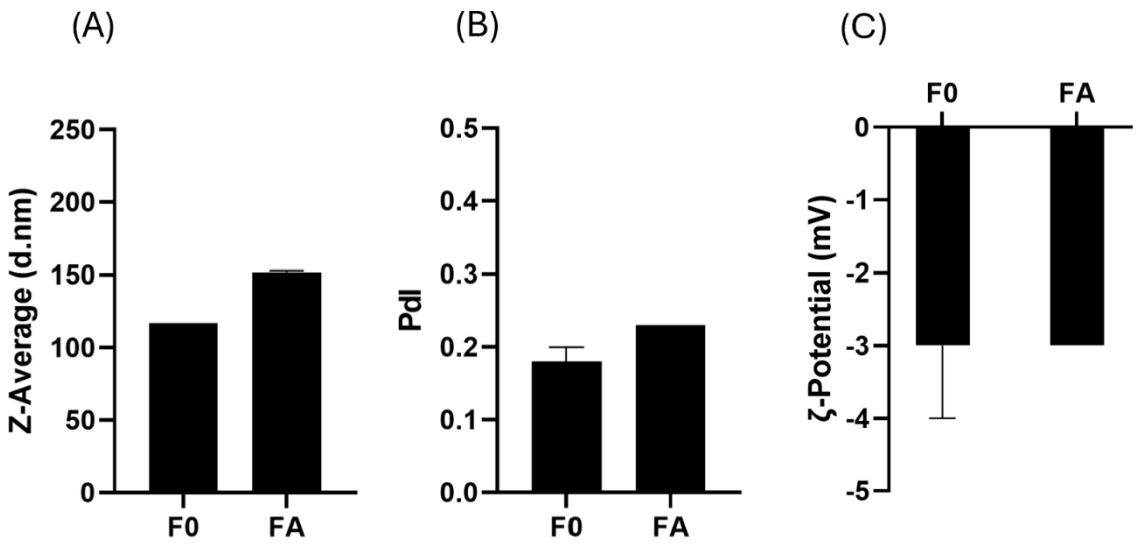


Figure 8. Size, PdI, and surface charge characterization of LNPs prepared by thin-film hydration followed by extrusion. (A) Z-Average (nm), (B) PdI, and (C) ζ-potential (mV). Data corresponds to formulations F0 and FA after 2.5 extrusion cycles through a 200 nm membrane. Full compositions and process parameters are provided in **Table 2** of **section 3.2.1**. Measurements were performed in 10 mM KCl; Data are shown as mean ± SD and three technical replicates were performed per condition (n = 1).

Nevertheless, extrusion remains a reliable technique for generating PEGylated LNPs with the target physicochemical profile at bench scale and is useful for small-batch confirmation studies. When higher throughput is required, options such as automated high-pressure extruders or alternative size-reduction steps (for example – controlled sonication) should be considered.

4.1.2 Microfluidics method

Microfluidic method was another technique tested to produce LNPs since it combines reproducibility, precise control over process variables, and scalability[217,218]. Additionally, microfluidic method has also been reported to improve encapsulation efficiency for some cargos compared with conventional bulk methods, although improvements are cargo-dependent[218,220,221]. A systematic formulation screening was performed to identify optimal lipid ratios, PEG molecular weights, and the potential benefit of cationic lipids for producing NPs with the desired physicochemical profile (Z-average < 200 nm, PdI ≤0.3 and neutral surface charge as supported in **section 1.4.2.**), while enabling efficient encapsulation of Tir.

The screening started from the base formulation FMB, and progressed through a series of variants designed to probe PEG fraction, PEG chain length, cholesterol content, and the inclusion of cationic lipids. Early formulations (FMC–FMH) explored different PEG fractions and flow-rate ratios (FRR), while FMI introduced Tir. A focused optimization series (F1–F8, F10) then systematically varied PEG molecular weight (DSPE-PEG_{10k} vs. DSPE-PEG_{2k}), cholesterol levels, and the

incorporation of cationic lipids (DOTAP or DOTMA). Process conditions tested several organic:aqueous FRRs (700:1400, 500:1400, 350:1400, and 350:350 µL/min) to identify parameters yielding optimal characteristics at target production masses (25 mg). Full compositions and process parameters are provided in **Table 3** of **section 3.2.2**.

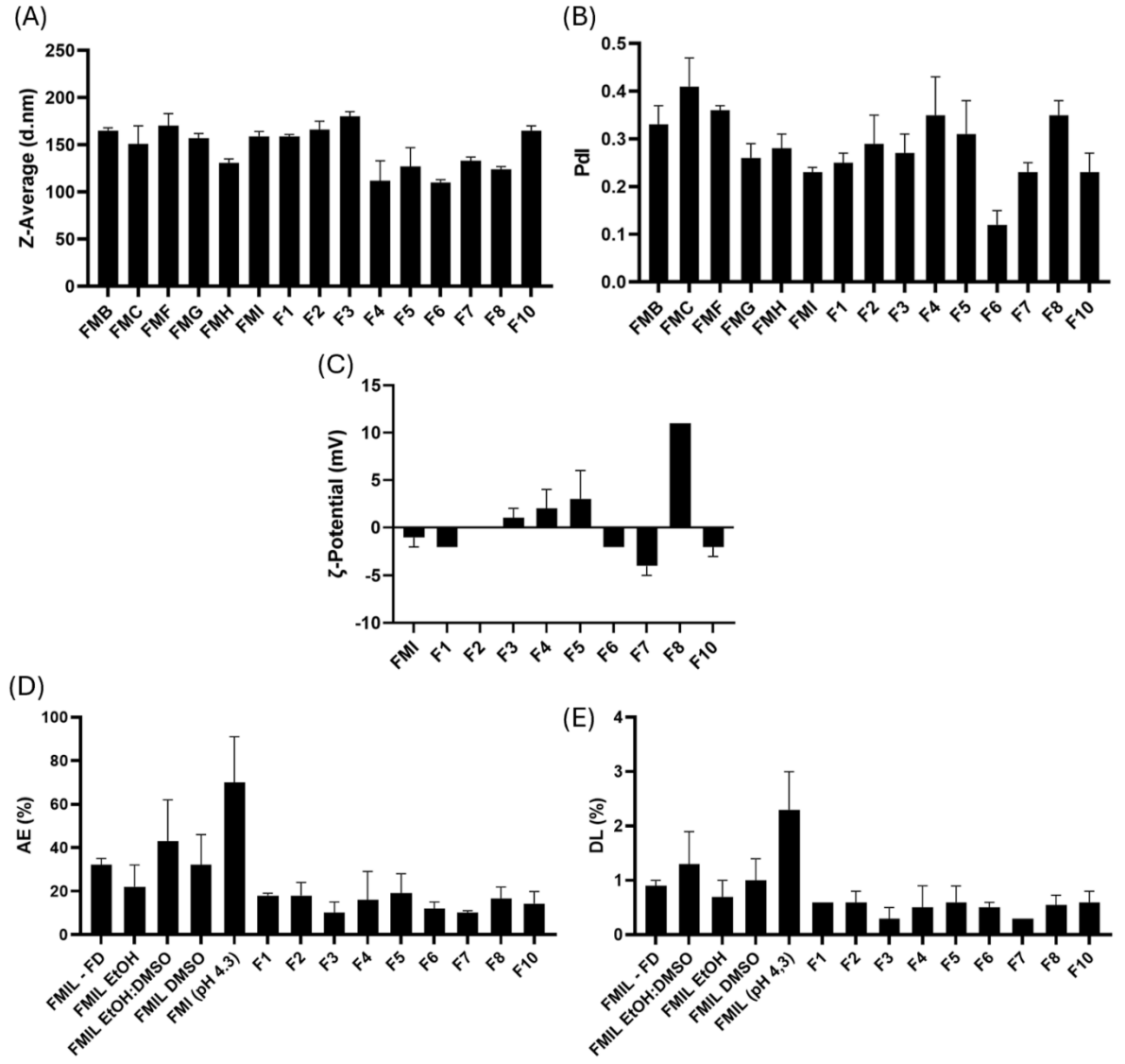


Figure 9. Physicochemical characterization of LNPs produced by microfluidics. (A) Z-Average (nm), (B) PdI, (C) ζ-potential (mV), (D) Directly measured AE (%), (E) Directly measured DL (%). Full compositions and process parameters are provided in **Table 3** of **section 3.2.2**). Data is shown as mean ± SD from three independent replicates (*n* = 3). An ANOVA one-way was applied to compare the samples FMIL – FD, FMIL EtOH, FMIL EtOH:DMSO and FMI DMSO in both panel D and E and did not find any statistical difference between the groups (*p-value* = 0.3321 in panel D and *p-value* = 0.3669 in panel E).

The ζ-potential values for FMB, FMC, FMF, FMG, and FMH were excluded from Figure 9C because their measurements were conducted in ultrapure water, a medium subsequently found to be unsuitable for this type of measurement as it lacks the necessary conductivity required to measure electrophoretic mobility accurately[222]. The poor conductivity of pure water leads to field distortion, an effect known as electrode polarization, resulting in unstable and artificially inflated readings. This phenomenon manifested as unexpectedly negative values (up to –20 mV) that do not reflect genuine changes in surface chemistry but are caused by the absence of ionic screening. Subsequent measurements of the other formulations in 10 mM KCl, a standard electrolyte solution used to prevent these issues, showed near-neutral ζ-potential. This aligns the expected behavior conferred by the PEG corona, which dominates the surface behavior by masking the charge, and demonstrates that the water-measured values were incorrect.

From a particle formation perspective, the most relevant observations when compared to the base formulation FMB were: (1) Reducing the flow rate ratio (FRR) to 1:1 (F6, 350:350 µL/min) reduced size and homogeneity, producing smaller particles (110 nm, **Figure 9A**) with a PdI closer to 0.10 (**Figure 9B**). (2) Decreasing the PEG-lipid fraction from 30% (w/w %) to 10% (w/w %) did not greatly affect LNP size. This was consistent for both DSPE-PEG_{10k} (F1 vs F3, ~160-170 nm) and DSPE-PEG_{2k} (F4 vs F5, ~130-140 nm) formulations. (3) However, at a constant 30% weight fraction, switching from DSPE-PEG_{10k} (F1, ~160 nm) to DSPE-PEG_{2k} (F4, ~120 nm) slightly reduced the particle size, which was expected considering that the shorter polymer chain provides a thinner steric barrier on the LNP surface. (4) Additionally, the incorporation of cationic lipids (DOTAP or DOTMA)[223] did not drastically alter the ζ-potential. Only a slight shift from neutral (FMI) to moderately positive values (≈+10 mV) was observed for formulation F8, which contained the highest fraction of DOTAP (11%) (**Figure 9C**). This again suggests that the PEG corona effectively masks surface charge, and only a high fraction of cationic lipid can partially counteract this shielding effect to display a minimal positive charge. Additionally, the LNPs produced by microfluidic method were spherical and indeed had a similar size between them coherent with PdI, as confirmed by TEM analysis of FMI (**Figure 10**).

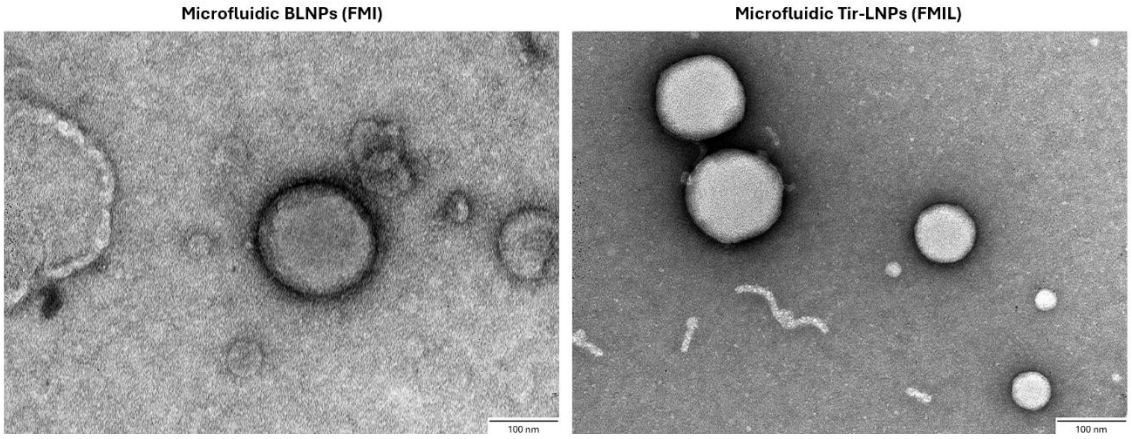


Figure 10. Transmission electron microscopy (TEM) images of LNPs produced by microfluidic technique. TEM images show LNPs with a spherical shape for empty FMI LNPs and loaded FMI (FMIL) LNPs. Full compositions and process parameters are provided in **Table 3** of **section 3.2.2**. Scale bars represent 100 nm.

The incorporation of the antidiabetic peptide Tir into LNPs demonstrated to be the major hurdle throughout the project. Since the FMI formulation was established before many others formulations tried, specifically the F1-F8 and F10 series, and as it presented acceptable Z-average, PdI and ζ-Potential values, it was used as the first formulation where it was tried to encapsulate Tir. Although introducing the peptide into the FMI formulation (FMIL) did not modified its physicochemical properties (**Figure 9 and 10**), with Z-average, PdI, and ζ-potential values being equal or very similar to those of empty FMI (and thus also referred to as FMI in **Figure 9 A-C**), reaching significant drug loading was difficult. Loading experiments used FMI compositions with theoretical drug loads scaled to approach the lowest clinical dose (5 mg) per batch, showing a nanosystem saturation at 872 µg of Tir per 25 mg formulation (DL of 3.5% becoming the theoretical drug loading). To accurately measure the amount of Tir encapsulated, different methods were tried for FMI disruption in order to separate the peptide from the lipid matrix for quantification. Initial techniques, including dialysis and high-speed centrifugation at 40,000 *g* for 20 min at 4ºC, yielded undetectable AE and DL (not shown), suggesting either complete peptide release or that the method was too gentle to break apart the LNPs and liberate the drug. Alternative methods were then explored, including freeze-drying (FD) the entire suspension (FMIL-FD) and, direct solubilization of the LNPs using organic solvents, specifically 100% (*v/v*) EtOH (FMIL EtOH), a 1:1 EtOH:DMSO mixture (FMIL EtOH:DMSO), and 100% (*v/v*) DMSO (FMIL DMSO). A parallel solubilization assay confirmed that Tir exhibited higher solubility in DMSO (3.3 mg/mL) compared to EtOH (1.9 mg/mL) **(Table 6)**. The results from these direct organic solvent disruption methods, as shown in **Figure 9D** and **9E**, were consistent and provided the first reliable evidence of encapsulation. The directly measured AE for the FMI formulation was approximately 30%, corresponding to a DL of about 1%,

which was very similar to that obtained using the FD method. This was corroborated by the lack of statistically significant differences in AE or DL values between the different disruption methods (Figure 9).

Table 6. Solubility assessment of Tir in EtOH, DMSO, ultrapure water, PBS (pH 7.4) and citrate buffer (pH 4.3).

Solvent:	EtOH	DMSO	Ultrapure water	PBS (pH 7.4)	Citrate Buffer (pH = 4.3)
Tir solubility (mg/mL):	1.9	3.3	>4	>4	0.006

EtOH: Ethanol 100% (v/v); **Tir**: Tirzepatide; **DMSO**: Dimethyl sufoxide 100% (v/v); **PBS:** Phosphate-buffered saline.

Based on these findings, solubilization of the LNPs in 100% (*v/v*) DMSO was selected as the standard disruption method for subsequent formulations due to its high solubility for Tir, its ability to provide consistent results, and its rapid processing time (completed in less than one hour) compared to the FD process, which required approximately one day.

Although both direct and indirect measurements of AE and DL were made, the values were not congruent. Direct measurements yielded relatively low values (AE ≈ 30%, DL ≈ 1%), while indirect methods suggested significantly higher results (not shown). This discrepancy suggests potential drug loss during production (*e.g.,* adsorption to Amicon® filters) leading to overestimation by indirect methods. Therefore, direct measurement was determined to be the more reliable approach, and all reported AE and DL values in this study were obtained through direct disruption of the LNPs.

To increase the encapsulation of Tir into LNPs, two strategies were explored: (1) reduce peptide solubility in the aqueous phase; and/or (2) promote ionic pairing with charged lipids (such as the cationic lipid DOTAP). To perform the strategy (1), firstly, the Tir charge profile was determined, being positively charged at acidic pH (pH 2), neutral at its isoelectric point (pI = 4.3, where it precipitates) and negatively charged at physiological pH 7.4 (**Figure 11**). After determining the pI of Tir, the aqueous phase of the FMI was shifted from PBS (pH 7.4, FMIL DMSO) to citrate buffer (pH 4.3), which was translated in the development of LNPs with higher AE and DL for Tir (PBS: AE = 30% ± 1%, DL = 0.7% ± 0.0%; Citrate: AE ≈ 70 ± 21 %, DL ≈ 2.3 ± 0.7 %) (**Figure 9D and 9E**). The release assay was conducted for the FMI produced with citrate buffer (pH 4.3) as aqueous phase and for the F1, with the LNPs releasing around 100 % of Tir content within 15 min under gastric acidic conditions (**Figure 12**), which might be associated to surface adsorption or co-precipitation of Tir rather than bilayer or core entrapment. To understand what was happening, free Tir in citrate buffer was filtered through Amicon® tubes, revealing that the peptide

precipitated at pH 4.3 (its pI), causing most of it to be retained on the filter. This result indicated that the AE and DL had been grossly overestimated when using citrate buffer pH 4.3 as aqueous phase, as the peptide was being retained on the filtration membranes during the LNP concentration step. Hence, in citrate buffer the measured AE and DL reflected peptide precipitate co-located with the NPs retained in the Amicon filter®. In PBS the peptide remained soluble and passed through the Amicon® filter, providing reliable AE and DL values. Overall, PBS was the aqueous phase selected for subsequent formulations.

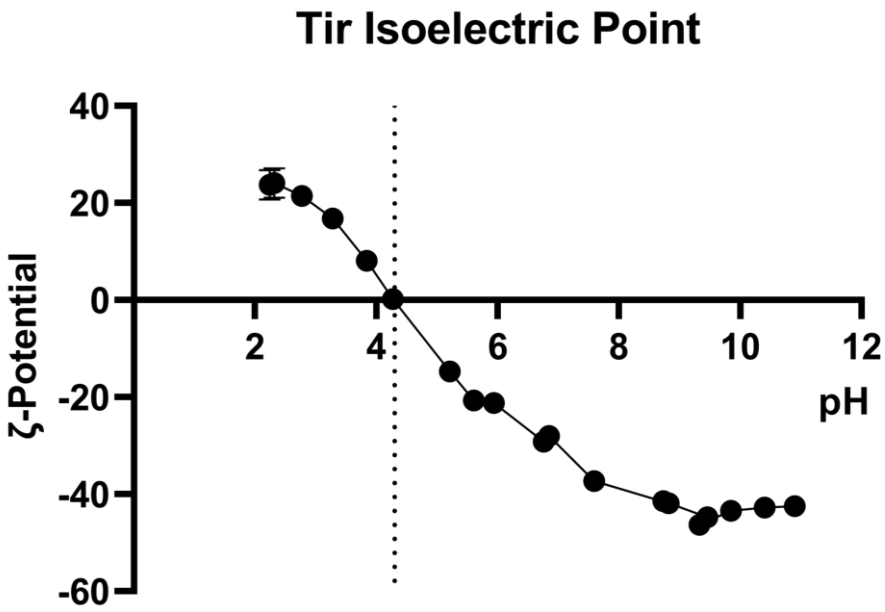


Figure 11. Tir isoelectric point (pI). The pI was determined by pH titration combined with assessment of peptide charge and solubility across pH 2–12. Tir demonstrated to be cationic at strongly acidic pH, electrically neutral at pH 4.3 (pI), and anionic at physiological pH (~7.4). Error bars denote mean ± SD.

The strategy (2) tested ionic pairing and bilayer modification by incorporating cationic lipids (DOTAP or DOTMA) or by pre-incubating the peptide with cationic lipid prior to microfluidic mixing. As shown in **Figure 9D** and **9E**, the incorporation of 5% (*w/w*) DOTAP (F1), 11% (*w/w*) DOTAP (F8), or 5% *(w/w*) DOTMA (F10) did not yield a significant or reproducible increase in AE or DL compared to the FMI. The AE remained below 20% and DL below 1.5% for all cationic formulations tested. Variations in other components, such as increased cholesterol (F2, F7) or the use of shorter PEG chains (F4, F5), effectively tuned size and PdI, but were likewise ineffective at promoting core entrapment of Tir (**Figure 9D and 9E**). Notably, formulation F6, which utilized a 1:1 FRR (350:350 µL/min), produced the smallest particles (≈115 nm) with the best homogeneity (PdI ≈ 0.10), but still failed to improve Tir loading.

The *in vitro* release shows the lack of true entrapment of Tir in the LNPs (**Figure 12**). The release profile shows that both FMI (without cationic lipid) and F1 (with 5% (*w/w*) DOTAP) exhibited a release kinetics virtually identical to that of free, unencapsulated Tir. In the gastric phase buffer (0-120 min), nearly 100% of the measured Tir content was released from the LNPs within the first 15 min. This rapid and complete release suggests that the peptide was not stably encapsulated within the LNPs core but was merely associated with the LNP surface, likely through weak adsorption. This superficial association is instantly disrupted upon exposure to acidic gastric buffer, leading to immediate peptide dissociation.

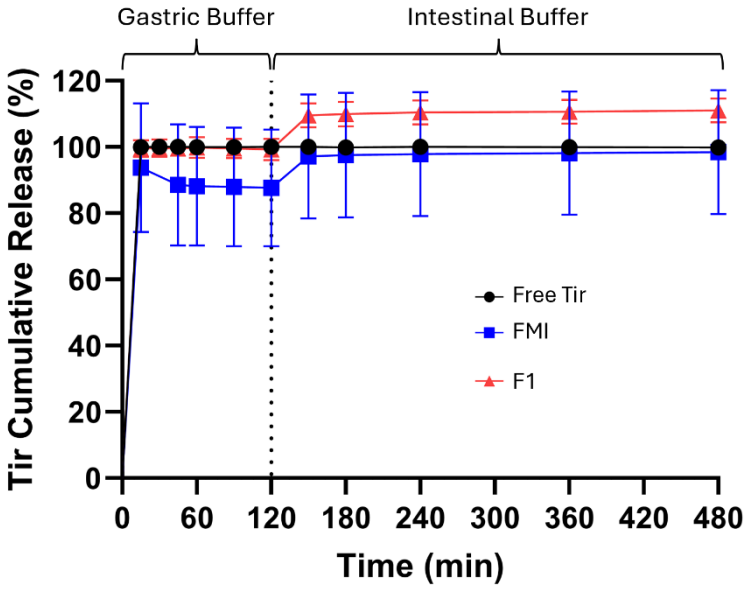


Figure 12. *In vitro* release profile of Tir from loaded LNPs. Mean percentage of Tir released over 480 min from formulation FMI (**blue squares**), formulation F1 (**red triangles**) and free Tir control (**black circles**). The experiment comprised an initial gastric phase conditions (pH 1.2) from 0 to 120 min followed by transfer into intestinal buffer (pH 6.8) at 120 min, indicated by the dashed vertical line. Full compositions and process parameters are provided in **Table 3** of **section 3.2.2**. Error bars denote mean ± SD.

Overall, microfluidics proved to be an outstanding method for producing monodisperse, PEGylated empty LNPs, and for the rapid screening of formulations. However, it was not possible to obtain stable LNPs with high Tir AE and DL. The principal reason was hypothesized to be the intrinsic amphiphilic behavior of the peptide, which confers a low tendency to partition into the lipid core when disposes of a higher volume of aqueous phase during microfluidic mixing. This was evidenced by a solubility assay, where Tir dissolved readily in both organic solvents such as EtOH (1.9 mg/mL) and DMSO (3.3 mg/mL), and in aqueous media such as water and PBS (>4 mg/mL) **(Table 6)**. These results confirm the amphiphilic character of Tir, while also indicating a preference for aqueous environments over the lipid phase

under formulation conditions. Consequently, during microfluidic assembly, Tir is more likely to remain in the external aqueous phase rather than partitioning into the lipid core, which explains the rapid release and low encapsulation obtained. To overcome this, future work should focus on formulation strategies that favor core internalization and entrapment, such as the use of ionizable lipids with a pKa tuned to transiently bind the peptide for subsequent release at physiological pH, lipids with deeper hydrophobic anchors, or polymer–lipid hybrid matrices[192,223-225]. Only by fundamentally altering the peptide–lipid interaction can the throughput and reproducibility advantages of the microfluidic method be fully exploited to produce a lipid-based nanosystem designed for oral Tir delivery.

4.1.3 Vortex-mixing method

Vortex-mixing is an alternative simple method to produce LNPs. For this method, the formulations tested were composed of lecithin, DSPE-PEG10K, cholesterol, DOTAP or DOTMA, and Tir. Full compositions of the formulations are described in **Table 4** of **section 3.2.3**. All these components were solubilized in EtOH before being added to the stirring PBS, promoting the self-assembly of the lipids into the LNPs. Formulations tested in this method all contained 30% (*w/w*) DSPE-PEG_{10K}, with varying proportions of DOTAP or DOTMA to yield the effect of cationic content.

This method constantly produced relatively monodisperse LNPs with a Z-average between 107 nm and 116 nm, and PdI values from 0.18 to 0.26, and with neutral surface charge (**Figure 13A-C**). However, the AE and DL values remained relatively low (AE < 20%, DL < 1%) (**Figure 13D-E**). Among the formulations, the highest AE and DL values were observed with F12, which contained 9% (w/v) DOTAP instead of 5% (w/v). This suggested a potential role for the increased cationic ratio in stabilizing peptide association via electrostatic interactions. However, without any statistical significance, neither significant improvements were made comparative with the previous techniques. The substitution of DOTAP with DOTMA (F11) did not confer measurable benefits.

In summary, vortex-mixing proved to be a simple, rapid, and accessible method for generating small, monodisperse, PEGylated LNPs, but it failed to overcome the challenge of achieving a high Tir entrapment. Although, higher DOTAP ratios improved AE and DL, the increases were insufficient for translational development. From a methodological standpoint, vortex-mixing remains valuable as a rapid exploratory tool at the bench scale. However, its high operator-dependence and poor encapsulation performance relative to other methods exclude it as a viable production strategy for oral Tir-LNPs.

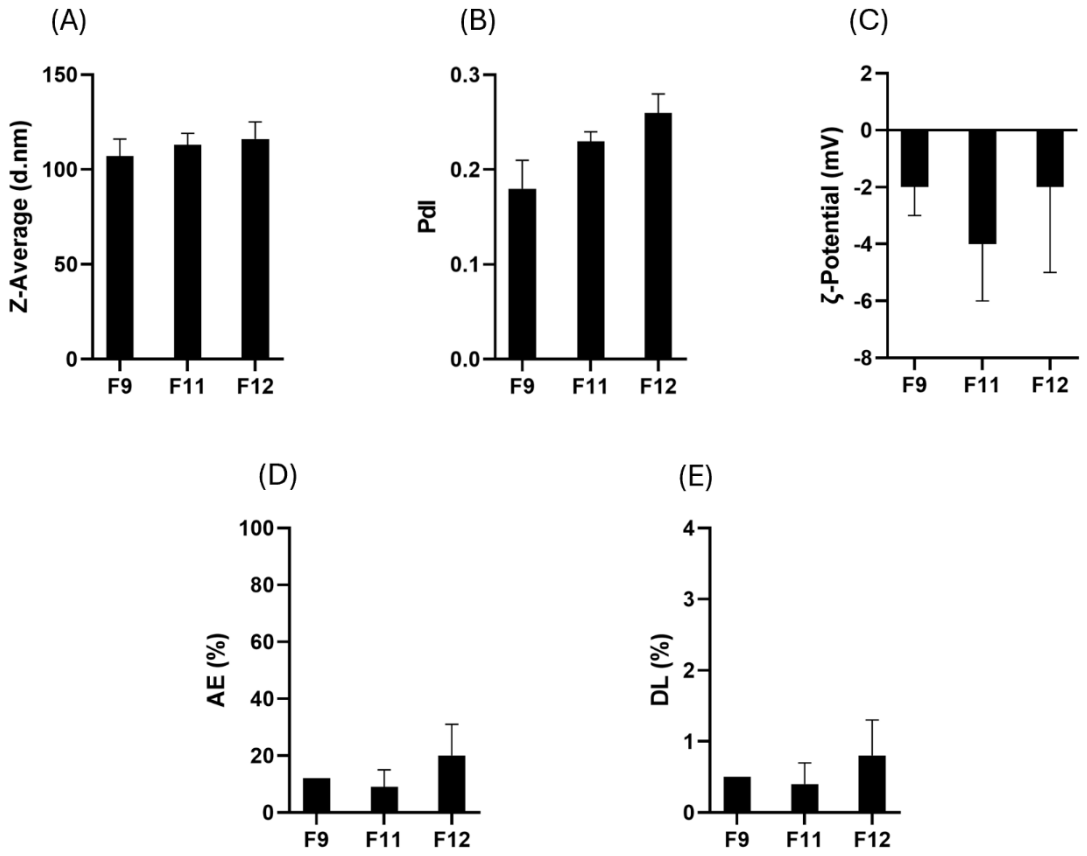


Figure 13. Physicochemical characterization of LNPs produced by vortex-mixing. (A) Z-Average (nm), (B) PdI, (C) ζ-potential (mV), (D) Directly measured AE (%) and (E) Directly measured DL (%) for different LNP microfluidic formulations. Full compositions and process parameters are provided in **Table 4** of **section 3.2.3**. Data is shown as mean ± SD from three independent replicates (*n* = 3).

4.1.4 Thin-film hydration followed by sonication method

The thin-film hydration followed by sonication method was the last method tested to overcome the insufficient AE and DL observed with the other production approaches. In this method, the lipid films were composed of lecithin, DSPE-PEG_{2K}, cholesterol, and a cationic lipid (either DOTAP or DOTMA) solubilized in chloroform, and Tir solubilized directly in the PBS that was used for hydration. The detailed lipidic composition and producing method can be found on **Table 5** of **section 3.2.4**. Since this method requires markedly lower aqueous volumes compared with microfluidic or vortex-mixing, it was hypothesized that the drug would have a higher probability of becoming entrapped within the lipid structures during self-assembly upon film hydration. However, to avoid the highly time-consuming extrusion step, which had previously limited scalability, film-hydrated suspensions were instead homogenized by probe sonication.

Both formulations produced NPs of similar hydrodynamic diameter (Tir-LNPs: 121 ± 10 nm; F17: 127 ± 6 nm) and ζ-potentials around −6 mV, and TEM confirmed predominantly spherical vesicles for BLNPs and Tir-LNPs (**Figure 15, Figure 14A** and **14C**). However, the suspensions were relatively polydisperse (PdI ≈ 0.31 - 0.35, **Figure 14B**) for both formulations, indicating heterogeneous size populations and inferior size homogenization relative to extrusion or microfluidic production. Notwithstanding this heterogeneity, thin-film hydration followed by sonication was the first method to yield meaningful peptide association: Tir-LNPs achieved AE ≈ 70% and DL ≈ 2.3%, and F17 achieved AE ≈ 65% and DL ≈ 2%, substantially higher than the values obtained by microfluidics or vortex-mixing. On balance, Tir-LNPs was selected as the formulation for downstream functionalization and *in-vitro* testing due to its superior payload.

In summary, thin-film hydration followed by sonication was the only method in this study that yielded LNPs with relevant AE and DL. A key limitation of this method was the suboptimal particle size distribution, yielding populations with a PdI ≈ 0.3-0.4). This heterogeneity may contribute to intra-batch variability, thus not ensuring the same performance for all the NPs produced[153,226] (see **section 1.4.2)**. Future work should therefore aim to optimize this promising platform by implementing more controlled size homogenization techniques, such as a more controlled probe-sonication[227], or even optimized extrusion procedure that is not so time costly to achieve monodispersity (PdI < 0.2) while preserving the high drug loading capacity.

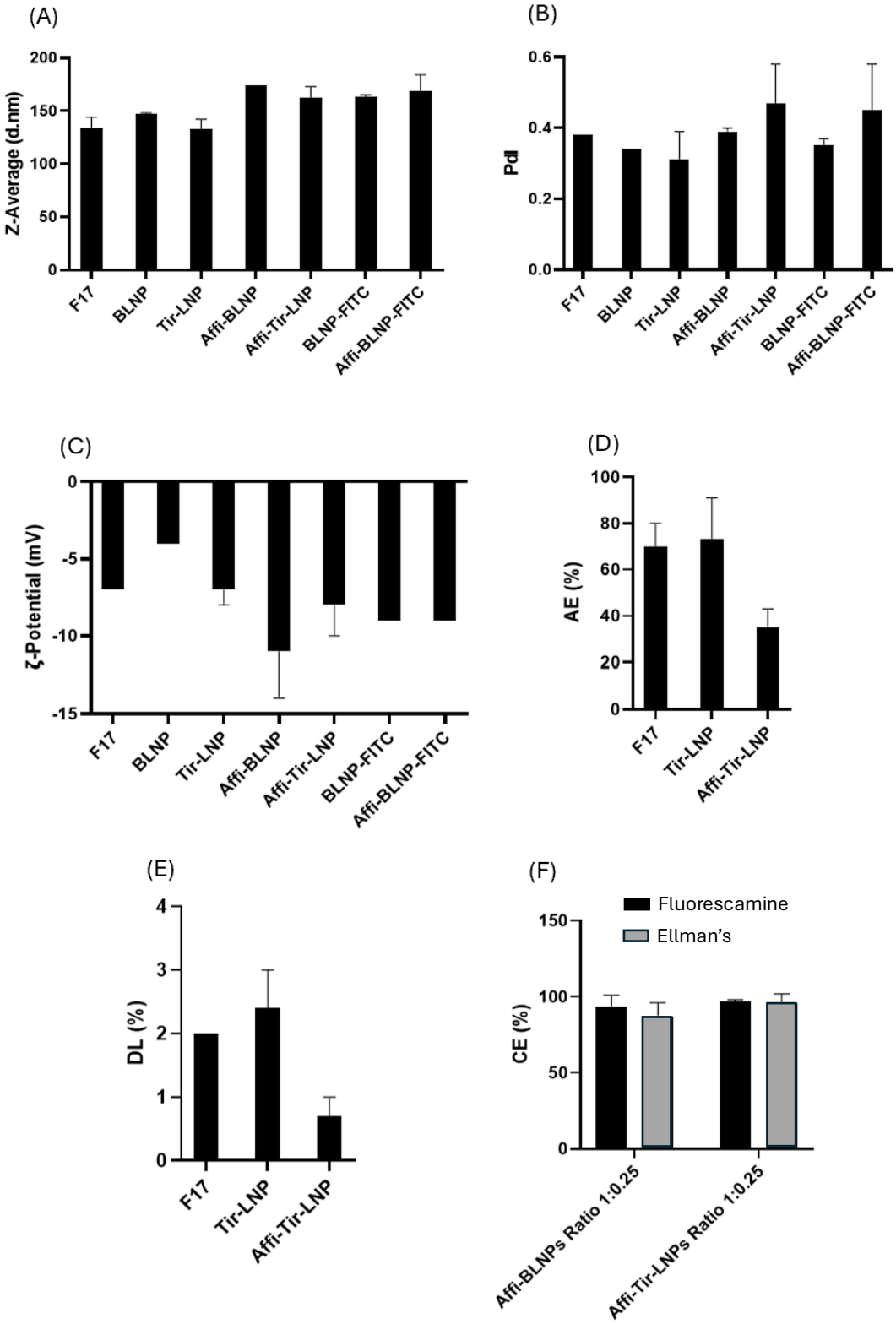


Figure 14. Physicochemical characterization of LNPs produced by thin-film hydration followed by sonication. (A) Z-average (nm), (B) PdI, (C) ζ-potential (mV, (D) Directly measured AE (%), (E) Directly measured DL (%) and (F) indirect CE (%) detected using both fluorescamine assay (black bars) and Ellman's assay (grey bars). (Data correspond to the formulations indicated on the x-axis (F17, BLNP, Tir-LNP, Affi-BLNP, Affi-Tir-LNP, BLNP-FITC, Affi-BLNP-FITC). Full compositions and process parameters are provided in **Table 4** of **section 3.2.4**. Data is shown as mean ± SD from three independent replicates (*n* = 3).

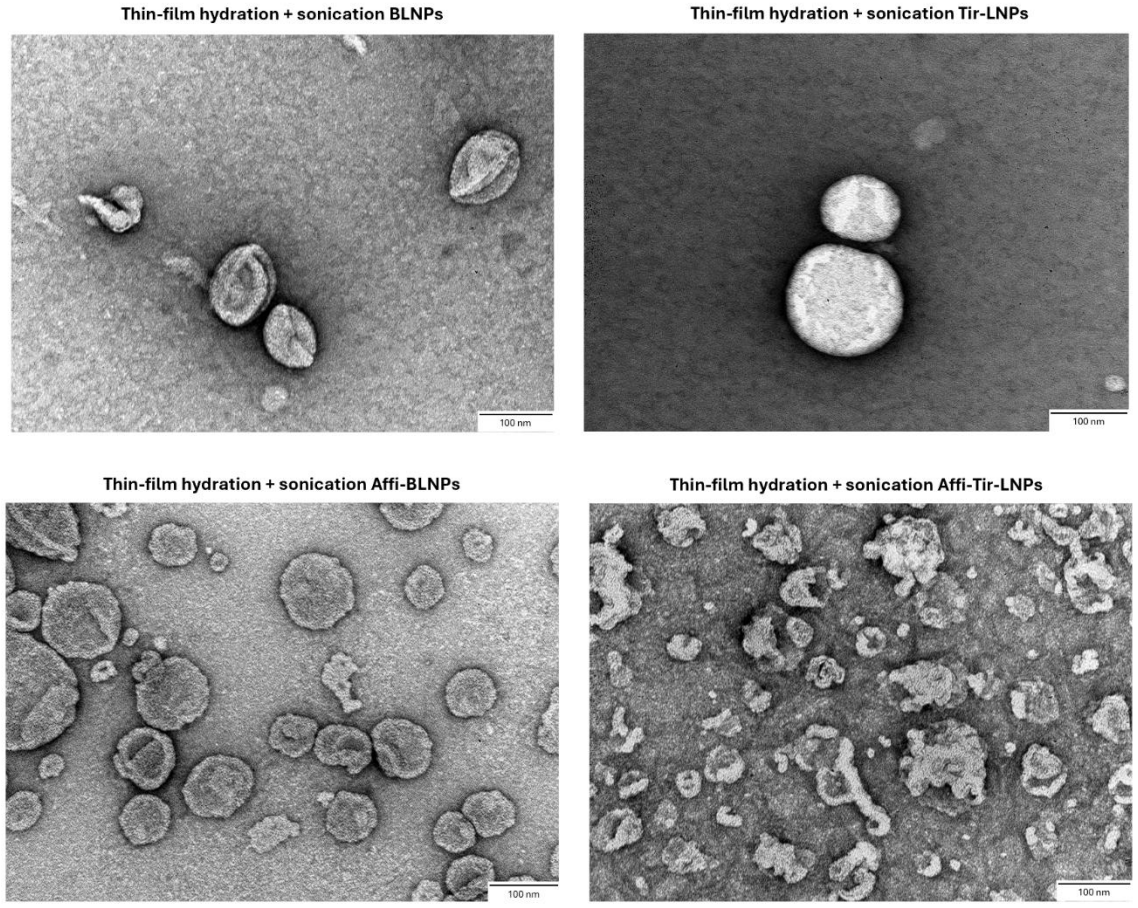


Figure 15. Transmission electron microscopy (TEM) images of thin-film hydration followed sonication and functionalized LNPs. The images show BLNPs, Tir-LNPs, Affi-BLNPs, and Affi-Tir-LNPs. Spherical morphology of the particles was preserved upon Tir loading, whereas functionalization with FcRn-targeting Affi induced surface roughness, most observed in Affi-Tir-LNPs, suggesting increased structural heterogeneity. Scale bars represent 100 nm.

4.2. Functionalization of lipid-based nanoparticles with FcRn-targeting affibody

The optimized formulation (Tir-LNPs, prepared by thin-film hydration with probe sonication) was functionalized with the FcRn-specific Affi Z_{FcRn_16}, which contains a C-terminal Cys residue. Site-directed conjugation was achieved *via* Mal–thiol chemistry using DSPE-PEG_{2K}-Mal pre-inserted into the LNPs bilayer during the manufacturing process. Briefly, the free thiol group of the Cys residue located on the C-terminal of the amino acid sequence of Z_{FcRn_16} was covalently linked to the Mal ring of the DSPE-PEG_{2K} -Mal. This strategy orients the Affi outward, preserving its FcRn-binding interface and conferring FcRn-specific conjugation to the LNPs to enable their uptake and transcytosis across the intestinal epithelium[98].

The determination of CE was performed by indirect method, using Ellman's reagent (to detect unreacted thiol groups) and fluorescamine assay (to detect free

primary amines). At a 1:0.25 ratio of LNPs:Affibody, CE values were at least 85%, showing coherence between assays: Affi-BLNPs exhibited 93 ± 8% CE (fluorescamine) and 87 ± 9% (Ellman's), while Affi-Tir-LNPs showed 97 ± 1% and 96 ± 6%, respectively (**Figure 14F**). According to these data, 1:0.25 ratio of LNPs: Z_{FcRn_16} was selected for further experiments based on its consistently high conjugation readouts, closer resemblance of the CE values between both methods of quantification (Fluorescamine and Ellman's methods), and due to the CE value of ~90% that corresponds to an affibody surface density of around 242 μM, which is higher than the nanomolar FcRn binding affinity (dissociation constant (K_d) of 72 nM)[98], ensuring receptor saturation while conserving reagent. The high and consistent coupling efficiencies confirm that the functionalization protocol was both efficient and robust.

The functionalization of LNPs with the Affi slightly increased the hydrodynamic diameter of the particles from 133 nm (Tir-LNPs) to 162 nm (Affi-Tir-LNPs), and PdI from 0.31 to 0.45, indicating a shift toward greater population heterogeneity following ligand insertion (**Figure 14A-B**). The ζ-potential remained got slightly negative (ζ-potential ~ -8 mV) (**Figure 14C**). This same pattern can also be seen for the BLNPs and Affi-BLNPs, although not so significantly, with Z-Average increasing from 150 nm to 160 nm; PdI from 0.37 to 0.39; ζ-Potential from -4 mV to -11 mV) (**Figure 14A-C**). Importantly, the association of Tir to the LNPs was reduced after functionalization, with AE decreasing from 70% (Tir-LNPs) to 35% (Aff-Tir-LNPs), and DL from 2.1% (Tir-LNPs) to 1.2% (Aff-Tir-LNPs) (**Figure 14D-E**), which can be associated to the release of the antidiabetic peptide during the two concentration steps performed during the manufacturing process: the first one to remove the unbound antidiabetic peptide to LNPs, and the second corresponding to the removal of the unbound affibody to LNPs. TEM imaging of Affi-BLNPs showed largely spherical particles with a "wrinkled" surface and increased particle–particle contacts versus non-functionalized LNPs, whereas Affi-Tir-LNPs displayed more pronounced clustering and partial loss of uniform spherical contrast, consistent with mild aggregation (**Figure 15**). These data indicate that the Mal–thiol coupling strategy that required additional purification steps might be introducing measurable compromise in payload retention and colloidal homogeneity.

Overall, the results highlight a recurring trade-off in ligand–nanoparticle engineering: high-affinity targeting was achieved at the cost of some loss of encapsulated drug and a modest compromise in colloidal homogeneity. Nevertheless, the ability to reproducibly obtain a CE higher than 85% demonstrated the robustness of the DSPE-PEG_{2K}-Mal coupling strategy and established a lipid-based nanosystem suitable for biological evaluation of FcRn-mediated transport.

4.3. *In vitro* biological assays

4.3.1. Effect of FcRn-targeted lipid-based nanoparticles in the metabolic activity of intestinal cells

The metabolic activity of enterocyte-mimicking cells (Caco-2 cells) and mucus-producing like goblet cells (HT29-MTX cells) when treated with different concentrations of LNPs and free Tir was assessed using a resazurin reduction assay. Both intestinal cell lines were treated with free Tir, BLNPs, Tir-LNPs, Affi-BLNPs and Affi-Tir-LNPs at Tir equivalent concentrations of 0.2, 1.0, 5.04, 25.2 and 126 µg/mL for 4 h and 24 h. The results showed that none of the treatments interfered with the cellular viability of Caco-2 and HT29-MTX cells, since in all the conditions at both 4 h and 24 h time-points, the metabolic activity levels were equal or higher than 70%[228], and no systematic, dose-dependent loss of viability was observed across the formulations (**Figure 16**). Consequently, the highest concentration tested (126 µg/mL peptide equivalent) was selected for subsequent in *vitro* permeability studies, as described in **section 4.3.3**.

According to the data, the overall safety profile of the tested LNPs and Tir was expected, as the literature indicates that LNPs are generally well-tolerated and biocompatible since they are mainly composed of naturally occurring lipids that do not typically trigger an immunological response[229-232], and GLP-1RA, such as semaglutide and liraglutide, commonly show good cell viability whenever applied in cell-culture studies[98,233-235].

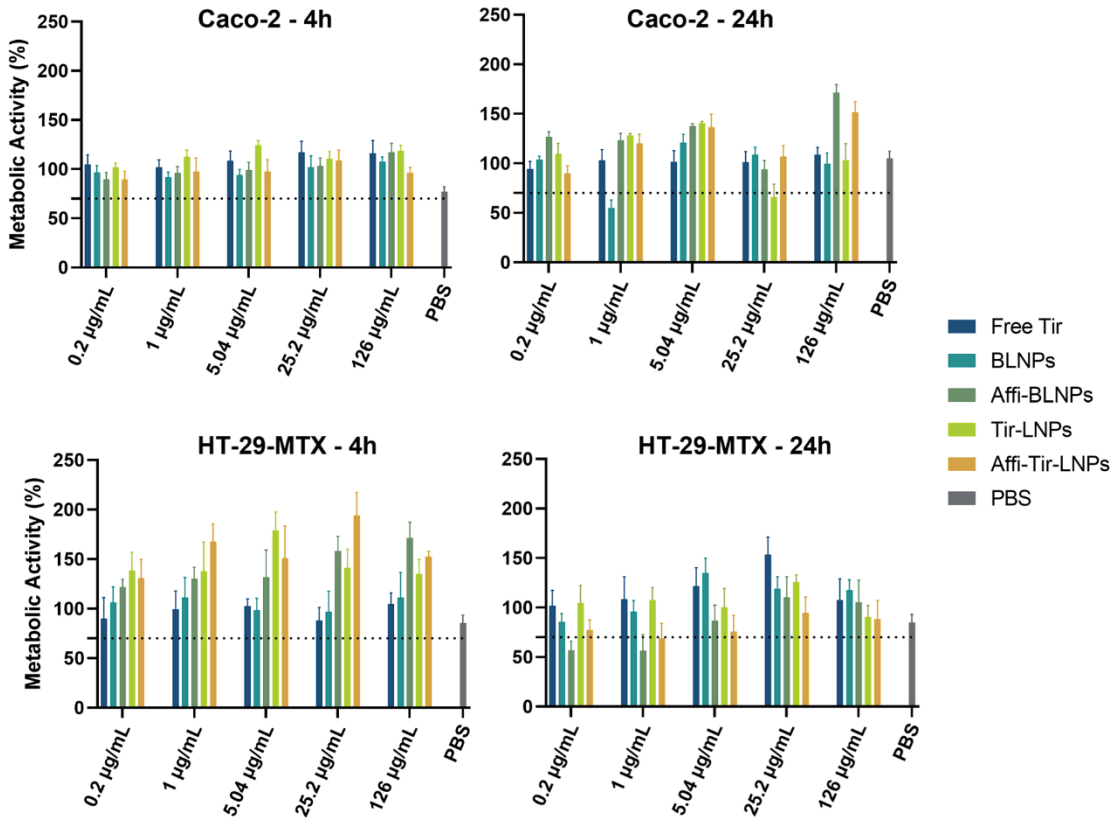


Figure 16. Metabolic activity of Caco-2 and HT29-MTX cells after incubation with LNPs and free Tir. The cellular metabolic activity of both intestinal cells was measured by resazurin, after 4 h and 24 h of exposure to: free tirzepatide (Free Tir), empty LNPs (BLNPs), affibody-functionalized empty LNPs (Affi-BLNPs), tirzepatide-loaded LNPs (Tir-LNPs), affibody-functionalized tirzepatide-loaded LNPs (Affi-Tir-LNPs), and PBS as a control group. LNPs samples were applied at peptide-equivalent concentrations of 0.2, 1.0, 5.04, 25.2 and 126 µg/mL. Fluorescence values were blank-corrected (medium without cells) and normalized to untreated control cells, which are set to 100% viability. Data are shown as mean ± SD and six technical replicates were performed per condition (n = 1). The dotted horizontal line marks 70% metabolic activity, the cytotoxicity threshold.

4.3.2. Interaction studies between the FcRn-targeted lipid-based nanoparticles and intestinal cells

The intestinal cellular interaction of LNPs with Caco-2 cells was quantitatively assessed by flow cytometry analysis, after 4 h of exposure to 100, 500, and 1000 µg/mL of BLNPs and Affi-BLNPs, both formulations fluorescently labelled with FITC. The Caco-2 cells was chosen for this interaction study since it is a well-established *in vitro* model for studying nanoparticle uptake mechanisms in the intestinal epithelium[207], and for its high expression of FcRn, which is critically involved in transcytosis mechanisms relevant to nanoparticle delivery systems, aligning with the purpose of this study[208,209].

The 4-h exposure window was selected to approximate the upper-intestinal residence time relevant to oral formulations and thus, ensure physiological relevance, as it mimic the upper-intestinal residence time relevant to nanoparticle–epithelium interactions [210-212]. Two complementary parameters were evaluated, namely the percentage of positive cells and MFI (**Figure 17A and 17B**).

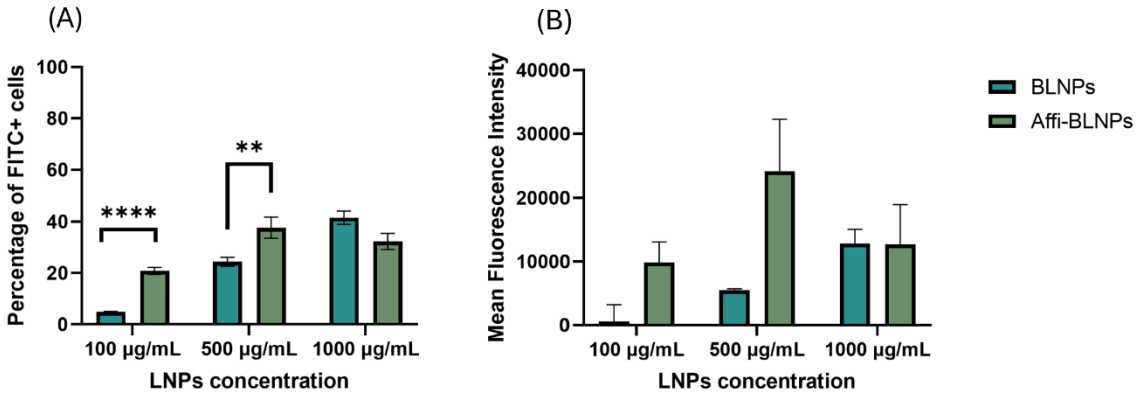


Figure 17. Intestinal cellular interaction of BLNPs and Affi-BLNPs in Caco-2 cells after 4 h incubation. Results are expressed as (A) percentage of FITC-positive cells and (B) mean fluorescence intensity (MFI) at 100–1000 µg/mL. T-test student revealed a statistically significant difference in the percentage of FITC-positive cells between BLNPs and Affi-BLNPs at 100 µg/mL ($p = 0.000038$) and 500 µg/mL ($p = 0.006720$). Data represent the mean ± SD of three technical replicates measurements (n = 1). Significance is denoted as *$p < 0.05$, **$p < 0.01$, ***$p < 0.001$ and ****$p < 0.0001$.

The data showed that the percentage of positive cells increased dose-dependently for BLNPs and Affi-BLNPs. It was observed that the lowest concentration of NPs tested (100 µg/mL) translated in a percentage of positive cells of 8.5- and 1.8-fold lower than the highest concentration studied (1000 µg/mL) of BLNPs (4.9% vs 41.5%) and Affi-BLNPs (20.9% vs 32.3%), respectively. At 100 µg/mL and 500 µg/mL, Affi-BLNPs interacted significantly more with cells, yielding 4.3- and 1.5-fold higher positive cell percentages than BLNPs, respectively (20.9% vs 4.9% for 100 µg/mL, and 37.7% vs. 24.4% for 500 µg/mL). This data suggested that probably the Affi-BLNPs were interacting with Caco-2 cells *via* hFcRn pathway. However, at the highest concentration tested (1000 µg/mL), BLNPs exceeded Affi-BLNPs (41.5% vs. 32.3%). These results suggest that the FcRn-targeting effect was most pronounced at low-to-intermediate doses. Notwithstanding, the percentage of positive cells treated with Affi-BLNPs was similar between the concentrations of 500 µg/mL and 1000 µg/mL, which may indicate receptor saturation at higher LNP concentrations. Under such conditions, nonspecific uptake pathways—such as macropinocytosis or adsorptive endocytosis—likely become dominant and may

mask the relative advantage of targeted particles[236,237], as appears to have occurred at 1000 µg/mL.

MFI results presented a large variability but provided further insight into per-cell uptake. At 100 µg/mL, Affi-BLNPs produced an MFI 16.8-fold higher than BLNPs, while at 500 µg/mL the difference was 4.4-fold. At 1000 µg/mL the two formulations were essentially equivalent, which could consolidate the hypothesis that at this concentration might be occurring the saturation of hFcRn receptor.

Taken together, the flow cytometry results provided evidence suggestive that the affibody Z_{FcRn_16} conjugated with LNPs enhanced the interaction of the particles with Caco-2 cells**,** particularly at low concentrations (100 µg/mL). However, the data did not constitute definitive proof of receptor-mediated internalization. It is important to note that flow cytometry cannot differentiate between interaction of NPs-cell membrane and internalization[238]. Thus, to confirm effective intracellular internalization, future work should include confocal microscopy, which enables observation of NPs localization on the cells. Notwithstanding, the interaction of Affi-BLNPs by Caco-2 cells *via* hFcRn pathway could also be proved by performing a competition assay by flow cytometry analysis, in which the cells are prior incubated with the affibody. Additionally, a flow cytometry analysis in a cell line knock-out for hFcRn receptors, such as HeLa cells (cervical adenocarcinoma cell line)[98], could also be considered to demonstrate the targeting-specificity of the particles.

4.3.3. *In vitro* permeability profile of FcRn-targeted lipid-based nanoparticles through an intestinal double-culture model

The intestinal permeability profile of Tir incorporated into Affi-BLNPs was assessed in a 2D Transwell® co-culture model, composed of Caco-2 and HT29-MTX in a cellular ratio of 9:1, thus accurately mimicking the physiological intestinal epithelial barrier[208,239,240]. The model was maintained in culture for 21 days and the TEER values were monitored to ensure the formation of the monolayer and barrier integrity. Free Tir, Tir-LNPs and Affi-Tir-LNPs (126 µg/mL Tir equivalent), previously diluted in HBSS at pH 6.5, were applied on the apical side of the insert, while the basolateral compartment contained HBSS at pH 7.4. The model was maintained in culture for 21 days and the TEER values were monitored to ensure the formation of the monolayer and barrier integrity. Free Tir, Tir-LNPs and Affi-Tir-LNPs (126 µg/mL Tir equivalent), previously diluted in HBSS at pH 6.5, were applied on the apical side of the insert, while the basolateral compartment contained HBSS at pH 7.4. This apical-to-basolateral pH gradient (apical pH 6.5 and basolateral pH 7.4) was built to exploit the pH-dependent binding mechanism of FcRn, a fundamental characteristic that governs its biological function in intestinal transcytosis (see **section 1.3.** This experimental setup should therefore enable the well-established

biochemical behavior of FcRn to effectively test its potential for enhancing oral delivery.

Throughout the 21 days of culture, the TEER values of the double-culture model increased steadily from ≈330 Ω·cm^2 at day 7 to a plateau around 630 Ω·cm^2 by day 21 (**Figure 18**). This progressive increase indicates the formation of a tight, functional epithelial monolayer, a critical characteristic for reliable permeability studies. The incorporation of HT29-MTX cells into the Caco-2 monolayer creates a co-culture that better resembles the human intestinal epithelium. The distinct protein expression profiles and intercellular interactions between these two cell types result in a monolayer with a tightness that is more physiologically relevant than a Caco-2 monoculture. TEER serves as a key quantitative measure of this epithelial integrity, reflecting the formation and strength of tight junctions.

The TEER values achieved in this work were higher than those reported by Araújo F. et al.[208], for the same 9:1 Caco-2:HT29-MTX model, which showed a steady increase from approximately 100 Ω·cm^2 to 200 Ω·cm^2 over 21 days. This discrepancy can likely be attributed to the use of a different Caco-2 clone passage, which might exhibit an different capacity in forming tighter monolayers, and variations in culture conditions[207]. Despite the difference in absolute values, the consistent upward trend and eventual plateau in TEER in both studies confirm the successful formation of a tight epithelial barrier.

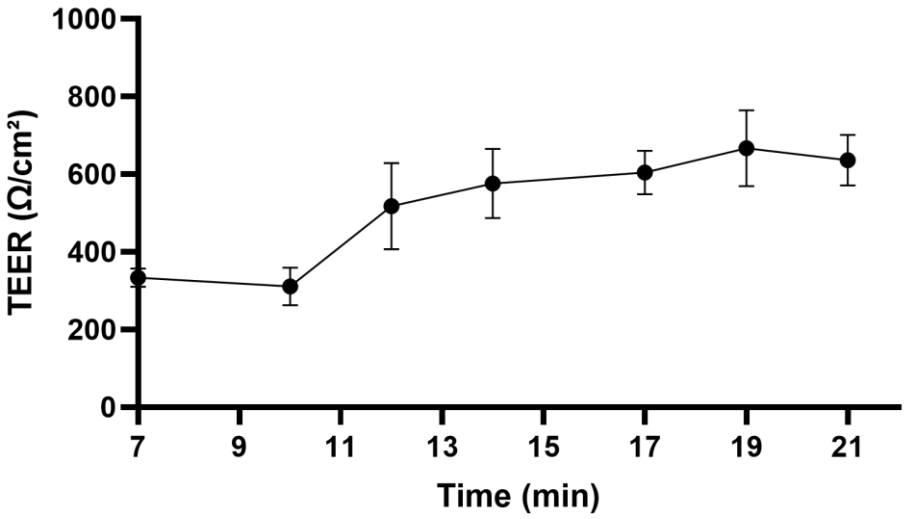


Figure 18. Transepithelial electrical resistance (TEER) of Caco-2:HT29-MTX (90:10) co-culture during 21 days. TEER values increased from 330 Ω·cm^2 at day 7 to 630 Ω/cm^2 at day 21. The TEER values are represented as mean ± SD. Twelve technical replicates were performed per condition (n = 1). Values represent the mean ± SD.

The permeability experiment was conducted on day 21 of culture, and the TEER values and aliquots of samples from the basolateral side of the insert was performed for over 4 h. Throughout the time of the assay, TEER values were practically maintained its integrity, ranging from 300 Ω·cm^2 to 200 Ω·cm^2 across all conditions (**Figure 19**).

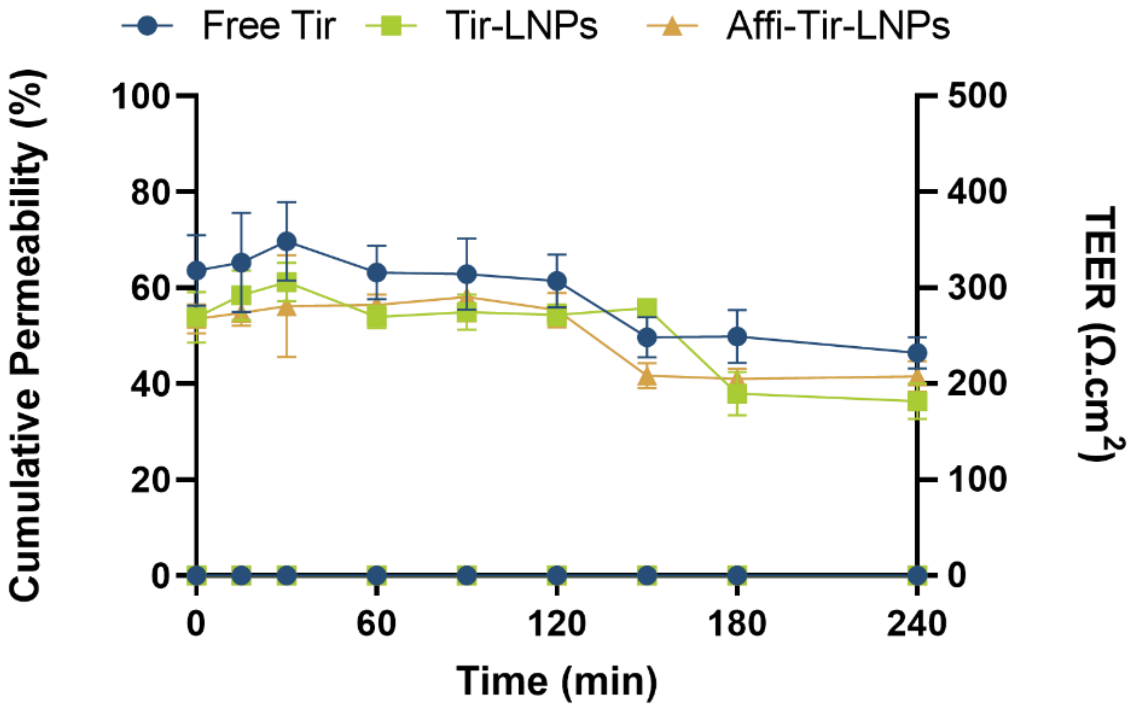


Figure 19. TEER values and permeability profile (% of the initial amount) of free Tir, Tir-LNPs, and Affi-Tir-LNPs through the Caco-2/HT29-MTX co- culture *in vitro* model. All results are represented as mean ± SD (n = 3)

Nonetheless, HPLC analysis of the basolateral samples collected up to 240 minutes revealed no detectable Tir for any of the tested free Tir, Tir-LNPs and Affi-Tir-LNPs conditions after 4 hours of incubation. This shows that neither the non-functionalized nor the FcRn-targeted LNPs improved the passage of Tir across the intestinal epithelial barrier compared with the free peptide.

The outcome of the permeability assay complements the uptake assay results, showing that although FcRn-targeted NPs displayed enhanced cellular interaction, this did not translate into measurable transepithelial transport under the conditions used. Some possible explanations for this observation are: (i) Tir may not have been sufficiently protected by the LNPs from apical degradation or from endo-lysosomal proteolysis, leading to loss of intact detectable peptide; (ii) LNPs may be routed predominantly into degradative compartments (late endosomes/lysosomes) rather than FcRn-mediated transcytosis pathways; (iii) LNPs were weakly associated with the peptide and released it too soon.

5. Conclusion

In conclusion, this dissertation developed and characterized LNPs to further improve the oral delivery of the antidiabetic peptide Tir. Among the various production techniques evaluated, thin-film hydration followed by probe sonication produced the LNPs with the highest peptide association (AE ~70%, DL ~2.3%) but also yielded polydisperse nanoparticles populations (PdI ≈ 0.31) with an Z-average of ≈ 130 nm and a neutral surface charge. The subsequent functionalization of these LNPs with the FcRn-targeting Z_{FcRn_16} affibody via Mal-thiol chemistry was highly efficient, achieving a CE of approximately 85%, which was demonstrated by performing both fluorescamine and Ellman's methods. However, this process increased particle size (≈160 nm) and heterogeneity (PdI ≈0.40), maintained a neural ζ-potential (≈−8 mV), and markedly reduced the Tir associated with the LNPs (AE ~35%, DL ~1.2%).

The biological assessment revealed a favorable safety profile, as all formulated LNPs and conditions tested did not interfere with the metabolic activity of intestinal epithelial (Caco-2) and mucus-producing (HT29-MTX) cell lines. Crucially, functionalization of LNPs with the affibody significantly enhanced the interaction of the targeted formulations with Caco-2 cells, as demonstrated by flow cytometry analysis, which showed a markedly higher percentage of positive cells and MFI for Affi-BLNPs than the non-functionalized counterparts, particularly at lower concentrations (4.3- and 1.5-fold higher at 100 µg/mL and 500 µg/mL, respectively). This suggests a probably targeted, receptor-mediated interaction, likely facilitated by the FcRn pathway. However, this enhanced cellular association did not translate into improved translocation across a physiologically relevant intestinal barrier model. The permeability studies using a Caco-2/HT29-MTX co-culture model demonstrated that the free peptide, non-functionalized Tir-LNPs and Affi-Tir-LNPs were not capable of permeating the intestinal epithelial model, and thus, neither non-functionalized nor FcRn-targeted LNPs produced were capable to enhance the transepithelial passage of Tir compared with the free peptide.

It is important to note that the *in vitro* release profile of the peptide, which indicated rapid Tir release in earlier microfluidic formulations, was not performed on the final Tir-LNPs produced by thin-film hydration followed by sonication that were used in the permeability assay. This represents a limitation of the current study, and therefore the release profile and stability of the encapsulated payload of the LNPs produced by thin-film hydration followed by sonication should be addressed in the future. Additionally, the lack of transcytosis, despite confirmed cellular interaction, also suggests that the FcRn-mediated pathway may not have been fully engaged for complete transcellular transport. Potential reasons could include insufficient protection of Tir within the LNPs, leading to premature release

or degradation in endocytic compartments before transcytosis could occur, or routing of the particles towards lysosomal degradation instead of the transcytosis pathway.

Overall, this work highlights both the progress and the challenges of developing FcRn-targeted nanocarriers for oral peptide delivery, underscoring that enhanced cellular uptake is necessary, but not sufficient for effective oral delivery. Future research must prioritize strategies that ensure true, stable core encapsulation of Tir and minimize payload loss during functionalization. Crucially, a thorough characterization of the drug release profile under gastrointestinal conditions and detailed investigation of the intracellular trafficking via techniques like confocal microscopy are essential next steps to fully harness the FcRn-mediated transcytosis pathway for oral peptide delivery.

6. Future Perspectives

Building upon the findings of this work, future research should focus on overcoming the intrinsic challenges of peptide encapsulation and translocation. To achieve true core entrapment of Tir, thereby enhancing protection from the harsh conditions of the GIT, advanced formulation strategies must be explored. Ion-pairing with hydrophobic counterions could shield the charge of Tir and improve its partition into the lipid core[241]. Furthermore, the incorporation of ionizable lipids (with pKa tuned to the endosomal pH) or lipids with deeper hydrophobic anchors could facilitate a more stable encapsulation and potentially enable lysosomal escape, working synergistically with the FcRn pathway[192,223]. Alternatively, the design of lipid-polymer hybrid carriers could merge the biocompatibility of lipids with the enhanced stability and controlled release properties of polymers[224,242]. Prodrug approaches, such as the reversible hydrophobic conjugation to Tir, represent another promising avenue to drastically increase the lipophilicity and subsequent loading within the lipid matrix[242].

Alternative nanoparticle platforms that may offer superior peptide encapsulation capabilities should also be considered. Silica-based nanoparticles, including porous silicon (pSi) and mesoporous silica nanoparticles (MSNs), have demonstrated great[243] promise for peptide delivery applications. These materials possess several advantages over conventional lipid carriers, including large surface areas, tunable pore sizes (2-50 nm range, well-suited for peptides), and adjustable pore architectures[92,244]. Importantly, MSNs have shown high peptide loading capabilities, significantly superior to the lipid systems evaluated in this work[244]. The rigid silica framework provides enhanced thermal and chemical stability, better protecting encapsulated peptides during processing, storage, and administration[243,244]. Additionally, the surface silanol groups enable straightforward functionalization with targeting moieties while maintaining structural integrity[243,244].

Beyond encapsulation, the FcRn-targeting strategy requires deeper mechanistic validation. Confocal microscopy studies are essential to visually confirm the internalization and intracellular trafficking of functionalized LNPs, distinguishing surface binding from genuine uptake and potentially colocalizing them with FcRn and late endosome/lysosome markers[238]. This should be complemented by competitive binding assays using free affibody to demonstrate the specificity of the interaction. Additionally, flow cytometry assays should be performed using cell lines that do not express human FcRn, such as HeLa cells[98], to confirm the receptor-specific binding and exclude non-specific cellular interactions[98]. Concurrently, the functionalization protocol itself must be optimized, for instance by exploring other "post-insertion" techniques, to minimize the drug loss incurred during the conjugation and purification steps[245].

To robustly validate the translational potential of this platform, a more comprehensive biological evaluation pipeline is necessary. *In vitro*, this should include mucus penetration testing (MPT) studies to demonstrate the transport capacity of PEGylated LNPs through mucus barriers. MPT allows for quantitative assessment of nanoparticle mobility in mucus by tracking individual particle movements, providing crucial insights into the fractions of particles that effectively penetrate versus those that remain adherent to mucus components. Such studies have consistently demonstrated the importance of surface modifications in enabling mucus penetration for enhanced drug delivery efficacy[246].

More complex 3D intestinal models should also be applied, *(e.g.,* organoids[98] or Transwell 3D epithelium-stroma-endothelium model[204]) that better recapitulate the the cellular diversity, tissue architecture, and physiological transport mechanisms of the human intestinal tract compared to conventional 2D co-cultures. Such systems could provide critical insights into the complex interplay between nanoparticles, mucus, epithelial barriers, and underlying stromal components that influence transcellular transport[204]. Ultimately, *in vivo* studies in diabetic animal models are indispensable to assess the pharmacokinetic profile, the absolute oral bioavailability, and the consequent pharmacodynamic effects (*e.g.,* glycemic control and production/secretion of insulin by pancreatic β cells)[106]. For this studies, hFcRn transgenic mice model should be considered to suitably recapitulate the human response[106].

Finally, from a translational standpoint, scale-up feasibility must be considered early. Although sonication was effective for lab-scale production, microfluidic technologies should be revisited for their superior control over particle size, polydispersity, and batch-to-batch reproducibility, which are critical for future industrial scaling[217].

In conclusion, by integrating rational, next-generation formulation design with increasingly physiologically relevant testing models and a focus on scalability, the potential of FcRn-targeted lipid nanosystems can be fully unlocked to enable efficient oral delivery of therapeutic peptides. This multifaceted approach leverages lipid-based nanosystems not only for the oral delivery of Tir, but also as a broad platform strategy for the non-invasive administration of peptide-based therapeutics.

7. References

1 ElSayed, N. A. *et al.* 2. Classification and Diagnosis of Diabetes: Standards of Care in Diabetes-2023. *Diabetes Care* **46**, S19-s40 (2023). https://doi.org/10.2337/dc23-S002

2 International Diabetes Federation. IDF Diabetes Atlas, 11th edn. Brussels, Belgium: 2025. Available at: https://www.diabetesatlas.org

3 Asgarian, S. *et al.* Examining the clinical and genetic spectrum of maturity-onset diabetes of the young (MODY) in Iran. *Sci. Rep.* **14**, 19860 (2024). https://doi.org/10.1038/s41598-024-70864-y

4 Dzhemileva, L. U. *et al.* Current views on etiology, diagnosis, epidemiology and gene therapy of maturity onset diabetes in the young. *Frontiers in Endocrinology* **Volume 15 - 2024**, 1497298 (2025). https://doi.org/10.3389/fendo.2024.1497298

5 Aamodt, K. I. & Powers, A. C. The pathophysiology, presentation and classification of Type 1 diabetes. *Diabetes Obes Metab* **27 Suppl 6**, 15-27 (2025). https://doi.org/10.1111/dom.16628

6 Martins, L. M. *et al.* Type B insulin resistance syndrome: a systematic review. *Arch Endocrinol Metab* **64**, 337-348 (2020). https://doi.org/10.20945/2359-3997000000257

7 Zhao, X. *et al.* The crucial role and mechanism of insulin resistance in metabolic disease. *Frontiers in Endocrinology* **Volume 14 - 2023** (2023). https://doi.org/10.3389/fendo.2023.1149239

8 Norton, L., Shannon, C., Gastaldelli, A. & DeFronzo, R. A. Insulin: The master regulator of glucose metabolism. *Metabolism* **129**, 155142 (2022). https://doi.org/10.1016/j.metabol.2022.155142

9 Sami, A. *et al.* Genetics of diabetes and its complications: a comprehensive review. *Diabetology & Metabolic Syndrome* **17**, 185 (2025). https://doi.org/10.1186/s13098-025-01748-y

10 Laakso, M. & Fernandes Silva, L. Genetics of Type 2 Diabetes: Past, Present, and Future. *Nutrients* **14** (2022). https://doi.org/10.3390/nu14153201

11 Al-Goblan, A. S., Al-Alfi, M. A. & Khan, M. Z. Mechanism linking diabetes mellitus and obesity. *Diabetes Metab Syndr Obes* **7**, 587-591 (2014). https://doi.org/10.2147/dmso.S67400

12 Aldhaeefi, M. *et al.* Updates in the Management of Hyperglycemic Crisis. *Front Clin Diabetes Healthc* **2**, 820728 (2021). https://doi.org/10.3389/fcdhc.2021.820728

13 Wu, H. *et al.* Diabetes and Its Cardiovascular Complications: Comprehensive Network and Systematic Analyses. *Front Cardiovasc Med* **9**, 841928 (2022). https://doi.org/10.3389/fcvm.2022.841928

14 Tommerdahl, K. L., Shapiro, A. L. B., Nehus, E. J. & Bjornstad, P. Early microvascular complications in type 1 and type 2 diabetes: recent developments and updates. *Pediatr Nephrol* **37**, 79-93 (2022). https://doi.org/10.1007/s00467-021-05050-7

15 Sun, H. *et al*. IDF Diabetes Atlas: Global, regional and country-level diabetes prevalence estimates for 2021 and projections for 2045. *Diabetes Res Clin Pract* **183**, 109119 (2022). https://doi.org/10.1016/j.diabres.2021.109119

16 Ong, K. L. *et al*. Global, regional, and national burden of diabetes from 1990 to 2021, with projections of prevalence to 2050: a systematic analysis for the Global Burden of Disease Study 2021. *The Lancet* **402**, 203-234 (2023). https://doi.org/10.1016/S0140-6736(23)01301-6

17 Reed, J., Bain, S. C. & Kanamarlapudi, V. The Regulation of Metabolic Homeostasis by Incretins and the Metabolic Hormones Produced by Pancreatic Islets. *Diabetes Metab Syndr Obes* **17**, 2419-2456 (2024). https://doi.org/10.2147/dmso.S415934

18 van Gerwen, J., Shun-Shion, A. S. & Fazakerley, D. J. Insulin signalling and GLUT4 trafficking in insulin resistance. *Biochem Soc Trans* **51**, 1057-1069 (2023). https://doi.org/10.1042/bst20221066

19 Li, M. *et al*. Trends in insulin resistance: insights into mechanisms and therapeutic strategy. *Signal Transduction and Targeted Therapy* **7**, 216 (2022). https://doi.org/10.1038/s41392-022-01073-0

20 Judge, S. *et al*. Analysis of Multiple Insulin Actions in Single Muscle Fibers From Insulin-Resistant Mice Reveals Selective Defect in Endogenous GLUT4 Translocation. *Diabetes* **74**, 1121-1134 (2025). https://doi.org/10.2337/db25-0022

21 Dludla, P. V. *et al*. Pancreatic β-cell dysfunction in type 2 diabetes: Implications of inflammation and oxidative stress. *World J Diabetes* **14**, 130-146 (2023). https://doi.org/10.4239/wjd.v14.i3.130

22 Pappachan, J. M., Fernandez, C. J. & Ashraf, A. P. Rising tide: The global surge of type 2 diabetes in children and adolescents demands action now. *World J Diabetes* **15**, 797-809 (2024). https://doi.org/10.4239/wjd.v15.i5.797

23 Nadeau, K. J. *et al*. Youth-Onset Type 2 Diabetes: What We've Learned From Key Youth-Onset Type 2 Diabetes Studies, What We Still Don't Know, and Why It Is Important. *Diabetes Care* **48**, 1136-1149 (2025). https://doi.org/10.2337/dc25-0001

24 Salari, N., Ahmadi, M., Ghasemi, H., Yarani, R. & Mohammadi, M. The Global Prevalence of Sedentary Time in Diabetes and Metabolic Syndrome: A Systematic Review and Meta-Analysis. *Iran J Public Health* **53**, 2020-2029 (2024). https://doi.org/10.18502/ijph.v53i9.16455

25 Kovács, N., Shahin, B., Andrade, C. A. S., Mahrouseh, N. & Varga, O. Lifestyle and metabolic risk factors, and diabetes mellitus prevalence in European countries from three waves of the European Health Interview Survey. *Sci. Rep.* **14**, 11623 (2024). https://doi.org/10.1038/s41598-024-62122-y

26 Deng, M.-G. *et al.* Physical activity, sedentary behavior, and the risk of type 2 diabetes: A two-sample Mendelian Randomization analysis in the European population. *Frontiers in Endocrinology* **Volume 13 - 2022**, 964132 (2022). https://doi.org/10.3389/fendo.2022.964132

27 Sagastume, D. *et al.* The effectiveness of lifestyle interventions on type 2 diabetes and gestational diabetes incidence and cardiometabolic outcomes: A systematic review and meta-analysis of evidence from low- and middle-income countries. *EClinicalMedicine* **53**, 101650 (2022). https://doi.org/10.1016/j.eclinm.2022.101650

28 American Diabetes Association Professional Practice, C. 9. Pharmacologic Approaches to Glycemic Treatment: Standards of Care in Diabetes-2025. *Diabetes Care* **48**, S181-s206 (2025). https://doi.org/10.2337/dc25-S009

29 Corrao, S., Falcone, F., Mirarchi, L., Amodeo, S. & Calvo, L. Type 2 Diabetes Mellitus Remission, Dream or Reality? A Narrative Review of Current Evidence and Integrated Care Strategies. *Diabetes Therapy* **16**, 1557-1579 (2025). https://doi.org/10.1007/s13300-025-01761-4

30 Patel, M. R. Financial Toxicity in Diabetes: The State of What We Know. *Curr Diab Rep* **25**, 32 (2025). https://doi.org/10.1007/s11892-025-01588-0

31 American Diabetes Association Professional Practice Committee. 1. Improving Care and Promoting Health in Populations: Standards of Care in Diabetes—2025. *Diabetes Care* **48**, S14-S26 (2024). https://doi.org/10.2337/dc25-S001

32 Kwon, S. Y. & Moon, J. S. Advances in Continuous Glucose Monitoring: Clinical Applications. *Endocrinol Metab (Seoul)* **40**, 161-173 (2025). https://doi.org/10.3803/EnM.2025.2370

33 Davies, M. J. *et al.* Management of Hyperglycemia in Type 2 Diabetes, 2022. A Consensus Report by the American Diabetes Association (ADA) and the European Association for the Study of Diabetes (EASD). *Diabetes Care* **45**, 2753-2786 (2022). https://doi.org/10.2337/dci22-0034

34 Dahlén, A. D. *et al.* Trends in Antidiabetic Drug Discovery: FDA Approved Drugs, New Drugs in Clinical Trials and Global Sales. *Front Pharmacol* **12**, 807548 (2021). https://doi.org/10.3389/fphar.2021.807548

35 Helmstädter, J. *et al.* Glucagon-like peptide-1 (GLP-1) receptor agonists and their cardiovascular benefits-The role of the GLP-1 receptor. *Br J Pharmacol* **179**, 659-676 (2022). https://doi.org/10.1111/bph.15462

36 Monney, M., Jornayvaz, F. R. & Gariani, K. GLP-1 receptor agonists effect on cognitive function in patients with and without type 2 diabetes. *Diabetes & Metabolism* **49**, 101470 (2023). https://doi.org/https://doi.org/10.1016/j.diabet.2023.101470

37 Goldenberg, R. M. *et al.* Benefits of GLP-1 (Glucagon-Like Peptide 1) Receptor Agonists for Stroke Reduction in Type 2 Diabetes: A Call to Action for Neurologists. *Stroke* **53**, 1813-1822 (2022). https://doi.org/10.1161/STROKEAHA.121.038151

38 McIntyre, R. S. *et al.* The neuroprotective effects of GLP-1: Possible treatments for cognitive deficits in individuals with mood disorders. *Behavioural Brain Research* **237**, 164-171 (2013). https://doi.org/https://doi.org/10.1016/j.bbr.2012.09.021

39 Abdrabou Abouelmagd, A. *et al.* Efficacy and safety of retatrutide, a novel GLP-1, GIP, and glucagon receptor agonist for obesity treatment: a systematic review and meta-analysis of randomized controlled trials. *Proc (Bayl Univ Med Cent)* **38**, 291-303 (2025). https://doi.org/10.1080/08998280.2025.2456441

40 Sanyal, A. J. *et al.* Triple hormone receptor agonist retatrutide for metabolic dysfunction-associated steatotic liver disease: a randomized phase 2a trial. *Nature Medicine* **30**, 2037-2048 (2024). https://doi.org/10.1038/s41591-024-03018-2

41 Brixner, D., Edelman, S. V., Sieradzan, R. & Gavin, J. R., 3rd. Addressing the Burden of Multiple Daily Insulin Injections in Type 2 Diabetes with Insulin Pump Technology: A Narrative Review. *Diabetes Ther* **15**, 1525-1534 (2024). https://doi.org/10.1007/s13300-024-01598-3

42 Petry, S. F., Petry, F. W., Petry, J. K., Gäth, S. & Heinemann, L. Diabetes Technology and Waste: A Real-World Study in a Specialized Practice in Germany. *J Diabetes Sci Technol*, 19322968241257004 (2024). https://doi.org/10.1177/19322968241257004

43 Tian, T. *et al.* Quantifying Environmental Waste From Diabetes Devices in the U.S. *Diabetes Care* **48**, 1198-1203 (2025). https://doi.org/10.2337/dc24-2522

44 Jiao, Q., Huang, Y., He, J. & Xu, Y. Advances in Oral Biomacromolecule Therapies for Metabolic Diseases. *Pharmaceutics* **17** (2025). https://doi.org/10.3390/pharmaceutics17020238

45 Nauck, M. A. & Meier, J. J. Incretin hormones: Their role in health and disease. *Diabetes Obes Metab* **20 Suppl 1**, 5-21 (2018). https://doi.org/10.1111/dom.13129

46 Nauck, M. A. & Müller, T. D. Incretin hormones and type 2 diabetes. *Diabetologia* **66**, 1780-1795 (2023). https://doi.org/10.1007/s00125-023-05956-x

47 Rosenberg, J. *et al.* Incretin Hormones: Pathophysiological Risk Factors and Potential Targets for Type 2 Diabetes. *J Obes Metab Syndr* **30**, 233-247 (2021). https://doi.org/10.7570/jomes21053

48 Zheng, Z. *et al.* Glucagon-like peptide-1 receptor: mechanisms and advances in therapy. *Signal Transduction and Targeted Therapy* **9**, 234 (2024). https://doi.org/10.1038/s41392-024-01931-z

49 Jiang, Y. *et al.* GLP-1 Improves Adipocyte Insulin Sensitivity Following Induction of Endoplasmic Reticulum Stress. *Frontiers in Pharmacology* **Volume 9 - 2018**, 1168 (2018). https://doi.org/10.3389/fphar.2018.01168

50 Jeon, J. Y. *et al.* GLP-1 improves palmitate-induced insulin resistance in human skeletal muscle via SIRT1 activity. *Int J Mol Med* **44**, 1161-1171 (2019). https://doi.org/10.3892/ijmm.2019.4272

51 Movahednasab, M. *et al.* GLP-1-based therapies for type 2 diabetes: from single, dual and triple agonists to endogenous GLP-1 production and L-cell differentiation. *Diabetology & Metabolic Syndrome* **17**, 60 (2025). https://doi.org/10.1186/s13098-025-01623-w

52 Singh, A. K. Dipeptidyl peptidase-4 inhibitors: Novel mechanism of actions. *Indian J Endocrinol Metab* **18**, 753-759 (2014). https://doi.org/10.4103/2230-8210.141319

53 Andreasen, C. R., Andersen, A., Knop, F. K. & Vilsbøll, T. Understanding the place for GLP-1RA therapy: Translating guidelines for treatment of type 2 diabetes into everyday clinical practice and patient selection. *Diabetes, Obesity and Metabolism* **23**, 40-52 (2021). https://doi.org/https://doi.org/10.1111/dom.14500

54 Pechenov, S. *et al.* Development of an orally delivered GLP-1 receptor agonist through peptide engineering and drug delivery to treat chronic disease. *Sci Rep* **11**, 22521 (2021). https://doi.org/10.1038/s41598-021-01750-0

55 Rasmussen, M. F. The development of oral semaglutide, an oral GLP-1 analog, for the treatment of type 2 diabetes. *Diabetol Int* **11**, 76-86 (2020). https://doi.org/10.1007/s13340-019-00423-8

56 Hughes, S. & Neumiller, J. J. Oral Semaglutide. *Clin Diabetes* **38**, 109-111 (2020). https://doi.org/10.2337/cd19-0079

57 Liu, Q. K. Mechanisms of action and therapeutic applications of GLP-1 and dual GIP/GLP-1 receptor agonists. *Front Endocrinol (Lausanne)* **15**, 1431292 (2024). https://doi.org/10.3389/fendo.2024.1431292

58 Marassi, M. & Fadini, G. P. Real-world Evidence on Oral Semaglutide for the Management of Type 2 Diabetes. A Narrative Review for Clinical Practice. *Clinical Therapeutics* **47**, 102-110 (2025). https://doi.org/https://doi.org/10.1016/j.clinthera.2024.11.005

59 Solis-Herrera, C., Kane, M. P. & Triplitt, C. Current Understanding of Sodium N-(8-[2-Hydroxylbenzoyl] Amino) Caprylate (SNAC) as an Absorption Enhancer: The Oral Semaglutide Experience. *Clin Diabetes* **42**, 74-86 (2024). https://doi.org/10.2337/cd22-0118

60 Alqahtani, M. S., Kazi, M., Alsenaidy, M. A. & Ahmad, M. Z. Advances in Oral Drug Delivery. *Frontiers in Pharmacology* **Volume 12 - 2021**, 618411 (2021). https://doi.org/10.3389/fphar.2021.618411

61 Kalra, S., Das, S. & Zargar, A. H. A Review of Oral Semaglutide Available Evidence: A New Era of Management of Diabetes with Peptide in a Pill Form. *Indian J Endocrinol Metab* **26**, 98-105 (2022). https://doi.org/10.4103/ijem.ijem_522_21

62 Baral, K. C. & Choi, K. Y. Barriers and Strategies for Oral Peptide and Protein Therapeutics Delivery: Update on Clinical Advances. *Pharmaceutics* **17** (2025). https://doi.org/10.3390/pharmaceutics17040397

63 Al Tahan, M. A., Al-Khattawi, A. & Russell, C. Oral peptide delivery Systems: Synergistic approaches using polymers, lipids, Nanotechnology, and needle-based carriers. *Journal of Drug Delivery Science and Technology* **112**, 107205 (2025). https://doi.org/https://doi.org/10.1016/j.jddst.2025.107205

64 Nicze, M. et al. The Current and Promising Oral Delivery Methods for Protein- and Peptide-Based Drugs. *Int J Mol Sci* 25 (2024). https://doi.org/10.3390/ijms25020815

65 Wang, X. *et al*. Obstacles, research progress, and prospects of oral delivery of bioactive peptides: a comprehensive review. *Frontiers in Nutrition* **Volume 11 - 2024**, 1496706 (2024). https://doi.org/10.3389/fnut.2024.1496706

66 Herath, M., Hosie, S., Bornstein, J. C., Franks, A. E. & Hill-Yardin, E. L. The Role of the Gastrointestinal Mucus System in Intestinal Homeostasis: Implications for Neurological Disorders. *Frontiers in Cellular and Infection Microbiology* **Volume 10 - 2020**, 248 (2020). https://doi.org/10.3389/fcimb.2020.00248

67 Krupa, L. *et al*. Comparing the permeability of human and porcine small intestinal mucus for particle transport studies. *Sci Rep* **10**, 20290 (2020). https://doi.org/10.1038/s41598-020-77129-4

68 Johansson, M. E. V. *et al*. Composition and functional role of the mucus layers in the intestine. *Cellular and Molecular Life Sciences* **68**, 3635-3641 (2011). https://doi.org/10.1007/s00018-011-0822-3

69 Ensign, L. M., Cone, R. & Hanes, J. Oral drug delivery with polymeric nanoparticles: The gastrointestinal mucus barriers. *Advanced Drug Delivery Reviews* **64**, 557-570 (2012). https://doi.org/https://doi.org/10.1016/j.addr.2011.12.009

70 Allen, A. & Flemström, G. Gastroduodenal mucus bicarbonate barrier: protection against acid and pepsin. *American Journal of Physiology-Cell Physiology* **288**, C1-C19 (2005). https://doi.org/10.1152/ajpcell.00102.2004

71 Boegh, M. & Nielsen, H. M. Mucus as a barrier to drug delivery – understanding and mimicking the barrier properties. *Basic Clin Pharmacol Toxicol* **116**, 179-186 (2015). https://doi.org/10.1111/bcpt.12342

72 Leal, J., Smyth, H. D. C. & Ghosh, D. Physicochemical properties of mucus and their impact on transmucosal drug delivery. *Int J Pharm* **532**, 555-572 (2017). https://doi.org/10.1016/j.ijpharm.2017.09.018

73 Kiela, P. R. & Ghishan, F. K. Physiology of Intestinal Absorption and Secretion. *Best Pract Res Clin Gastroenterol* **30**, 145-159 (2016). https://doi.org/10.1016/j.bpg.2016.02.007

74 Azman, M., Sabri, A. H., Anjani, Q. K., Mustaffa, M. F. & Hamid, K. A. Intestinal Absorption Study: Challenges and Absorption Enhancement Strategies in Improving Oral Drug Delivery. *Pharmaceuticals (Basel)* **15** (2022). https://doi.org/10.3390/ph15080975

75 Paradis, T., Bègue, H., Basmaciyan, L., Dalle, F. & Bon, F. Tight Junctions as a Key for Pathogens Invasion in Intestinal Epithelial Cells. *International Journal of Molecular Sciences* **22**, 2506 (2021). https://doi.org/10.3390/ijms22052506

76 Morales, E. A., Gaeta, I. & Tyska, M. J. Building the brush border, one microvillus at a time. *Curr Opin Cell Biol* **80**, 102153 (2023). https://doi.org/10.1016/j.ceb.2023.102153

77 Delbaere, K. *et al*. The small intestine: dining table of host–microbiota meetings. *FEMS Microbiology Reviews* **47** (2023). https://doi.org/10.1093/femsre/fuad022

78 Yu, Y., Yang, W., Li, Y. & Cong, Y. Enteroendocrine Cells: Sensing Gut Microbiota and Regulating Inflammatory Bowel Diseases. *Inflamm Bowel Dis* **26**, 11-20 (2020). https://doi.org/10.1093/ibd/izz217

79 Chen, G., Kang, W., Li, W., Chen, S. & Gao, Y. Oral delivery of protein and peptide drugs: from non-specific formulation approaches to intestinal cell targeting strategies. *Theranostics* **12**, 1419-1439 (2022). https://doi.org/10.7150/thno.61747

80 Schoultz, I. & Keita Å, V. The Intestinal Barrier and Current Techniques for the Assessment of Gut Permeability. *Cells* **9** (2020). https://doi.org/10.3390/cells9081909

81 Yamamoto, K. *et al*. Intestinal Morphology and Glucose Transporter Gene Expression under a Chronic Intake of High Sucrose. *Nutrients* **16** (2024). https://doi.org/10.3390/nu16020196

82 Horowitz, A., Chanez-Paredes, S. D., Haest, X. & Turner, J. R. Paracellular permeability and tight junction regulation in gut health and disease. *Nat Rev*

Gastroenterol Hepatol **20**, 417-432 (2023). https://doi.org/10.1038/s41575-023-00766-3

83 Mehrotra, S., Kalyan Bg, P., Nayak, P. G., Joseph, A. & Manikkath, J. Recent Progress in the Oral Delivery of Therapeutic Peptides and Proteins: Overview of Pharmaceutical Strategies to Overcome Absorption Hurdles. *Adv Pharm Bull* **14**, 11-33 (2024). https://doi.org/10.34172/apb.2024.009

84 Peng, H. *et al.* Challenges and opportunities in delivering oral peptides and proteins. *Expert Opin Drug Deliv* **20**, 1349-1369 (2023). https://doi.org/10.1080/17425247.2023.2237408

85 Lombardi, L., Genio, V. D., Albericio, F. & Williams, D. R. Advances in Peptidomimetics for Next-Generation Therapeutics: Strategies, Modifications, and Applications. *Chemical Reviews* **125**, 7099-7166 (2025). https://doi.org/10.1021/acs.chemrev.4c00989

86 Kim, J. C., Park, E. J. & Na, D. H. Gastrointestinal Permeation Enhancers for the Development of Oral Peptide Pharmaceuticals. *Pharmaceuticals (Basel)* **15** (2022). https://doi.org/10.3390/ph15121585

87 Dan, N., Samanta, K. & Almoazen, H. An Update on Pharmaceutical Strategies for Oral Delivery of Therapeutic Peptides and Proteins in Adults and Pediatrics. *Children (Basel)* **7** (2020). https://doi.org/10.3390/children7120307

88 Zhu, Q. *et al.* Oral delivery of proteins and peptides: Challenges, status quo and future perspectives. *Acta Pharm Sin B* **11**, 2416-2448 (2021). https://doi.org/10.1016/j.apsb.2021.04.001

89 Gao, X., Li, J., Li, J., Zhang, M. & Xu, J. Pain-free oral delivery of biologic drugs using intestinal peristalsis–actuated microneedle robots. *Science Advances* **10**, eadj7067 (2024). https://doi.org/doi:10.1126/sciadv.adj7067

90 Vasquez-Martínez, N., Guillen, D., Moreno-Mendieta, S. A., Sanchez, S. & Rodríguez-Sanoja, R. The Role of Mucoadhesion and Mucopenetration in the Immune Response Induced by Polymer-Based Mucosal Adjuvants. *Polymers (Basel)* **15** (2023). https://doi.org/10.3390/polym15071615

91 Cheng, H. *et al.* Mucoadhesive versus mucopenetrating nanoparticles for oral delivery of insulin. *Acta Biomater* **135**, 506-519 (2021). https://doi.org/10.1016/j.actbio.2021.08.046

92 Guo, Y. *et al.* Mucus Penetration of Surface-Engineered Nanoparticles in Various pH Microenvironments. *ACS Nano* **17**, 2813-2828 (2023). https://doi.org/10.1021/acsnano.2c11147

93 Limenh, L. W. A review on oral novel delivery systems of insulin through the novel delivery system formulations: A review. *SAGE Open Med* **12**, 20503121231225319 (2024). https://doi.org/10.1177/20503121231225319

94 Dan, N., Samanta, K. & Almoazen, H. An Update on Pharmaceutical Strategies for Oral Delivery of Therapeutic Peptides and Proteins in Adults

and Pediatrics. *Children (Basel)* **7** (2020). https://doi.org/10.3390/children7120307

95 Panou, D. A., Pedersen, S. F., Kristensen, M. & Nielsen, H. M. Epithelium dynamics differ in time and space when exposed to the permeation enhancers penetramax and EGTA. A head-to-head mechanistic comparison. *Frontiers in Drug Delivery* **Volume 3 - 2023**, 1221628 (2023). https://doi.org/10.3389/fddev.2023.1221628

96 Nicze, M. *et al*. The Current and Promising Oral Delivery Methods for Protein- and Peptide-Based Drugs. *Int J Mol Sci* **25** (2024). https://doi.org/10.3390/ijms25020815

97 Zheng, Y. *et al*. Transepithelial transport of nanoparticles in oral drug delivery: From the perspective of surface and holistic property modulation. *Acta Pharm Sin B* **14**, 3876-3900 (2024). https://doi.org/10.1016/j.apsb.2024.06.015

98 Pinto, S. *et al*. Nanoparticles targeting the intestinal Fc receptor enhance intestinal cellular trafficking of semaglutide. *J Control Release* **366**, 621-636 (2024). https://doi.org/10.1016/j.jconrel.2024.01.015

99 Pridgen, E. M. *et al*. Transepithelial transport of Fc-targeted nanoparticles by the neonatal fc receptor for oral delivery. *Sci Transl Med* **5**, 213ra167 (2013). https://doi.org/10.1126/scitranslmed.3007049

100 Pyzik, M., Kozicky, L. K., Gandhi, A. K. & Blumberg, R. S. The therapeutic age of the neonatal Fc receptor. *Nat. Rev. Immunol.* **23**, 415-432 (2023). https://doi.org/10.1038/s41577-022-00821-1

101 Qi, T. & Cao, Y. In Translation: FcRn across the Therapeutic Spectrum. *Int J Mol Sci* **22** (2021). https://doi.org/10.3390/ijms22063048

102 Ma, G. *et al*. Differential effects of FcRn antagonists on the subcellular trafficking of FcRn and albumin. *JCI Insight* **9** (2024). https://doi.org/10.1172/jci.insight.176166

103 Sand, K. M. *et al*. Unraveling the Interaction between FcRn and Albumin: Opportunities for Design of Albumin-Based Therapeutics. *Front Immunol* **5**, 682 (2014). https://doi.org/10.3389/fimmu.2014.00682

104 Pyzik, M., Kozicky, L. K., Gandhi, A. K. & Blumberg, R. S. The therapeutic age of the neonatal Fc receptor. *Nat Rev Immunol* **23**, 415-432 (2023). https://doi.org/10.1038/s41577-022-00821-1

105 Pannek, A., Becker-Gotot, J., Dower, S. K., Verhagen, A. M. & Gleeson, P. A. The endosomal system of primary human vascular endothelial cells and albumin-FcRn trafficking. *J Cell Sci* **136** (2023). https://doi.org/10.1242/jcs.260912

106 Pinto, S. *et al*. Bioengineered Nanomedicines Targeting the Intestinal Fc Receptor Achieve the Improved Glucoregulatory Effect of Semaglutide in a

Type 2 Diabetic Mice Model. *ACS Nano* **18**, 28406-28424 (2024). https://doi.org/10.1021/acsnano.4c11172

107 Cho, H., Jeon, S. I., Ahn, C. H., Shim, M. K. & Kim, K. Emerging Albumin-Binding Anticancer Drugs for Tumor-Targeted Drug Delivery: Current Understandings and Clinical Translation. *Pharmaceutics* **14** (2022). https://doi.org/10.3390/pharmaceutics14040728

108 Strohl, W. R. Fusion Proteins for Half-Life Extension of Biologics as a Strategy to Make Biobetters. *BioDrugs* **29**, 215-239 (2015). https://doi.org/10.1007/s40259-015-0133-6

109 Haqqani, A. S., Bélanger, K. & Stanimirovic, D. B. Receptor-mediated transcytosis for brain delivery of therapeutics: receptor classes and criteria. *Front Drug Deliv* **4**, 1360302 (2024). https://doi.org/10.3389/fddev.2024.1360302

110 Richel, E. *et al.* Antigen-dependent modulation of immune responses to antigen-Fc fusion proteins by Fc-effector functions. *Front Immunol* **14**, 1275193 (2023). https://doi.org/10.3389/fimmu.2023.1275193

111 Junker, F., Gordon, J. & Qureshi, O. Fc Gamma Receptors and Their Role in Antigen Uptake, Presentation, and T Cell Activation. *Front Immunol* **11**, 1393 (2020). https://doi.org/10.3389/fimmu.2020.01393

112 Sadler, C. J. *et al.* Adding a Twist to Lateral Flow Immunoassays: A Direct Replacement of Antibodies with Helical Affibodies, from Selection to Application. *J Am Chem Soc* **147**, 11925-11940 (2025). https://doi.org/10.1021/jacs.4c17452

113 Visentin, C. *et al.* Affibodies as valuable tool to prevent β(2)m aggregation under lysosomal-like conditions. *Biol Direct* **20**, 67 (2025). https://doi.org/10.1186/s13062-025-00659-2

114 Hjelm, L. C., Lindberg, H., Ståhl, S. & Löfblom, J. Affibody Molecules Intended for Receptor-Mediated Transcytosis via the Transferrin Receptor. *Pharmaceuticals (Basel)* **16** (2023). https://doi.org/10.3390/ph16070956

115 Oroujeni, M. *et al.* Comparison of approaches for increasing affinity of affibody molecules for imaging of B7-H3: dimerization and affinity maturation. *EJNMMI Radiopharm Chem* **9**, 30 (2024). https://doi.org/10.1186/s41181-024-00261-3

116 Giang, K. A. *et al.* An Anti-BCMA Affibody Affinity Protein for Therapeutic and Diagnostic Use in Multiple Myeloma. *Int J Mol Sci* **26** (2025). https://doi.org/10.3390/ijms26115186

117 Chen, S. *et al.* Engineered-affibody conjugates contribute to the specific targeting and cellular retention of polyplexes in Erbb3 overexpressed lung cancer cells. *Eur J Pharm Sci* **209**, 107090 (2025). https://doi.org/10.1016/j.ejps.2025.107090

118 Westerberg, C., Mestre Borras, A., Ståhl, S. & Löfblom, J. Affibody-based HER2 prodrug shows conditional cytotoxic effect on HER2-positive cancer cells. *Biochemical and Biophysical Research Communications* **758**, 151660 (2025). https://doi.org/https://doi.org/10.1016/j.bbrc.2025.151660

119 Zhang, C. *et al.* Co-delivery of 5-fluorodeoxyuridine and doxorubicin via gold nanoparticle equipped with affibody-DNA hybrid strands for targeted synergistic chemotherapy of HER2 overexpressing breast cancer. *Sci. Rep.* **10**, 22015 (2020). https://doi.org/10.1038/s41598-020-79125-0

120 Xia, X. *et al.* A novel HER2 targeting nanoagent self-assembled from affibody-epothilone B conjugate for cancer therapy. *Journal of Nanobiotechnology* **22**, 502 (2024). https://doi.org/10.1186/s12951-024-02754-4

121 Ståhl, S. *et al.* Affibody Molecules in Biotechnological and Medical Applications. *Trends Biotechnol* **35**, 691-712 (2017). https://doi.org/10.1016/j.tibtech.2017.04.007

122 Malik, S., Muhammad, K. & Waheed, Y. Emerging Applications of Nanotechnology in Healthcare and Medicine. *Molecules* **28** (2023). https://doi.org/10.3390/molecules28186624

123 Shan, X. *et al.* Current approaches of nanomedicines in the market and various stage of clinical translation. *Acta Pharm Sin B* **12**, 3028-3048 (2022). https://doi.org/10.1016/j.apsb.2022.02.025

124 Etter, E. L., Mei, K. C. & Nguyen, J. Delivering more for less: nanosized, minimal-carrier and pharmacoactive drug delivery systems. *Adv. Drug Deliv. Rev.* **179**, 113994 (2021). https://doi.org/10.1016/j.addr.2021.113994

125 Jia, Y. *et al.* Approved Nanomedicine against Diseases. *Pharmaceutics* **15** (2023). https://doi.org/10.3390/pharmaceutics15030774

126 Hou, X., Zaks, T., Langer, R. & Dong, Y. Lipid nanoparticles for mRNA delivery. *Nature Reviews Materials* **6**, 1078-1094 (2021). https://doi.org/10.1038/s41578-021-00358-0

127 Wilson, B. & Geetha, K. M. Lipid nanoparticles in the development of mRNA vaccines for COVID-19. *J Drug Deliv Sci Technol* **74**, 103553 (2022). https://doi.org/10.1016/j.jddst.2022.103553

128 Liu, Q., Zou, J., Chen, Z., He, W. & Wu, W. Current research trends of nanomedicines. *Acta Pharm Sin B* **13**, 4391-4416 (2023). https://doi.org/10.1016/j.apsb.2023.05.018

129 Alghamdi, M. A. *et al.* The Promise of Nanotechnology in Personalized Medicine. *J Pers Med* **12** (2022). https://doi.org/10.3390/jpm12050673

130 Svensson, E., von Mentzer, U. & Stubelius, A. Achieving Precision Healthcare through Nanomedicine and Enhanced Model Systems. *ACS Materials Au* **4**, 162-173 (2024). https://doi.org/10.1021/acsmaterialsau.3c00073

131 Tewabe, A., Abate, A., Tamrie, M., Seyfu, A. & Abdela Siraj, E. Targeted Drug Delivery - From Magic Bullet to Nanomedicine: Principles, Challenges, and Future Perspectives. *J Multidiscip Healthc* **14**, 1711-1724 (2021). https://doi.org/10.2147/jmdh.S313968

132 Ly, P.-D. *et al.* Recent advances in surface decoration of nanoparticles in drug delivery. *Frontiers in Nanotechnology* **Volume 6 - 2024** (2024). https://doi.org/10.3389/fnano.2024.1456939

133 Thi, T. T. H. *et al.* Lipid-Based Nanoparticles in the Clinic and Clinical Trials: From Cancer Nanomedicine to COVID-19 Vaccines. *Vaccines (Basel)* **9** (2021). https://doi.org/10.3390/vaccines9040359

134 Bhatti, R. *et al.* Inorganic Nanoparticles: Toxic Effects, Mechanisms of Cytotoxicity and Phytochemical Interactions. *Adv Pharm Bull* **12**, 757-762 (2022). https://doi.org/10.34172/apb.2022.077

135 Elmowafy, M. *et al.* Polymeric Nanoparticles for Delivery of Natural Bioactive Agents: Recent Advances and Challenges. *Polymers* **15**, 1123 (2023). https://doi.org/10.3390/polym15051123

136 Xuan, L., Ju, Z., Skonieczna, M., Zhou, P. K. & Huang, R. Nanoparticles-induced potential toxicity on human health: Applications, toxicity mechanisms, and evaluation models. *MedComm (2020)* **4**, e327 (2023). https://doi.org/10.1002/mco2.327

137 Sabourian, P. *et al.* Effect of Physico-Chemical Properties of Nanoparticles on Their Intracellular Uptake. *Int J Mol Sci* **21** (2020). https://doi.org/10.3390/ijms21218019

138 Joudeh, N. & Linke, D. Nanoparticle classification, physicochemical properties, characterization, and applications: a comprehensive review for biologists. *Journal of Nanobiotechnology* **20**, 262 (2022). https://doi.org/10.1186/s12951-022-01477-8

139 Rennick, J. J., Johnston, A. P. R. & Parton, R. G. Key principles and methods for studying the endocytosis of biological and nanoparticle therapeutics. *Nature Nanotechnology* **16**, 266-276 (2021). https://doi.org/10.1038/s41565-021-00858-8

140 Rejman, J., Oberle, V., Zuhorn, I. S. & Hoekstra, D. Size-dependent internalization of particles via the pathways of clathrin- and caveolae-mediated endocytosis. *Biochem J* **377**, 159-169 (2004). https://doi.org/10.1042/bj20031253

141 Peng, Y. *et al.* Nanomaterials in Medicine: Understanding Cellular Uptake, Localization, and Retention for Enhanced Disease Diagnosis and Therapy. *Aging Dis* **16**, 168-208 (2024). https://doi.org/10.14336/ad.2024.0206-1

142 Gemperle, J. *et al.* Live-cell magnetic manipulation of recycling endosomes reveals their direct effect on actin protrusions to promote invasive

migration. *Sci Adv* **11**, eadu6361 (2025). https://doi.org/10.1126/sciadv.adu6361

143 Wang, C. *et al.* Investigation of endosome and lysosome biology by ultra pH-sensitive nanoprobes. *Adv. Drug Deliv. Rev.* **113**, 87-96 (2017). https://doi.org/10.1016/j.addr.2016.08.014

144 Huotari, J. & Helenius, A. Endosome maturation. *Embo j* **30**, 3481-3500 (2011). https://doi.org/10.1038/emboj.2011.286

145 Guo, S. *et al.* Research on the fate of polymeric nanoparticles in the process of the intestinal absorption based on model nanoparticles with various characteristics: size, surface charge and pro-hydrophobics. *Journal of Nanobiotechnology* **19**, 32 (2021). https://doi.org/10.1186/s12951-021-00770-2

146 Schleh, C. *et al.* Size and surface charge of gold nanoparticles determine absorption across intestinal barriers and accumulation in secondary target organs after oral administration. *Nanotoxicology* **6**, 36-46 (2012). https://doi.org/10.3109/17435390.2011.552811

147 Suri, K. *et al.* Oral delivery of stabilized lipid nanoparticles for nucleic acid therapeutics. *Drug Deliv. Transl. Res.* **15**, 1755-1769 (2025). https://doi.org/10.1007/s13346-024-01709-4

148 Foroozandeh, P. & Aziz, A. A. Insight into Cellular Uptake and Intracellular Trafficking of Nanoparticles. *Nanoscale Research Letters* **13**, 339 (2018). https://doi.org/10.1186/s11671-018-2728-6

149 Kattel, P. *et al.* Effect of Nanoparticle Weight on the Cellular Uptake and Drug Delivery Potential of PLGA Nanoparticles. *ACS Omega* **8**, 27146-27155 (2023). https://doi.org/10.1021/acsomega.3c02273

150 Zhang, W. *et al.* Effects of morphology and size of nanoscale drug carriers on cellular uptake and internalization process: a review. *RSC Advances* **13**, 80-114 (2023). https://doi.org/10.1039/D2RA06888E

151 Xue, J. *et al.* Nanoparticles with rough surface improve the therapeutic effect of photothermal immunotherapy against melanoma. *Acta Pharm Sin B* **12**, 2934-2949 (2022). https://doi.org/10.1016/j.apsb.2021.11.020

152 Yin, B. *et al.* Sub-10 nm Substrate Roughness Promotes the Cellular Uptake of Nanoparticles by Upregulating Endocytosis-Related Genes. *Nano Letters* **21**, 1839-1847 (2021). https://doi.org/10.1021/acs.nanolett.0c04932

153 Danaei, M. *et al.* Impact of Particle Size and Polydispersity Index on the Clinical Applications of Lipidic Nanocarrier Systems. *Pharmaceutics* **10** (2018). https://doi.org/10.3390/pharmaceutics10020057

154 John, R., Monpara, J., Swaminathan, S. & Kalhapure, R. Chemistry and Art of Developing Lipid Nanoparticles for Biologics Delivery: Focus on Development and Scale-Up. *Pharmaceutics* **16** (2024). https://doi.org/10.3390/pharmaceutics16010131

155 Balog, S., de Almeida, M. S., Taladriz-Blanco, P., Rothen-Rutishauser, B. & Petri-Fink, A. Does the surface charge of the nanoparticles drive nanoparticle–cell membrane interactions? *Current Opinion in Biotechnology* **87**, 103128 (2024). https://doi.org/https://doi.org/10.1016/j.copbio.2024.103128

156 Önal Acet, B., Gül, D., Stauber, R. H., Odabaşı, M. & Acet, Ö. A Review for Uncovering the "Protein-Nanoparticle Alliance": Implications of the Protein Corona for Biomedical Applications. *Nanomaterials (Basel)* **14** (2024). https://doi.org/10.3390/nano14100823

157 Farjadian, F. *et al.* Physically stimulus-responsive nanoparticles for therapy and diagnosis. *Front Chem* **10**, 952675 (2022). https://doi.org/10.3389/fchem.2022.952675

158 Makhani, E. Y., Zhang, A. & Haun, J. B. Quantifying and controlling bond multivalency for advanced nanoparticle targeting to cells. *Nano Converg* **8**, 38 (2021). https://doi.org/10.1186/s40580-021-00288-1

159 Choi, Y. *et al.* Controlled spatial characteristics of ligands on nanoparticles: Determinant of cellular functions. *J. Control. Release* **360**, 672-686 (2023). https://doi.org/https://doi.org/10.1016/j.jconrel.2023.07.020

160 Woythe, L., Madhikar, P., Feiner-Gracia, N., Storm, C. & Albertazzi, L. A Single-Molecule View at Nanoparticle Targeting Selectivity: Correlating Ligand Functionality and Cell Receptor Density. *ACS Nano* **16**, 3785-3796 (2022). https://doi.org/10.1021/acsnano.1c08277

161 Romero-Carmona, C. E. *et al.* Nanoparticle and microparticle-based systems for enhanced oral insulin delivery: A systematic review and meta-analysis. *J Nanobiotechnology* **22**, 802 (2024). https://doi.org/10.1186/s12951-024-03045-8

162 Adwani, G., Bharti, S. & Kumar, A. Engineered nanoparticles in non-invasive insulin delivery for precision therapeutics of diabetes. *International Journal of Biological Macromolecules* **275**, 133437 (2024). https://doi.org/https://doi.org/10.1016/j.ijbiomac.2024.133437

163 Pinto, S. F. T., Santos, H. A. & Sarmento, B. New insights into nanomedicines for oral delivery of glucagon-like peptide-1 analogs. *Wiley Interdiscip Rev Nanomed Nanobiotechnol* **16**, e1952 (2024). https://doi.org/10.1002/wnan.1952

164 Subedi, L. *et al.* An oral liraglutide nanomicelle formulation conferring reduced insulin-resistance and long-term hypoglycemic and lipid metabolic benefits. *J Control Release* **378**, 637-655 (2025). https://doi.org/10.1016/j.jconrel.2024.12.039

165 Kim, G. L., Song, J. G. & Han, H.-K. Enhanced Oral Efficacy of Semaglutide via an Ionic Nanocomplex with Organometallic Phyllosilicate in Type 2 Diabetic Rats. *Pharmaceutics* **16**, 886 (2024). https://doi.org/10.3390/pharmaceutics16070886

166 Poudwal, S., Misra, A. & Shende, P. Role of lipid nanocarriers for enhancing oral absorption and bioavailability of insulin and GLP-1 receptor agonists. *J Drug Target* **29**, 834-847 (2021). https://doi.org/10.1080/1061186x.2021.1894434

167 Sangnim, T. *et al.* Chitosan in Oral Drug Delivery Formulations: A Review. *Pharmaceutics* **15** (2023). https://doi.org/10.3390/pharmaceutics15092361

168 Li, S. *et al.* Application of chitosan/alginate nanoparticle in oral drug delivery systems: prospects and challenges. *Drug Deliv* **29**, 1142-1149 (2022). https://doi.org/10.1080/10717544.2022.2058646

169 Moammeri, A. *et al.* Current advances in niosomes applications for drug delivery and cancer treatment. *Mater Today Bio* **23**, 100837 (2023). https://doi.org/10.1016/j.mtbio.2023.100837

170 Hosseini Sharifabad, A., Behzad, T. & Salami-Kalajahi, M. Smart glucose-responsive PAMAM dendrimers anchored on nanocrystalline cellulose for controlled insulin release. *Int J Biol Macromol* **318**, 145235 (2025). https://doi.org/10.1016/j.ijbiomac.2025.145235

171 Abedi-Gaballu, F. *et al.* PAMAM dendrimers as efficient drug and gene delivery nanosystems for cancer therapy. *Appl Mater Today* **12**, 177-190 (2018). https://doi.org/10.1016/j.apmt.2018.05.002

172 Pang, H., Huang, X., Xu, Z. P., Chen, C. & Han, F. Y. Progress in oral insulin delivery by PLGA nanoparticles for the management of diabetes. *Drug Discov Today* **28**, 103393 (2023). https://doi.org/10.1016/j.drudis.2022.103393

173 Godase, S. S., Kulkarni, N. S. & Dhole, S. N. A Comprehensive Review on Novel Lipid-Based Nano Drug Delivery. *Adv Pharm Bull* **14**, 34-47 (2024). https://doi.org/10.34172/apb.2024.012

174 Amatya, R. *et al.* Long-Lasting Exendin-4-Coated Gold Nanoparticles: Synthesis and In Vivo Evaluation of Hypoglycemic Activity. *Pharmaceuticals (Basel)* **17** (2024). https://doi.org/10.3390/ph17111475

175 Yan, J. *et al.* Porous silicon and silica carriers for delivery of peptide therapeutics. *Drug Deliv. Transl. Res.* **14**, 3549-3567 (2024). https://doi.org/10.1007/s13346-024-01609-7

176 Zangabad, P. S. *et al.* Porous Silicon Microparticles Enable Sustained Release of GLP-1R Agonist Peptides for the Treatment of Type 2 Diabetes. *Advanced Therapeutics* **7**, 2400136 (2024). https://doi.org/https://doi.org/10.1002/adtp.202400136

177 Gaber, D. A. *et al.* Synthesized nano particles of glimepiride via spray freezing into cryogenic liquid: characterization, antidiabetic activity, and bioavailability. *Drug Deliv* **29**, 364-373 (2022). https://doi.org/10.1080/10717544.2021.2018524

178 Bao, X., Qian, K. & Yao, P. Oral delivery of exenatide-loaded hybrid zein nanoparticles for stable blood glucose control and β-cell repair of type 2 diabetes mice. *Journal of Nanobiotechnology* **18**, 67 (2020). https://doi.org/10.1186/s12951-020-00619-0

179 Marassi, M. & Fadini, G. P. Real-world Evidence on Oral Semaglutide for the Management of Type 2 Diabetes. A Narrative Review for Clinical Practice. *Clin Ther* **47**, 102-110 (2025). https://doi.org/10.1016/j.clinthera.2024.11.005

180 Mehta, M. *et al.* Lipid-Based Nanoparticles for Drug/Gene Delivery: An Overview of the Production Techniques and Difficulties Encountered in Their Industrial Development. *ACS Materials Au* **3**, 600-619 (2023). https://doi.org/10.1021/acsmaterialsau.3c00032

181 Mehrdadi, S. Lipid-Based Nanoparticles as Oral Drug Delivery Systems: Overcoming Poor Gastrointestinal Absorption and Enhancing Bioavailability of Peptide and Protein Therapeutics. *Adv Pharm Bull* **14**, 48-66 (2024). https://doi.org/10.34172/apb.2024.016

182 Mall, J. *et al.* Nanostructured lipid carriers as a drug delivery system: A comprehensive review with therapeutic applications. *Intelligent Pharmacy* **3**, 243-255 (2025). https://doi.org/https://doi.org/10.1016/j.ipha.2024.09.005

183 Piunti, C. & Cimetta, E. Microfluidic approaches for producing lipid-based nanoparticles for drug delivery applications. *Biophys Rev (Melville)* **4**, 031304 (2023). https://doi.org/10.1063/5.0150345

184 Viegas, C. *et al.* Solid Lipid Nanoparticles vs. Nanostructured Lipid Carriers: A Comparative Review. *Pharmaceutics* **15** (2023). https://doi.org/10.3390/pharmaceutics15061593

185 Fonte, P., Nogueira, T., Gehm, C., Ferreira, D. & Sarmento, B. Chitosan-coated solid lipid nanoparticles enhance the oral absorption of insulin. *Drug Deliv. Transl. Res.* **1**, 299-308 (2011). https://doi.org/10.1007/s13346-011-0023-5

186 Wang, T. *et al.* "Oil-soluble" reversed lipid nanoparticles for oral insulin delivery. *Journal of Nanobiotechnology* **18**, 98 (2020). https://doi.org/10.1186/s12951-020-00657-8

187 Chen, D., Liu, J., Wu, J. & Suk, J. S. Enhancing nanoparticle penetration through airway mucus to improve drug delivery efficacy in the lung. *Expert Opin Drug Deliv* **18**, 595-606 (2021). https://doi.org/10.1080/17425247.2021.1854222

188 Singh, A. *et al.* Hijacking the intrinsic vitamin B(12) pathway for the oral delivery of nanoparticles, resulting in enhanced in vivo anti-leishmanial activity. *Biomater Sci* **10**, 5669-5688 (2022). https://doi.org/10.1039/d2bm00979j

189 Hädrich, G. *et al.* Development of a Novel Lipid-Based Nanosystem Functionalized with WGA for Enhanced Intracellular Drug Delivery. *Pharmaceutics* **14**, 2022 (2022). https://doi.org/10.3390/pharmaceutics14102022

190 Sarkhel, S. *et al.* Nanotechnology-Based Approaches for the Management of Diabetes Mellitus: An Innovative Solution to Long-Lasting Challenges in Antidiabetic Drug Delivery. *Pharmaceutics* **16** (2024). https://doi.org/10.3390/pharmaceutics16121572

191 Ansari, M. J. *et al.* Enhanced oral bioavailability of insulin-loaded solid lipid nanoparticles: pharmacokinetic bioavailability of insulin-loaded solid lipid nanoparticles in diabetic rats. *Drug Deliv* **23**, 1972-1979 (2016). https://doi.org/10.3109/10717544.2015.1039666

192 Oyama, D. *et al.* Enhanced oral insulin delivery with charge-reversible lipid nanoparticles. *Biochem Biophys Res Commun* **750**, 151420 (2025). https://doi.org/10.1016/j.bbrc.2025.151420

193 Shrestha, N. *et al.* The stimulation of GLP-1 secretion and delivery of GLP-1 agonists via nanostructured lipid carriers. *Nanoscale* **10**, 603-613 (2018). https://doi.org/10.1039/c7nr07736j

194 Subedi, L. *et al.* An oral liraglutide nanomicelle formulation conferring reduced insulin-resistance and long-term hypoglycemic and lipid metabolic benefits. *J. Control. Release* **378**, 637-655 (2025). https://doi.org/https://doi.org/10.1016/j.jconrel.2024.12.039

195 Gonçalves, L. M. *et al.* Development of solid lipid nanoparticles as carriers for improving oral bioavailability of glibenclamide. *Eur J Pharm Biopharm* **102**, 41-50 (2016). https://doi.org/10.1016/j.ejpb.2016.02.012

196 Ilyas, U. *et al.* Nanostructured Lipid Carrier-Based Delivery of Pioglitazone for Treatment of Type 2 Diabetes. *Frontiers in Pharmacology* **Volume 13 - 2022**, 934156 (2022). https://doi.org/10.3389/fphar.2022.934156

197 Mansour, N. M., El-Masry, A. A., El-Sherbiny, D. T. & Moustafa, M. A. White analytical insight for sensitive fluorescent determination of semaglutide and tirzepatide in pharmaceuticals and biological matrices. *Spectrochimica Acta Part A: Molecular and Biomolecular Spectroscopy* **313**, 124159 (2024). https://doi.org/https://doi.org/10.1016/j.saa.2024.124159

198 Ghisaidoobe, A. B. & Chung, S. J. Intrinsic tryptophan fluorescence in the detection and analysis of proteins: a focus on Förster resonance energy transfer techniques. *Int J Mol Sci* **15**, 22518-22538 (2014). https://doi.org/10.3390/ijms151222518

199 Chen, Y. & Erickson, H. P. Conformational changes of FtsZ reported by tryptophan mutants. *Biochemistry* **50**, 4675-4684 (2011). https://doi.org/10.1021/bi200106d

200 Azevedo, C. *et al.* Engineered albumin-functionalized nanoparticles for improved FcRn binding enhance oral delivery of insulin. *J Control Release* **327**, 161-173 (2020). https://doi.org/10.1016/j.jconrel.2020.08.005

201 Derayea, S. M. & Samir, E. A review on the use of fluorescamine as versatile and convenient analytical probe. *Microchemical Journal* **156**, 104835 (2020). https://doi.org/https://doi.org/10.1016/j.microc.2020.104835

202 Riener, C. K., Kada, G. & Gruber, H. J. Quick measurement of protein sulfhydryls with Ellman's reagent and with 4,4'-dithiodipyridine. *Anal Bioanal Chem* **373**, 266-276 (2002). https://doi.org/10.1007/s00216-002-1347-2

203 Macedo, M. H., Martinez, E., Barrias, C. C. & Sarmento, B. Development of an Improved 3D in vitro Intestinal Model to Perform Permeability Studies of Paracellular Compounds. *Frontiers in Bioengineering and Biotechnology* **Volume 8 - 2020**, 524018 (2020). https://doi.org/10.3389/fbioe.2020.524018

204 Macedo, M. H., Barros, A. S., Martínez, E., Barrias, C. C. & Sarmento, B. All layers matter: Innovative three-dimensional epithelium-stroma-endothelium intestinal model for reliable permeability outcomes. *J. Control. Release* **341**, 414-430 (2022). https://doi.org/https://doi.org/10.1016/j.jconrel.2021.11.048

205 Jaradat, A. *et al.* Prediction of the enhanced insulin absorption across a triple co-cultured intestinal model using mucus penetrating PLGA nanoparticles. *International Journal of Pharmaceutics* **585**, 119516 (2020). https://doi.org/https://doi.org/10.1016/j.ijpharm.2020.119516

206 Petiti, J., Revel, L. & Divieto, C. Standard Operating Procedure to Optimize Resazurin-Based Viability Assays. *Biosensors (Basel)* **14** (2024). https://doi.org/10.3390/bios14040156

207 Macedo, M. H., Araújo, F., Martínez, E., Barrias, C. & Sarmento, B. iPSC-Derived Enterocyte-like Cells for Drug Absorption and Metabolism Studies. *Trends in Molecular Medicine* **24**, 696-708 (2018). https://doi.org/https://doi.org/10.1016/j.molmed.2018.06.001

208 Araújo, F. & Sarmento, B. Towards the characterization of an in vitro triple co-culture intestine cell model for permeability studies. *Int J Pharm* **458**, 128-134 (2013). https://doi.org/10.1016/j.ijpharm.2013.10.003

209 Lozoya-Agullo, I. *et al.* Usefulness of Caco-2/HT29-MTX and Caco-2/HT29-MTX/Raji B Coculture Models To Predict Intestinal and Colonic Permeability Compared to Caco-2 Monoculture. *Molecular Pharmaceutics* **14**, 1264-1270 (2017). https://doi.org/10.1021/acs.molpharmaceut.6b01165

210 Hua, S. Advances in Oral Drug Delivery for Regional Targeting in the Gastrointestinal Tract - Influence of Physiological, Pathophysiological and Pharmaceutical Factors. *Frontiers in Pharmacology* **Volume 11 - 2020**, 524 (2020). https://doi.org/10.3389/fphar.2020.00524

211 Liu, W. *et al.* Biomimetic and temporal-controlled nanocarriers with ileum transporter targeting for achieving oral administration of chemotherapeutic drugs. *Journal of Nanobiotechnology* **20**, 281 (2022). https://doi.org/10.1186/s12951-022-01460-3

212 Diao, W. *et al.* PNA-Modified Liposomes Improve the Delivery Efficacy of CAPIRI for the Synergistic Treatment of Colorectal Cancer. *Front Pharmacol* **13**, 893151 (2022). https://doi.org/10.3389/fphar.2022.893151

213 Suk, J. S., Xu, Q., Kim, N., Hanes, J. & Ensign, L. M. PEGylation as a strategy for improving nanoparticle-based drug and gene delivery. *Adv. Drug Deliv. Rev.* **99**, 28-51 (2016). https://doi.org/10.1016/j.addr.2015.09.012

214 Kim, H. *et al.* Protein corona components of polyethylene glycol-conjugated organosilica nanoparticles modulates macrophage uptake. *Colloids and Surfaces B: Biointerfaces* **199**, 111527 (2021). https://doi.org/https://doi.org/10.1016/j.colsurfb.2020.111527

215 Huckaby, J. T. & Lai, S. K. PEGylation for enhancing nanoparticle diffusion in mucus. *Advanced Drug Delivery Reviews* **124**, 125-139 (2018). https://doi.org/https://doi.org/10.1016/j.addr.2017.08.010

216 Ong, S. G., Chitneni, M., Lee, K. S., Ming, L. C. & Yuen, K. H. Evaluation of Extrusion Technique for Nanosizing Liposomes. *Pharmaceutics* **8** (2016). https://doi.org/10.3390/pharmaceutics8040036

217 Shepherd, S. J., Issadore, D. & Mitchell, M. J. Microfluidic formulation of nanoparticles for biomedical applications. *Biomaterials* **274**, 120826 (2021). https://doi.org/10.1016/j.biomaterials.2021.120826

218 Prakash, G. *et al.* Microfluidic fabrication of lipid nanoparticles for the delivery of nucleic acids. *Adv. Drug Deliv. Rev.* **184**, 114197 (2022). https://doi.org/10.1016/j.addr.2022.114197

219 Shah, V. M. *et al.* Liposomes produced by microfluidics and extrusion: A comparison for scale-up purposes. *Nanomedicine* **18**, 146-156 (2019). https://doi.org/10.1016/j.nano.2019.02.019

220 Maeki, M., Uno, S., Niwa, A., Okada, Y. & Tokeshi, M. Microfluidic technologies and devices for lipid nanoparticle-based RNA delivery. *J Control Release* **344**, 80-96 (2022). https://doi.org/10.1016/j.jconrel.2022.02.017

221 Ota, A., Mochizuki, A., Sou, K. & Takeoka, S. Evaluation of a static mixer as a new microfluidic method for liposome formulation. *Front Bioeng Biotechnol* **11**, 1229829 (2023). https://doi.org/10.3389/fbioe.2023.1229829

222 Roth, R. S. *et al.* Effect of solution ions on the charge and performance of nanofiltration membranes. *npj Clean Water* **7**, 25 (2024). https://doi.org/10.1038/s41545-024-00322-9

223 Sun, D. & Lu, Z. R. Structure and Function of Cationic and Ionizable Lipids for Nucleic Acid Delivery. *Pharm Res* **40**, 27-46 (2023). https://doi.org/10.1007/s11095-022-03460-2

224 Hassan, A. A. A., Ramadan, E., Kristó, K., Regdon, G., Jr. & Sovány, T. Lipid-Polymer Hybrid Nanoparticles as a Smart Drug Delivery System for Peptide/Protein Delivery. *Pharmaceutics* **17** (2025). https://doi.org/10.3390/pharmaceutics17060797

225 Rao, S. & Prestidge, C. A. Polymer-lipid hybrid systems: merging the benefits of polymeric and lipid-based nanocarriers to improve oral drug delivery. *Expert Opin Drug Deliv* **13**, 691-707 (2016). https://doi.org/10.1517/17425247.2016.1151872

226 Schober, G. B., Story, S. & Arya, D. P. A careful look at lipid nanoparticle characterization: analysis of benchmark formulations for encapsulation of RNA cargo size gradient. *Sci. Rep.* **14**, 2403 (2024). https://doi.org/10.1038/s41598-024-52685-1

227 Sharma, K., Nilsuwan, K., Ma, L. & Benjakul, S. Effect of Liposomal Encapsulation and Ultrasonication on Debittering of Protein Hydrolysate and Plastein from Salmon Frame. *Foods* **12** (2023). https://doi.org/10.3390/foods12040761

228 International Organization for Standardization (ISO). ISO 10993-5: Biological evaluation of medical devices — Part 5: Tests for in vitro cytotoxicity. ISO 10993-5:2009.

229 Zhu, Y. *et al.* Screening for lipid nanoparticles that modulate the immune activity of helper T cells towards enhanced antitumour activity. *Nat Biomed Eng* **8**, 544-560 (2024). https://doi.org/10.1038/s41551-023-01131-0

230 Li, S. *et al.* Payload distribution and capacity of mRNA lipid nanoparticles. *Nat. Commun.* **13**, 5561 (2022). https://doi.org/10.1038/s41467-022-33157-4

231 Tenchov, R., Bird, R., Curtze, A. E. & Zhou, Q. Lipid Nanoparticles–From Liposomes to mRNA Vaccine Delivery, a Landscape of Research Diversity and Advancement. *ACS Nano* **15**, 16982-17015 (2021). https://doi.org/10.1021/acsnano.1c04996

232 Parvez, S., Karole, A. & Mudavath, S. L. Fabrication, physicochemical characterization and In vitro anticancer activity of nerolidol encapsulated solid lipid nanoparticles in human colorectal cell line. *Colloids and Surfaces B: Biointerfaces* **215**, 112520 (2022). https://doi.org/https://doi.org/10.1016/j.colsurfb.2022.112520

233 Li, L., Jin, L., Tian, Y. & Wang, J. Semaglutide enhances PINK1/Parkin-dependent mitophagy in hypoxia/reoxygenation-induced cardiomyocyte injury. *Mol Med Rep* **31** (2025). https://doi.org/10.3892/mmr.2025.13476

234 Takizawa, Y. *et al.* Impact of Glucagon-like Peptide-1 Receptor Agonists on Intestinal Epithelial Cell Barrier. *European Pharmaceutical Journal* **71**, 43-52 (2024). https://doi.org/10.2478/afpuc-2024-0008

235 Liu, D. X., Zhao, C. S., Wei, X. N., Ma, Y. P. & Wu, J. K. Semaglutide Protects against 6-OHDA Toxicity by Enhancing Autophagy and Inhibiting Oxidative Stress. *Parkinsons Dis* **2022**, 6813017 (2022). https://doi.org/10.1155/2022/6813017

236 Sahay, G., Alakhova, D. Y. & Kabanov, A. V. Endocytosis of nanomedicines. *J Control Release* **145**, 182-195 (2010). https://doi.org/10.1016/j.jconrel.2010.01.036

237 Cho, H. *et al.* Beyond nanoparticle-based oral drug delivery: transporter-mediated absorption and disease targeting. *Biomaterials Science* **12**, 3045-3067 (2024). https://doi.org/10.1039/D4BM00313F

238 Vranic, S. *et al.* Deciphering the mechanisms of cellular uptake of engineered nanoparticles by accurate evaluation of internalization using imaging flow cytometry. *Part Fibre Toxicol* **10**, 2 (2013). https://doi.org/10.1186/1743-8977-10-2

239 Umar, S. Intestinal Stem Cells. *Current Gastroenterology Reports* **12**, 340-348 (2010). https://doi.org/10.1007/s11894-010-0130-3

240 Béduneau, A. *et al.* A tunable Caco-2/HT29-MTX co-culture model mimicking variable permeabilities of the human intestine obtained by an original seeding procedure. *European Journal of Pharmaceutics and Biopharmaceutics* **87**, 290-298 (2014). https://doi.org/https://doi.org/10.1016/j.ejpb.2014.03.017

241 Ristroph, K. D. & Prud'homme, R. K. Hydrophobic ion pairing: encapsulating small molecules, peptides, and proteins into nanocarriers. *Nanoscale Adv* **1**, 4207-4237 (2019). https://doi.org/10.1039/c9na00308h

242 Renukuntla, J., Vadlapudi, A. D., Patel, A., Boddu, S. H. S. & Mitra, A. K. Approaches for enhancing oral bioavailability of peptides and proteins. *International Journal of Pharmaceutics* **447**, 75-93 (2013). https://doi.org/https://doi.org/10.1016/j.ijpharm.2013.02.030

243 Abeer, M. M. *et al.* Silica nanoparticles: A promising platform for enhanced oral delivery of macromolecules. *J. Control. Release* **326**, 544-555 (2020). https://doi.org/https://doi.org/10.1016/j.jconrel.2020.07.021

244 Xu, C., Lei, C. & Yu, C. Mesoporous Silica Nanoparticles for Protein Protection and Delivery. *Frontiers in Chemistry* **Volume 7 - 2019**, 290 (2019). https://doi.org/10.3389/fchem.2019.00290

245 Swart, L. E. *et al.* A robust post-insertion method for the preparation of targeted siRNA LNPs. *International Journal of Pharmaceutics* **620**, 121741 (2022). https://doi.org/https://doi.org/10.1016/j.ijpharm.2022.121741

246 Zimath, P., Pinto, S., Dias, S., Rafacho, A. & Sarmento, B. Zein nanoparticles as oral carrier for mometasone furoate delivery. *Drug Deliv. Transl. Res.* **13**, 2948-2959 (2023). https://doi.org/10.1007/s13346-023-01367-y